

PART I
IMPLEMENTATION OF
ABSORPTION-CORRECTED
FLUORESCENCE MEASUREMENTS

PART II
FLUOROMETRIC AND OTHER STUDIES
OF THE REACTION OF ALUMINUM (III)
AND FLAVONOL IN ABSOLUTE ETHANOL

Dissertation for the Degree of Ph. D.
MICHIGAN STATE UNIVERSITY
PATRICK MICHAEL KELLY
1976



This is to certify that the

thesis entitled
PART I: IMPLEMENTATION OF ABSORPTION-CORRECTED FLUORESCENCE MEASUREMENTS
PART II: FLUOROMETRIC AND OTHER STUDIES OF THE REACTION OF ALUMINUM (III) AND FLAVONOL IN ABSOLUTE ETHANOL
presented by

Patrick Michael Kelly

has been accepted towards fulfillment
of the requirements for

Ph.D. degree in Chemistry

Major professor

Date July 26, 1976

0-7639



FLUC
OF ALU

A sec
was const
include th
computer
tance sta
and the u
extend th

The p
nately ± 0
netric ac
while the

The i
work on a
Some of t
of the co

G101716

ABSTRACT

PART I

IMPLEMENTATION OF ABSORPTION-CORRECTED FLUORESCENCE MEASUREMENTS

PART II

FLUOROMETRIC AND OTHER STUDIES OF THE REACTION OF ALUMINUM (III) AND FLAVONOL IN ABSOLUTE ETHANOL

By

Patrick Michael Kelly

A second computer-centered spectrophotofluorometer was constructed. Improvements over the prototype instrument include the capability of using several different sources, computer controlled wavelength scans, the use of a reflectance standard to calibrate the emission detection system and the utilization of a methylene blue quantum counter to extend this calibration to 700 nm.

The photometric accuracy of the instrument is approximately $\pm 0.1\%$ T in the range from 1 to 100% T. The fluorometric accuracy was estimated to be approximately $\pm 5\%$, while the fluorometric precision was found to be $\pm 1\%$.

The instrument was used to extend some of the previous work on absorption-corrected fluorescence measurements. Some of the assumptions previously made in the derivation of the correction equation were carefully examined. This

critical ex
emission op
the assumpt
plementatio
ments based
measurement
found to be

This in
electronic
The band is
excitation
fluorescenc
sorption ba
although th

Based o
structures
been propos
and only on
experimenta
ing structu
identical e
ethoxide to
bridge conf

The pre
flavonol ch
in detail.

critical examination resulted in the construction of an emission optical system which met all of the criteria of the assumptions. A scheme was then developed for the implementation of absorption-corrected fluorescence measurements based on this model. Subsequently, absorption-corrected measurements were made up to an absorbance of 2.0 and were found to be accurate to $\pm 3\%$.

This instrument was used in the discovery of a new electronic absorption band in the spectrum of flavonol. The band is located in the spectral region near 410 nm, and excitation at this wavelength results in the emission of fluorescence at 484 nm. Tentatively, this electronic absorption band has been assigned to a (n, π^*) transition although the experimental results are somewhat inconclusive.

Based on the available experimental evidence, various structures for aluminum (III) in absolute ethanol have been proposed. All three are hexameric cyclic structures, and only one of these could be eliminated on the basis of the experimental evidence produced in this study. The two remaining structures seem to fit the experimental criteria of identical environments for all of the six aluminum ions, an ethoxide to aluminum (III) ratio of 2.5 and an alternating bridge configuration.

The previous work on the formation of aluminum (III)-flavonol chelates in absolute ethanol has been re-examined in detail. The formation of a 1:1 chelate in dilute base

and the 1:
unbuffered
In addition
aluminum-to
solutions.
and a series

for these
The flu
in solution
dilute base
chelates in
of 0.01, 0.
of the 1:1
absolute et
respectivel
been attrib
in unbuffer
intersystem

The pro
which presu
appear to
of various
proved uns
same ethan.
fortunatel
tallograph.

and the 1:1, 2:1 and 6:1 aluminum-to-flavonol chelates in unbuffered absolute ethanol solutions has been confirmed. In addition, this study has also shown that 1:1 and 2:1 aluminum-to-flavonol chelates also exist in acidic ethanol solutions. Based upon the proposed aluminum (III) structures and a series of potentiometric titrations, various structures for these chelates in absolute ethanol have been proposed.

The fluorescence quantum efficiencies of the chelates in solution have also been measured. The 1:1 chelate in dilute base, and the 1:1, 2:1 and 6:1 aluminum-to-flavonol chelates in unbuffered solutions, have quantum efficiencies of 0.01, 0.01, 0.03 and 0.70, respectively. The efficiencies of the 1:1 and 2:1 aluminum-to-flavonol chelates in acidic absolute ethanol solutions were found to be 0.03 and 0.45, respectively. These trends in quantum efficiencies have been attributed to an increase in rigidity for the chelates in unbuffered solutions and to a decrease in the rate of intersystem crossing for the acidic chelates.

The prospects for obtaining the solids of the chelates, which presumably exist in dilute absolute ethanol solutions, appear to be quite small. Crystallization by the addition of various solvents to the ethanolic chelate solutions has proved unsuccessful. Evaporation of the solvent from these same ethanolic solutions did yield crystalline powders. Unfortunately, the crystals were unsuitable for an X-ray crystallographic structure analysis. In addition, Raman, infrared

and aluminum

only one cl

the solid s

lieved to h

and aluminum-27 nmr spectroscopy have all indicated that only one chelate is formed in concentrated solutions and in the solid state. The stoichiometry of this chelate is believed to be three flavonate ions per aluminum ion.

IM

FLUORO
OF ALUMI

in

PART I

IMPLEMENTATION OF ABSORPTION-CORRECTED
FLUORESCENCE MEASUREMENTS

PART II

FLUOROMETRIC AND OTHER STUDIES OF THE REACTION
OF ALUMINUM (III) AND FLAVONOL IN ABSOLUTE ETHANOL

By

Patrick Michael Kelly

A DISSERTATION

Submitted to

Michigan State University

in partial fulfillment of the requirements

for the degree of

DOCTOR OF PHILOSOPHY

Department of Chemistry

1976

The au
guidance,
of this st

The au
for his ma

Specia
assistance
photofluoro
aid in the
system, to
Mr. Norman
Ronald Haas
tion far ex

ACKNOWLEDGMENTS

The author wishes to thank Dr. Andrew Timnick for his guidance, encouragement and friendship throughout the course of this study.

The author also wishes to thank Dr. Stanley R. Crouch for his many helpful suggestions as second reader.

Special thanks are given to Dr. John Holland for his assistance and advice during the construction of the spectrofluorometer, to Dr. Thomas Edwards for his invaluable aid in the design of part of the fluorometer emission optical system, to Mr. Deak Watters for his machining expertise, to Mr. Norman Young for his programming assistance and to Mr. Ronald Haas whose abilities in electronic design and fabrication far exceed his abilities as a fisherman and hunter.

LIST OF TAB

LIST OF FIG

Part I - IM
CO
ME

I. Introd

II. Theore

Evaluat

III. Instru

Optica

Electr

Comput

Instru

Instru

Precis

IV. Experi

Emissi

Absorp

Automa

V. Result

Basic

Implem

Correc

VI. Summa

TABLE OF CONTENTS

	Page
LIST OF TABLES	vii
LIST OF FIGURES	viii
Part I - IMPLEMENTATION OF ABSORPTION - CORRECTED FLUORESCENCE MEASURE- MENTS	1
I. Introduction	2
II. Theoretical	11
Evaluation of the Basic Assumptions	18
III. Instrumental	20
Optical	20
Electrical	22
Computer	26
Instrumental Improvements	28
Instrumental Accuracy and Precision	30
IV. Experimental	33
Emission Optical System	33
Absorption-Corrected Fluorescence	40
Automated Corrections	45
V. Results and Discussion	47
Basic Assumptions	47
Implementation	49
Correction Accuracy	50
VI. Summary and Conclusions	53

Chapter

Part II - F
O
A

I. Introd

II. Experi

Instru

Chemic

Purifi

Prepar

Experi

Sp

Ph

Ti

Ap

Em

Co

Ra

In

X-

Me

Al

III. Result

Absorp
of Fla

Emissi
77 K.

(n, π^*)

Absorp
of the

Emiss
at 77

Chelat

B

Chapter	Page
Part II - FLUOROMETRIC AND OTHER STUDIES OF THE REACTION OF ALUMINUM (III) AND FLAVONOL IN ABSOLUTE ETHANOL	54
I. Introduction.	55
II. Experimental.	61
Instrumentation	61
Chemicals	62
Purification of Flavonol.	63
Preparation of Stock Solutions.	64
Experimental Procedures	65
Spectrofluorometer.	65
Photometric and Fluorometric Titrations.	66
Apparent pH Measurements.	67
Emission Measurements	67
Concentrated Chelate Solutions.	67
Raman Spectra Measurements.	68
Infrared Spectra Measurements	68
X-ray Powder Diffraction Measurements.	69
Aluminum-27 NMR Measurements.	69
III. Results and Discussion.	71
Absorption and Fluorescence Spectra of Flavonol	71
Emission Spectrum of Flavonol at 77 K.	71
(n, π^*) Excited State of Flavonol.	76
Absorption and Fluorescence Spectra of the Chelates	84
Emission Spectra of the Chelates at 77 K	86
Chelate Stoichiometries	93
Basic Solutions	93

Chapter

N
A

Raman

Infra

Alumi

Poten

Alumi
in Ab

B
"
A

Chela

B
"
A

Chela

Prepa

IV. Summar

APPENDICES

Append
Assump

Append
Config

Append
Constr
Emissi
Table

Bu

Pr

Chapter	Page
Neutral Solutions	94
Acidic Solutions.	94
Raman Spectra	96
Infrared Spectra.	99
Aluminum-27 NMR	110
Potentiometric Titrations	114
Aluminum (III) Species Structures in Absolute Ethanol	123
Basic Solutions	123
"Neutral" Solutions	123
Acidic Solutions.	128
Chelate Structures.	129
Basic Solutions	129
"Neutral" Solutions	130
Acidic Solutions.	135
Chelate Quantum Efficiencies.	135
Preparation of Solid Chelates	139
IV. Summary and Conclusions	140
APPENDICES	
Appendix One - Mathematical Proof of Assumption Four	144
Appendix Two - Buffered Digital I/O Pin Configurations (DEC DR8-EA)	148
Appendix Three - Instructions for the Construction and Implementation of an Emission Detection System Correction Table	150
Building the Correction Table	151
Rhodamine B Section.	151
Methylene Blue Section	153
Program PMT	153

Chapter

D

Appen
Imple
Fluor

P

P

P

BIBLIOGRAP

Chapter	Page
Data Processing	157
Appendix Four - Instructions for the Implementation of Absorption-Corrected Fluorescence Measurements	161
Program LSSQ.	163
Section One.	164
Section Two.	166
Program RTFACT.	167
Program ARTCAL.	171
BIBLIOGRAPHY	181

Table

I Va
Fl

II De
ce
Wa
Ox

III D
C
E
P

IV P
a

V

LIST OF TABLES

Table		Page
I	Variables for 90°, Steady State Fluorescence Measurements	3
II	Dependence of the Delayed Fluores- cence of Flavonol on Excitation Wavelength and the Presence of Oxygen.	74
III	Dependence of Delayed Fluores- cence on Chelate Stoichiometry, Excitation Wavelength and the Presence of Oxygen.	88
IV	Raman Spectra of Flavonol, 2:1 and 6:1 Metal-to-Ligand Chelates.	97
V	Correlation of Quantum Efficiency with Chelate Stoichiometry and Ionic Charge.	137

Figure

1 Op
Ce

2 Ci
Os

3 Fl
ti
Po

4 El
mu

5 Ge
fo

6 Li
ce
So

7 Va
a
ta
ce

8 Fl
Ak
l.

9 Fl
AK
of
be
l
N

10 Al
S
E

11 Et
F

12 E
i

LIST OF FIGURES

Figure		Page
1	Optical Diagram for the Computer-Centered Spectrophotofluorometer.	21
2	Circuit for the Vibrating Bridge Oscillator.	23
3	Flag Circuit for Computer Recognition of the Vibrating Bridge Mirror Position.	25
4	Electronic Circuit for Photo-multiplier Signal Amplification	27
5	Geometric and Optical Configuration for the Collection of Fluorescence.	36
6	Limiting Conditions for the Fluorescence Observation Angles for Point Sources Across the Sample Cell.	37
7	Variation of Optical Parameters as a Function of Secondary Mask Distance from the Source of Fluorescence	38
8	Fluorescence as a Function of Absorbance for Quinine Sulfate in 1.0 N Sulfuric Acid	42
9	Fluorescence as a Function of Absorbance for Increasing Amounts of the Chromophore, 2,5-Dihydroxybenzoic Acid, in the Presence of 1×10^{-5} M Quinine Sulfate in 0.1 N Sulfuric Acid	43
10	Absorption and Fluorescence Spectra of Flavonol in Absolute Ethanol	72
11	Emission Spectrum at 77 K for Flavonol in Absolute Ethanol.	73
12	Excitation Spectrum of Flavonol in Absolute Ethanol	77

Figure

- 13 A:
S:
E:
- 14 P:
f:
O:
A:
- 15 A:
S:
A:
- 16 A:
S:
C:
- 17 E:
t:
F:
E:
- 18 E:
2:
C:
7:
- 19 S:
f:
A:
F:
I:
- 20A I:
F:
- 20B I:
F:
- 21A I:
t:
- 21B I:
2:
- 22A I:
6:
- 22B I:
6:

Figure		Page
13	Absorption and Fluorescence Spectra of Flavonol in Absolute Ethanol	78
14	Plot of Partial Quantum Efficiency (PQ) as a Function of Wavelength for Flavonol in Absolute Ethanol.	79
15	Absorption and Fluorescence Spectra of Flavonol in Acidic Absolute Ethanol.	81
16	Absorption and Fluorescence Spectra of the Aluminum-Flavonol Chelates in Absolute Ethanol.	85
17	Emission Spectrum at 77 K for the 2:1 and 6:1 Aluminum to Flavonol Chelates in Absolute Ethanol	87
18	Energy Level Diagrams for the 2:1 and 6:1 Aluminum to Flavonol Chelates in Absolute Ethanol at 77 K.	90
19	Spectrophotometric and Spectrofluorometric Titration Curves for Aluminum (III) Titrated with Flavonol with the Proton to Metal Ion Ratio 5:1	95
20A	Infrared Absorption Spectrum of Flavonol.	100
20B	Infrared Absorption Spectrum of Flavonol.	101
21A	Infrared Absorption Spectrum of the 2:1 Aluminum to Flavonol Chelate.	102
21B	Infrared Absorption Spectrum of the 2:1 Aluminum to Flavonol Chelate.	103
22A	Infrared Absorption Spectrum of the 6:1 Aluminum to Flavonol Chelate.	104
22B	Infrared Absorption Spectrum of the 6:1 Aluminum to Flavonol Chelate.	105

Figure

23A Ir
Re
ar
Ch

23B Ir
Re
ar
Ch

24A Ir
Ab

24B Ir
Ab

25 Ty
fo
Fo

26 A
O
S
t

27 A
O
R

28 P
f
H

29 P
f
t

30

31

Figure		Page
23A	Infrared Absorption Spectrum of the Residue Formed When the Solvent from an Alcoholic Solution of Aluminum Chloride is Evaporated.	106
23B	Infrared Absorption Spectrum of the Residue Formed When the Solvent from an Alcoholic Solution of Aluminum Chloride is Evaporated.	107
24A	Infrared Absorption Spectrum of Absolute Ethanol.	108
24B	Infrared Absorption Spectrum of Absolute Ethanol.	109
25	Typical Aluminum-27 NMR Spectrum for the Aluminum-Flavonol Chelates Formed in Absolute Ethanol.	111
26	Aluminum-27 NMR Shift as a Function of Aluminum (III) Concentration for Solutions with 2:1 and 6:1 Aluminum to Flavonol Ratios in Absolute Ethanol. . .	112
27	Aluminum-27 NMR Shift as a Function of the Aluminum to Flavonol Mole Ratio in Absolute Ethanol	113
28	Potentiometric Titration Curve for Aluminum (III) Titrated with Hydroxide Ions in Absolute Ethanol.	115
29	Potentiometric Titration Curves for the Titrations of Various Aluminum to Flavonol Ratios with Hydroxide Ions in Absolute Ethanol.	118
30	Potentiometric Titration Curves for the Titration of Various Aluminum to Flavonol Ratios with Hydroxide Ions in Absolute Ethanol.	119
31	Potentiometric Titration Curves for the Titration of Various Aluminum to Flavonol Ratios with Hydroxide Ions in Absolute Ethanol	120

Figure

32 P
t
F
i

33 P
F
A
T
A

34A V
A
E

34B V
A
E

35 V
t
C

36 V
t
C

37 V
t
C

38 P
l
C
E

39 P

40 P

41 P

Figure		Page
32	Potentiometric Titration Curves for the Titration of Various Aluminum to Flavonol Ratios with Hydroxide Ions in Absolute Ethanol	121
33	Potentiometric Titration Curves for Fresh and Aged Solutions with an Aluminum to Flavonol Ratio of 2:1 Titrated with Hydroxide Ions in Absolute Ethanol.	122
34A	Various Proposed Structures for Aluminum (III) in Absolute Ethanol	126
34B	Various Proposed Structures for Aluminum (III) in Absolute Ethanol	127
35	Various Proposed Structures for the 6:1 Aluminum to Flavonol Chelate in Absolute Ethanol	131
36	Various Proposed Structures for the 2:1 Aluminum to Flavonol Chelate in Absolute Ethanol	133
37	Various Proposed Structures for the 1:1 Aluminum to Flavonol Chelate in Absolute Ethanol	136
38	Proposed Structures for the 1:1 and 2:1 Aluminum to Flavonol Chelates in Acidic Absolute Ethanol	136
39	Program PMT Flowchart	156
40	Program LSSQ Flowchart.	170
41	Program ARTCAL Flowchart.	180

PART I
IMPLEMENTATION OF ABSORPTION-CORRECTED
FLUORESCENCE MEASUREMENTS

Fluore

important

fact, the

with the i

Consequent

tion and t

that preci

Only i

obtain hig

cause of t

the measur

and until

will remain

work has g

variables.

variables

tained in

For th

have been

source ins

splitter a

(1-3). Ur

distributi

I. INTRODUCTION

Fluorescence spectroscopy has become an increasingly important analytical tool in the past few decades. In fact, the volume of fluorescence literature has mushroomed with the introduction of each new fluorescence probe. Consequently, it is very important that the instrumentation and theory behind fluorescence be well understood so that precise and accurate measurements may be made.

Only in the past few years has it become possible to obtain high quality fluorescence spectra routinely. Because of the many instrumental and photophysical variables, the measurement of fluorescence is a complicated process and until these variables are eliminated or minimized, it will remain that way. Consequently, in recent years much work has gone into defining and eliminating many of these variables. A list of the instrumental and photophysical variables involved in fluorescence measurements is contained in Table I.

For the most part, many of the instrumental variables have been eliminated or minimized. The problems with source instability were overcome by the use of a beam splitter and second detector which monitored the source (1-3). Unfortunately, the problem of source spectral distribution was not remedied by this innovation. To solve

Table I
Variables for 90°, Steady State Fluorescence Measurements

Table I

Variables for 90°, Steady State Fluorescence Measurements

Instrumental	Photophysical
Source Stability	Primary Absorption Processes
Source Spectral Distribution	Secondary Absorption Processes
Excitation Optical System	Refractive Index
Cell Geometry	Scattered Light
Emission Optical System	Anisotropic Effects
Detector Sensitivity, Linearity and Stability	
Linearity and Stability of the Readout System	

this P
tor we
before
to a gr
wavelen
refinem
to the p
cell. T
intensit
tunately
had negl

In a
one serie
to monito
This fact
spectral c
wavelength
walls. To
had to hav
or to the
work has b
rections,
while quar
instrument
the use of
corrected

Much P

this problem partially, the beam splitter and second detector were placed after the wavelength isolation device, but before the sample cell (4-6). These systems were refined to a greater extent by correcting automatically for the wavelength dependence of the beam splitter (7,8), and further refinements led to the elimination of the beam splitter and to the placement of the second detector behind the sample cell. The fluorescence intensity was then ratioed to the intensity measured by this second detector (9,10). Unfortunately, this system could only be used with samples which had negligible absorbances.

In all of the systems described previously, there is one serious drawback. The second detector, which was used to monitor the source, had a non-linear spectral response. This fact precluded complete correction for the source spectral distribution, the transfer coefficient of the wavelength isolation device and any scattering at the cell walls. To correct for these variables, the source detector had to have a response which was proportional to the energy or to the number of quanta in the incident beam. Much work has been carried out in this area. For energy corrections, bolometers and thermopiles have been used (7,9,11), while quantum counters have been used in quantum-corrected instruments (8,12,13). Good results have been obtained by the use of these devices so that excitation and source-corrected fluorescence spectra are now routinely recorded.

Much progress has also been made in the elimination

of the emi
that almos
sion syste
devices wi
tum counte
fluorescen
are just n
choice is
linear res
of the dev
response.

success (1
advocated
tions for
At any rat
quite tedi

Quite
struct a s
corrective
plish thei
to collect
fluorescer
instrument
this date,
becoming c
quality fl

of the emission instrumental variables. It seems obvious that almost all of the instrumental variables in the emission system could be eliminated by the use of detection devices with linear responses such as a bolometer or a quantum counter. Unfortunately, due to the low levels of fluorescence intensities normally measured, such detectors are just not sensitive enough. The next most obvious choice is to compare a more sensitive device with a non-linear response, such as a photomultiplier tube, with one of the devices mentioned above or with a detector of known response. This has been done by several workers with good success (14,15). In addition, several other workers have advocated the use of a series of standard fluorophore solutions for the calibration of the emission detector (16,17). At any rate, most of the corrective procedures are either quite tedious or complicated.

Quite recently, extensive work was undertaken to construct a spectrofluorometer which incorporated all of the corrective measures mentioned previously (18). To accomplish their goal, Holland et al., utilized a minicomputer to collect, manipulate and correct both absorption and fluorescence data. The result was a fully automated and instrumentally corrected spectrophotofluorometer. As of this date, fully instrumentally corrected instruments are becoming commercially available and as a result, good quality fluorescence measurements, which are essentially

free from
routinely
about the

The ph
be divided
cludes bo
while the
tive indi
variables
is desira
tion.

Photo
in fluore
of the ph
system us
tensity i
fluoropho
selves as
in fluore
in mind,
been unde

The e
nature.
purificat
oxygenati
indices a

free from instrumental variables, can now be made routinely. On the other hand, the same cannot be said about the corrections for the photophysical variables.

The photophysical variables, as listed in Table I, may be divided into two subclasses. The intrinsic class includes both the primary and secondary absorption processes, while the extrinsic class includes the effects of refractive indices and scattering. Since these photophysical variables are not well understood by many researchers, it is desirable at this point to formulate a general definition.

Photophysical variables are those possible error sources in fluorescence measurements which result from the nature of the physical phenomenon observed or from the chemical system used. As a result, the measured fluorescence intensity is not proportional to the concentration of the fluorophore. These discrepancies usually manifest themselves as an apparent change in absorptivity or a change in fluorescence quantum efficiency. With this definition in mind, it is now desirable to examine the work which has been undertaken to eliminate these variables.

The extrinsic variables are usually of a controllable nature. Many times quenching can be controlled by careful purification of the solvent and reagents as well as deoxygenation. On the other hand, changes in refractive indices and scattering are not easily controlled. In

systems
scatter
ing can
measure
(19).
mathema
effects
if adequ
not the
and they
ments.

Intr
are some
observed
include t
attenuate
tion proc
cence fro
es will b
into two
occurs in
spectrum
spectrum.
called en
phores ar
cence whi

systems of suspended particles or macromolecules, Rayleigh scattering can be a considerable problem. Often scattering can be minimized by the use of filters or can be measured and manually subtracted as part of a background (19). In cases where refractive indices are a problem, mathematical corrections can be made (20,21). Thus, the effects of the extrinsic variables are usually not severe if adequate precautions are taken. Unfortunately, this is not the case with the intrinsic photophysical variables and they have consistently plagued fluorescence measurements.

Intrinsic variables or inner-filter effects, as they are sometimes called, are concerned with the nature of the observed phenomenon. In the case of fluorescence, these include the primary absorption processes, which act to attenuate the excitation beam, and the secondary absorption processes, which act to attenuate the emitted fluorescence from a fluorophore. The secondary absorption processes will be considered first. These processes can be divided into two categories. The first is self-absorption and it occurs in the spectral region where the fluorescence spectrum of a fluorophore overlaps its own absorption spectrum. The second category includes what might be called environmental-absorption and it occurs when chromophores and possibly other fluorophores absorb the fluorescence which is generated by the fluorophore of primary

concentr

fluores

attent

To dat

mathem

when se

more wo

The

measure

fluores

phore co

the case

cell, it

the abso

absorbinc

cence int

sity, mor

cell than

observed

phore con

than 0.06

gators (2

of workin

ever, thi

where the

concentra

concern. Both categories of processes lead to inaccurate fluorescence measurements and unfortunately, very little attention has been given to the elimination of their effects. To date, only one known attempt has been made to predict mathematically the expected fluorescence intensity measured when secondary absorption occurs (21). It is certain, that more work in this area will follow soon.

The other major intrinsic variable in fluorescence measurements is primary absorption. Intuitively, the fluorescence intensity should be proportional to the fluorophore concentration. Unfortunately, this is not always the case. As the excitation beam passes through the sample cell, its intensity is decreased exponentially because of the absorption by the fluorophore as well as any additional absorbing chromophores which are present. Since the fluorescence intensity is proportional to the excitation beam intensity, more fluorescence is generated in the front of the cell than in the back of the cell. As a result, the total observed fluorescence is not proportional to the fluorophore concentration in solutions with absorbances greater than 0.06. This effect has been noted by several investigators (22-24). To minimize it, the general recommendation of working with dilute solutions has been advocated. However, this is not a "universal" remedy. Consider the case where the fluorophore is initially present at a very low concentration level but the solution absorbance is high

due to
diluti
in a de
in con
sociati
the abs
large u
hand, f
error in
ments an
To circu
and Barn
Supposed
fluoresce
primary a
tion was
in the ca
Later, Pa
its applic
shore. L
mental ev
sult, man
tion fact
criteria
the resul
situation

due to the presence of other absorbing species. Continued dilution of such a system would not increase the accuracy in a determination. In addition, dilution may cause changes in conformation, bonding, solvation and the degree of association as well as other chemical events which may alter the absorption-fluorescence processes and thereby, introduce large unknown errors into the measurements. On the other hand, failure to dilute such a system will introduce serious error into the determination if the fluorescence measurements are not corrected for the primary absorption processes. To circumvent problems such as the one described, Parker and Barnes (25) proposed the use of a correction factor. Supposedly, when this factor was applied to the measured fluorescence, the fluorescence was then corrected for the primary absorption processes. Unfortunately, no derivation was presented and the correction factor was used only in the case of a chromophore and a fluorophore mixture. Later, Parker and Rees (26) extended its use by advocating its application to systems which contained only pure fluorophore. Like the first publication, no supportive experimental evidence was given for this extension. As a result, many investigators are reluctant to use a correction factor which has no apparent theoretical basis, no criteria for its proper application and no evaluation of the resultant corrections. In an effort to rectify this situation, several investigators have turned their

attention
fects on
geometric
partially
same resu
the deriv
a good at
the corre

Only
out by Ho
for the p
rection f
attempt h
intensiti
absorptio

The p
how the w
all of th
correctio
dition, t
plementat
cence mea
of this s
absorptio
been eval
capabilit

attention to the problem. Ohnesorge (27) examined the effects on fluorescence measurements with changes in the geometric model presented by Parker and Barnes. Gill (28) partially derived a correction factor which gives the same results as the Parker and Barnes factor. Although the derivation was not quite satisfactory, Gill did make a good attempt at elucidating the theoretical basis of the correction factor.

Only recently has the theoretical basis been worked out by Holland and others (29). In addition, the criteria for the proper application of the Parker and Barnes correction factor have been partially defined and an initial attempt has been made to correct measured fluorescence intensities automatically for the effects of the primary absorption processes.

The purpose of Part I of this thesis is to report on how the work of Holland et al. has been extended so that all of the criteria for the proper application of the correction factor have now been clearly defined. In addition, this report describes the procedures for the implementation of automated absorption-corrected fluorescence measurements which have been developed in the course of this study. Furthermore, the accuracy of the resultant absorption-corrected fluorescence measurements have also been evaluated with respect to the present instrumental capabilities and the availability of ideal chemical systems.

To date
cal basis
Barnes. I
tions nece
delineated
from its ap

Quite r
tion. Holl
correction
Their deriv
structed ar
The details
detailed de

The dev
configurati
Observation
the excitat
scattering f
Barnes confi
placed as cl
order that a
generated wi
the basic ge
next step wa

II. THEORETICAL

To date, very little has been known about the theoretical basis of the correction factor presented by Parker and Barnes. In addition, the chemical and experimental conditions necessary for its application have never been fully delineated, and the accuracy of the resultant corrections from its application never determined.

Quite recently, work was begun to remedy this situation. Holland, Teets and Timnick were able to derive a correction factor identical to the Parker and Barnes factor. Their derivation was based on a theoretical model constructed around certain chemical and experimental restraints. The details of their work are summarized below but a more detailed development may be found elsewhere (29).

The development of the model began with a geometrical configuration similar to the one chosen by Parker and Barnes. Observation of the fluorescence was to be made at 90° to the excitation beam and a mask was to be used to minimize scattering from the cell walls. Unlike the Parker and Barnes configuration, the edges of the mask were to be placed as close to the edges of the cell as possible in order that a maximum amount of the fluorescence would be generated within the window defined by this mask. Thus, the basic geometry of the system was established and the next step was to define the instrumental and chemical

restraints

Upon con
tions or re
include the

(1) The
int
tie
and
int
qua

(2) The
the

(3) The
the
the
the

restraints of the model.

Upon consideration of the problem, seven basic assumptions or requirements were enumerated or implied and they include the following:

- (1) The incident intensity, I_0 , and the transmitted intensity, I , represented by the measured quantities R (reference) and S (sample), respectively and the measured quantity, F , the fluorescence intensity, are proportional to the number of quanta, Q , involved.

$$R = kQ_r$$

$$S = kQ_s$$

$$F = k'Q_f$$

- (2) The absorption processes within the cell follow the Beer-Lambert Law.

$$I = I_0 e^{-abc}$$

- (3) The quanta fluoresced by the fluorophore within the observation window are linearly related to the quanta absorbed by that same species within the same window.

$$F_{\text{window}} = k''\phi(\Delta I)_{\text{window}}$$

(4) The
due
of
pho

(5) A f
gen
by

(6) Onl
is
cen

(7) The
dic
to

The last ste
was the deri
were used an
the sake of

Based on
tensity of th
length, w, f

- (4) The fraction of the total absorbance which is due to the fluorophore is equal to the fraction of the total quanta absorbed by that fluorophore.

$$\frac{A_f}{A_t} = \frac{Q_f}{Q_t}$$

- (5) A fixed fraction of the fluoresced radiation generated within the observation window is viewed by a detector with uniform sensitivity.

$$F_{\text{measured}} = k''' F_{\text{window}}$$

- (6) Only the fluorescence of a single fluorophore is measured and any absorption of this fluorescence is negligible.
- (7) The effects of scattered light, refractive indices and anisotropic characteristics are assumed to be negligible.

The last step in the development of the theoretical model was the derivation of a correction factor. Two approaches were used and both arrived at the same relationship. For the sake of brevity, only one of these will be outlined.

Based on assumptions 1 and 2, it was shown that the intensity of the excitation beam at any fraction of the cell length, w , from the point of entry could be calculated

from the fol

where I_w is

is the inten

T is the tra

expression f

where K is a

the absorban

of one or mo

citation bea

positioned a

combination

described th

quantities,

At this

was defined

average inte

vation windo

from the following equation,

$$I_w = R \exp(w \ln T) = RT^w \quad (1)$$

where I_w is the intensity at a fractional distance w , R is the intensity of the excitation beam before entry and T is the transmittance. From assumptions 3 and 4, the expression for the measured fluorescence was obtained,

$$F = K \frac{A_f}{A_f + A_c} (I_{w_1} - I_{w_2}) \quad (2)$$

where K is an instrumental and geometric factor, A_f is the absorbance of the fluorophore, A_c is the absorbance of one or more chromophores, and I_{w_1} and I_{w_2} are the excitation beam intensities at the mask edges which are positioned at the fractional distances of w_1 and w_2 . The combination of equations 1 and 2, yielded an equation which described the measured fluorescence in terms of measurable quantities,

$$F = 2.303 \frac{KA_f R}{\ln T} (T^{w_2} - T^{w_1}) \quad (3)$$

At this point, the absorption-corrected fluorescence was defined as the measured fluorescence divided by the average intensity of the excitation beam across the observation window from w_1 to w_2 . This definition is quite

logical since
of fluoresce
tion of the
for this gen

By substitut
ing the inte

The absorpt

This reduce

where the r

Note th

with the co

(25),

logical since absorption-corrected fluorescence is the amount of fluorescence that would have been measured if no absorption of the excitation beam had taken place. The expression for this general definition was written as,

$$F_{CO} = \frac{F}{\int_{w_1}^{w_2} \frac{I_w dw}{w_2 - w_1}} \quad (4)$$

By substituting Equation 1 into the denominator and performing the integration, the general definition yielded,

$$F_{CO} = \frac{F}{R} \frac{\ln T(w_2 - w_1)}{T^{w_2} - T^{w_1}} \quad (5)$$

The absorption correction factor, f_a , was defined as

$$f_a = \frac{\ln T(w_2 - w_1)}{T^{w_2} - T^{w_1}} \quad (6)$$

This reduced Equation 5 to the following expression,

$$F_{CO} = \frac{F}{R} \times f_a \quad (7)$$

where the ratio, $\frac{F}{R}$, is the source-corrected fluorescence.

Note that Equation 6 is identical, except in form, with the correction factor presented by Parker and Barnes (25),

where A is t
x₁ and x₂ ar
meters from
Holland, Tee
derivation f
have also en
met in order
gone one ste
substituting
was obtained

This express
escence is p
if Beer's la
geometry is
pression can

$$F_{co} =$$

where a is t
pathlength o
fluorophore.

$$f_a = \frac{2.303 A (x_1 - x_2)}{10^{-Ax_1} - 10^{-Ax_2}}$$

where A is the absorbance per centimeter pathlength and x_1 and x_2 are the distances of the mask edges in centimeters from the entry point of the cell. Consequently, Holland, Teets and Timnick have presented a theoretical derivation for the Parker and Barnes correction factor and have also enumerated the basic requirements which must be met in order for it to be valid. In addition, they have gone one step further. By solving Equation 3 for KA_f and substituting into Equation 5, the following relationship was obtained,

$$F_{CO} = 2.303 K A_f (w_2 - w_1) \quad (8)$$

This expression shows that the absorption-corrected fluorescence is proportional to the fluorophore concentration if Beer's law is followed and the observation and detection geometry is kept constant. Consequently, the overall expression can be written as,

$$F_{CO} = \frac{F}{R} \times \frac{\ln T (w_2 - w_1)}{T^{w_2} - T^{w_1}} = 2.303 K (w_2 - w_1) abc_f$$

where a is the absorptivity of the fluorophore, b is the pathlength of the cell and c_f is the concentration of the fluorophore.

Since th
only remaini
an optical g
quirements o
corrections
constructed,
which met th
corrections
chosen for t
previously b
liminary tes
and chromoph
absorption o
observation
fluorophore
that a gener
tests showed
tion-correct
absorbances
ment was cor
Consequently
the construc
for the foll

(1) To
the

Since the theoretical model had been developed, the only remaining task was to construct a fluorometer with an optical geometry which met all of the instrumental requirements of the model and in addition, could make the corrections automatically. Once this fluorometer had been constructed, tests could then be made with chemical systems which met the remaining requirements. The accuracy of the corrections could then be determined. The fluorometer chosen for these tests was one which was similar to that previously built by Holland, Teets and Timnick (18). Preliminary tests by these workers with various fluorophores and chromophores indicated that the effects of primary absorption on measured fluorescence was dependent on the observation window size and independent of wavelength and fluorophore which was used. Consequently, they showed that a general correction scheme was possible. Further tests showed that they were able to make automated absorption-corrected fluorescence measurements on solutions with absorbances up to 1.3. Unfortunately, when a second instrument was constructed, the same results could not be achieved. Consequently, this study, which was partially involved with the construction of this second instrument, was undertaken for the following purposes:

- (1) To re-evaluate the basic assumptions in the theoretical model.

- (2) To
si
- (3) To
co
- (4) To
re

EVALUATION

Upon in
sumptions,
the theore
category,
the first
tics of th
gory inclu
the instr

Since
study wer
theoretic
sumptions
are valid
ing assum
contained
which can
in the li
all of the

- (2) To make any instrumental modifications necessitated by this re-evaluation.
- (3) To clearly define the method by which absorption-corrected fluorescence measurements are made.
- (4) To evaluate the accuracy of the resultant corrected measurements.

EVALUATION OF THE BASIC ASSUMPTIONS

Upon inspection, it becomes obvious that the basic assumptions, which formed the basis for the development of the theoretical model, fall into two categories. The first category, which embodies all of the assumptions except for the first and the fifth, is concerned with the characteristics of the chemical systems involved. The second category includes the two remaining assumptions and deals with the instrumental aspects of the measurements.

Since the chemical systems for this and the previous study were carefully chosen to meet the criteria of the theoretical model, it must be assumed that all of the assumptions in the first category, except for number four, are valid. On the other hand, the validity of this remaining assumption was rigorously proved and the details are contained in Appendix one. In addition, another approach, which can lead to the same result, has recently appeared in the literature (30). In any case, it is certain that all of the assumptions in the first category are valid if

the correct

Consider

clusion that

warranted by

in this stud

does indeed

tional to th

only the val

Most certain

misundersto

its require

assumption

implementat

ments. Sin

optical sys

ments will

chapter, wh

optical sys

the correct chemical systems are utilized.

Consideration of the second category leads to the conclusion that assumption one is valid. This conclusion is warranted by the fact that the instrument, which was used in this study and described in the Instrumental chapter, does indeed, make intensity measurements which are proportional to the number of quanta involved. At this point, only the validity of assumption five remains questionable. Most certainly, it is the most complex and the most easily misunderstood of all of the assumptions. In addition, its requirements are difficult to fulfill and consequently, assumption five presents the largest impediment to the implementation of absorption-corrected fluorescence measurements. Since this assumption deals with the emission optical system of the spectrophotofluorometer, its requirements will be delineated and evaluated in the Experimental chapter, which deals in part with the construction of the optical system.

OPTICAL

Figure
photofluorom
of this stud
Holland et al
data acquis
is either an
a Hanovia 2
Powerpacs M
put is coll
the slits o
This monoch
in conjunc
1180 lines
the monoch
Beckman Vi
which is 1
splits the
tum counte
of rhodam
5 mm quar
selected
by a McPh

III. INSTRUMENTAL

OPTICAL

Figure 1 presents the optical diagram for the spectrofluorometer which was constructed during the course of this study. It is similar to the one constructed by Holland et al. (18) and likewise, uses a minicomputer for data acquisition, manipulation and correction. The source is either an Illumination Industries 150 watt Xenon arc or a Hanovia 200 watt Xenon-Mercury arc powered by an Electro Powerpacs Model 352 variable power supply. The source output is collimated by a quartz lens and is passed through the slits of a GCA McPherson Model EU-700 Monochromator. This monochromator utilizes a Czerny-Turner configuration in conjunction with a 48 x 48 mm grating which is ruled at 1180 lines per mm and is blazed for 2500 Å. After leaving the monochromator, the excitation beam is directed to a Beckman Vibrating Bridge Assembly (parts #571868 and B-28128) which is located in the sample compartment. This assembly splits the excitation beam in time and directs it to a quantum counter. The quantum counter consists of a solution of rhodamine B in ethylene glycol which is contained in a 5 mm quartz cell, a 6100 Å sharp cut-off filter, and a selected RCA 1P28A photomultiplier tube which is powered by a McPherson EU-42A high voltage supply. The useful

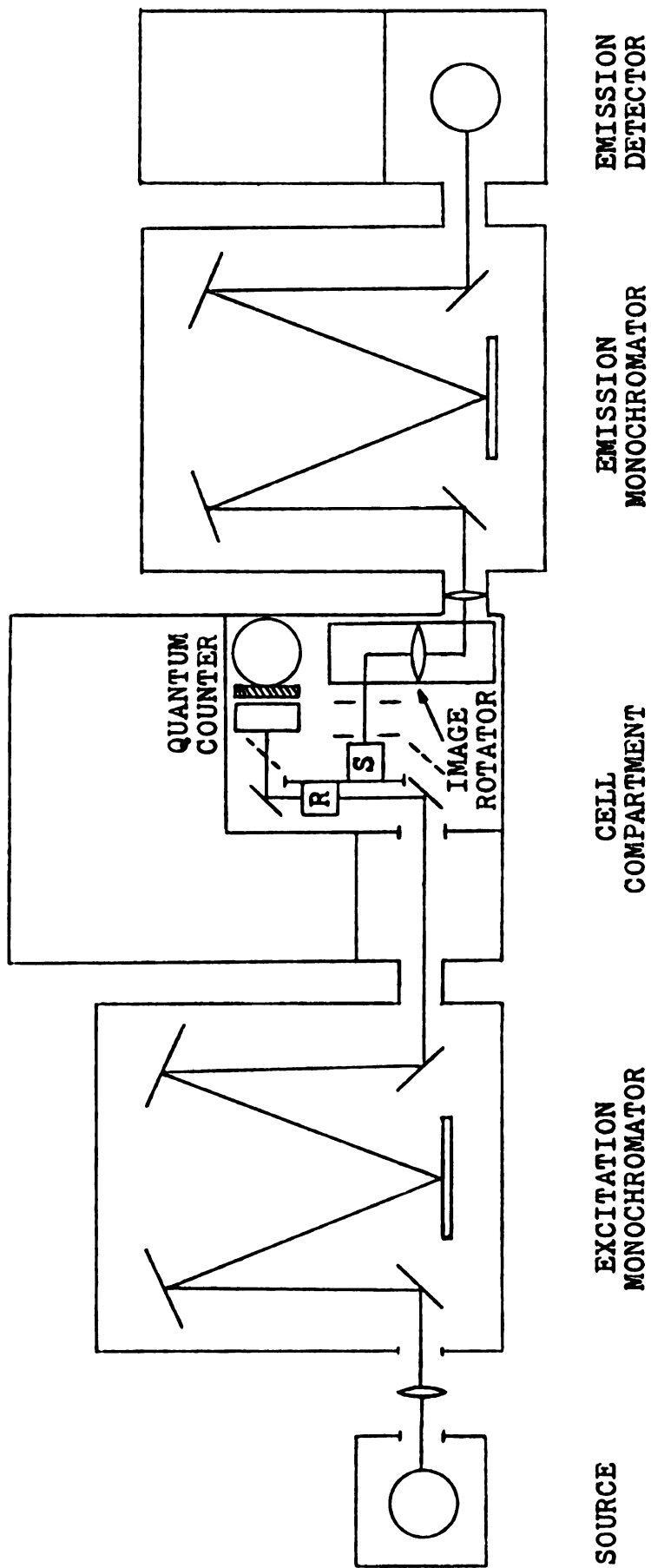


Figure 1. Optical Diagram for the Computer-Centered Spectrophotofluorometer.

spectral r

Å.

The fl
sample cel
a device c
rotates th
perpendicu
at the sli
lens is t
monochroma
the fluore
Ga-As phot
high volta

ELECTRICAL

The sc
drives the
Figure 2.
electric c
assembly.
any bridge
through an
configurat
of a power
ing the 10
switched b

spectral range of the quantum counter is from 2500 to 6000 Å.

The fluorescence radiation which is generated in the sample cell is gathered at 90° to the excitation beam by a device called an image rotator. This optical system rotates the fluorescence image 90° in the plane which is perpendicular to the optical axis and presents a 1:1 image at the slit of another McPherson monochromator. A field lens is then used to match the image size to the emission monochromator optics. Upon emergence from the monochromator, the fluorescence is then detected by a Hamamatsu Model R666 Ga-As photomultiplier tube which is powered by another McPherson high voltage power supply.

ELECTRICAL

The schematic diagram of the oscillator circuit, which drives the Beckman Vibrating Bridge Assembly, is shown in Figure 2. The circuit utilizes only one of the two opto-electric chopping devices which are a part of the bridge assembly. This opto-electric chopper is used to convert any bridge motion into an ac signal which is then passed through an operational amplifier which is used in a follower configuration. The signal is then ac coupled to the base of a power transistor which is biased above ground by adjusting the 10 kΩ potentiometer. As the power transistor is switched by the movement of the bridge assembly, current is

+115V

+15V

+15V

+115V



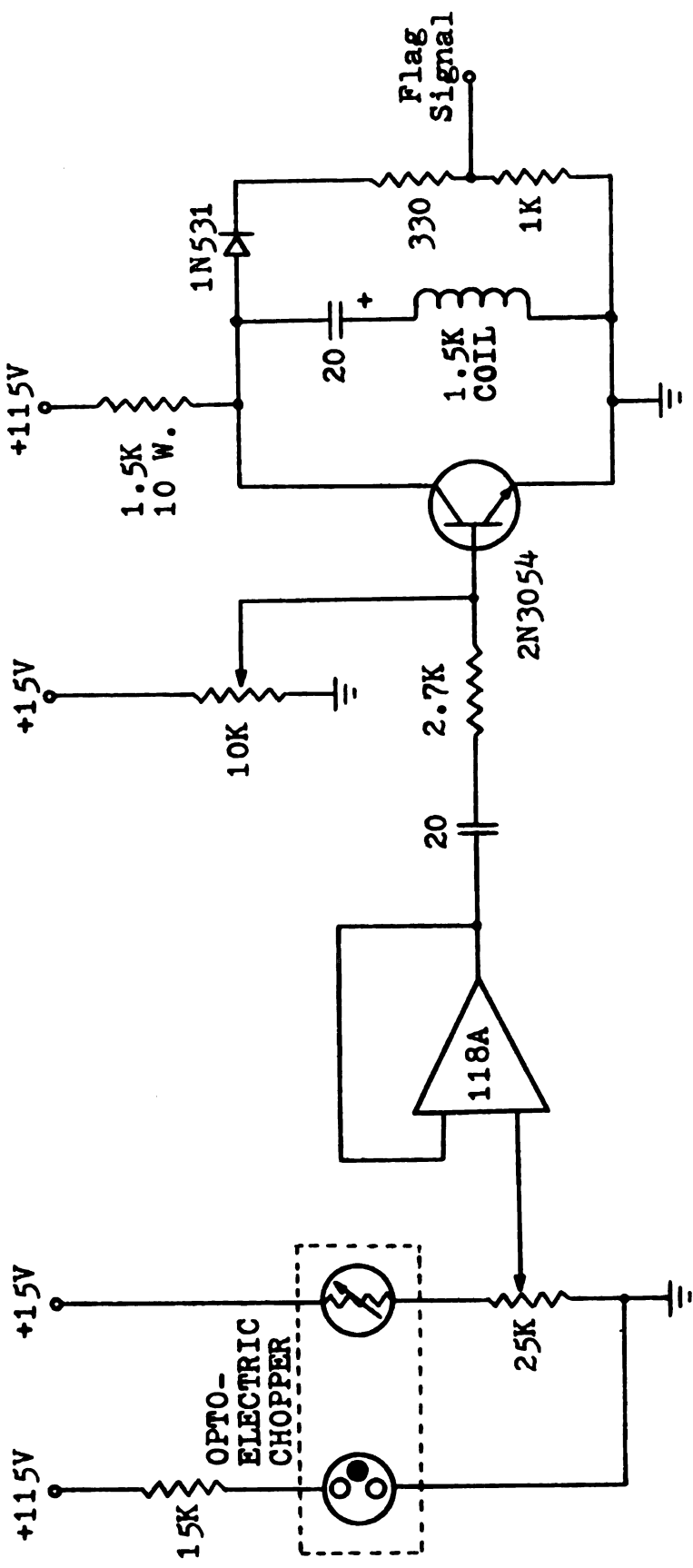


Figure 2. Circuit for the Vibrating Bridge Oscillator.

alternately
the bridge
is set up a
amplitude o
frequency,
at the ampl

Power f
made 115V c
powered by
used in a m

In add:
Assembly, t
plies a sid
with respect
nal is used
ure 3. The
the excita
data acqui
similar se
each set i
to positio
when the e
reference
set determ
to adjust
by the use
of the dat

alternately supplied to the electromagnet which controls the bridge movement. Consequently, a feedback situation is set up and the bridge will continue to oscillate. The amplitude of the bridge oscillation and consequently, the frequency, is controlled by the 10 turn 25 k Ω potentiometer at the amplifier input.

Power for the oscillator circuit is supplied by a home-made 115V dc supply while the operational amplifier is powered by a Deltron Model OS-15 bipolar 15V power supply used in a master-slave series tracking mode.

In addition to driving the Beckman Vibrating Bridge Assembly, the oscillator circuit described above also supplies a signal which indicates the position of the bridge with respect to the sample and reference cells. This signal is used by the flagging circuit which is shown in Figure 3. This circuit is used to notify the minicomputer of the excitation beam position and in addition, it also triggers data acquisition. The flagging circuit consists of two similar sets of monostables. The first monostable in each set is used as a delay and this delay time is adjusted to position the data flag for each channel to the time when the excitation beam is in the center of either the reference or the sample cell. The second monostable in each set determines the duration of each data flag and is used to adjust visually the delay times of the first monostables by the use of an oscilloscope. The negative going edges of the data flags initiate data acquisition by the



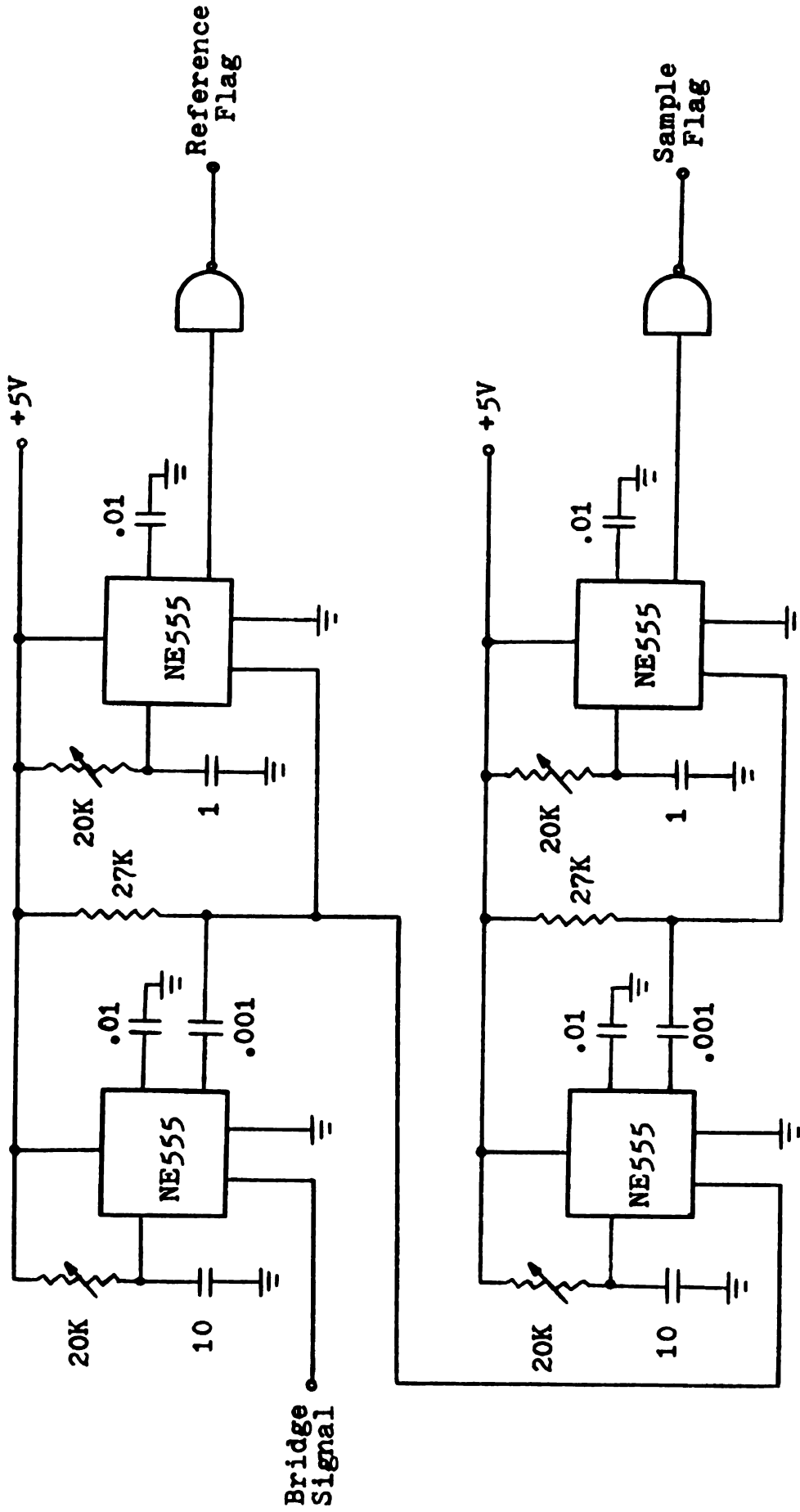


Figure 3. Flag Circuit for Computer Recognition of the Vibrating Bridge Mirror Position.

minicomputer

The amplifier

and fluorescent

one of the

The first stage

FET input of

stage configuration

Devices Model

with gain of

Model 118A

conjunction

stage is of

analog-to-digital

channel has

nanoampere.

ampere and

COMPUTER

The computer

throughout

Corporation

space of 8

with the

was loaded

TU56 DECT

converter

minicomputer.

The amplification system for both the reference-sample and fluorescence data channels is shown in Figure 4. Only one of the channels is shown since they are both identical. The first stage consists of an Analog Devices Model 142B FET input operational amplifier used in a current to voltage configuration. The second stage consists of an Analog Devices Model 183J operational amplifier used as an inverter with gain while the third stage utilizes an Analog Devices Model 118A operational amplifier as a follower with gain in conjunction with a low pass filter. The input to the third stage is offset so that the input limits of the computer analog-to-digital converter can be fully utilized. Each channel has a variable gain from zero to about one volt per nanoampere. The maximum sensitivity is about one picoampere and is limited by the stability of the offset.

COMPUTER

The computer utilized in conjunction with the fluorometer throughout the course of this study was a Digital Equipment Corporation (DEC) LAB 8/e minicomputer with a minimum core space of 8K. The following LAB 8/e peripherals were used with the spectrofluorometer. The fluorometer program FLUORO was loaded into the computer through the use of a DEC Model TU56 DEctape transport. A DEC Model AD8-EA analog-to-digital converter (ADC) was used for data acquisition. This ADC

.009

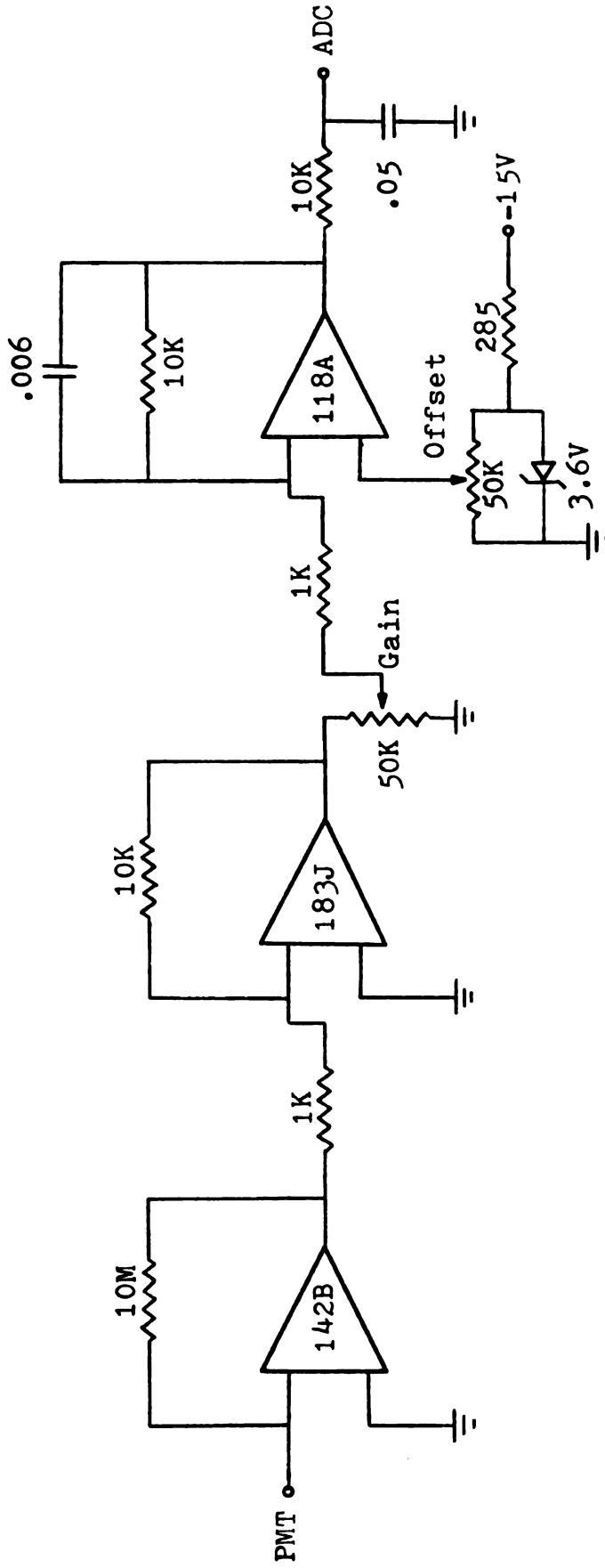


Figure 4. Electronic Circuit for Photomultiplier Signal Amplification.

is a 10 bit
a DEC Model
and the con
used for th
for the flu
sists of a
with a Hewl
display is
output rang
Model DR8-E
various ope
for the ref
negative gd
initiate da
used for th
pen drop co
DEC Buffer
they could

INSTRUMENT

Severa
which was
type built
the abilit
as the sou
especially

is a 10 bit successive approximation converter equipped with a DEC Model AM8-EA multiplexer. The input range is $\pm 1V$ and the conversion rate is 50 KHz maximum. Channel 0 was used for the reference-sample signals and channel 1 was used for the fluorescence. The fluorometer output display consists of a DEC Model VC8-E display control in conjunction with a Hewlett-Packard Model 7044A X-Y recorder. The DEC display is a two axis digital-to-analog converter with an output range of $\pm 5.12V$ and a resolution of 10 mV. The DEC Model DR8-EA 12 channel digital I/O buffer was used for various operations. Input channels 10 and 11 were used for the reference and sample data flags, respectively. A negative going transition for either of these flags can initiate data acquisition. Output channels 11 and 0 were used for the monochromator wavelength drive and the recorder pen drop control, respectively. The pin assignments for the DEC Buffered Digital I/O are given in Appendix Two since they could not be found in the DEC literature.

INSTRUMENTAL IMPROVEMENTS

Several improvements have been made in the instrument which was used in this study, when compared to the prototype built by Holland et al. (18). The first of these is the ability to use a xenon, mercury or a xenon-mercury lamp as the source. This improvement is a significant advantage especially when sensitivity is needed in a fluorometric

determinat
a mercury
the speed
in the new
length dri
computer s
speed whil
has the ad
acquisitio
tion, data
by deactiv
the most i
multiplier
Since the
up to abou
system eff
are much e
tube has e
the fluoro
system hav
of a methy
of the cor
from that
a reflecto
been used
from 2500

determination when the analyte absorbs in the region near a mercury line. The second improvement is concerned with the speed of data acquisition. Since the monochromators in the new instrument utilize stepping motors in the wavelength drive circuits, it is quite convenient to have the computer step the monochromators at their maximum scanning speed while pausing only for data acquisition. This process has the advantage of nearly zero dead time as well as data acquisition while the monochromators are stopped. In addition, data at one wavelength may be taken and averaged merely by deactivating the wavelength drives. The last and perhaps the most important improvement is the use of a Ga-As photomultiplier tube in place of a 1P28 for the emission detector. Since the spectral response of these types of tubes is good up to about 9000 Å, corrections for the emission optical system efficiency and the photomultiplier spectral response are much easier to make. In addition, the use of the Ga-As tube has extended the emission wavelength capabilities of the fluorometer, and corrections for the emission detection system have now been extended up to 7000 Å through the use of a methylene blue quantum counter (31). The construction of the computer correction table has been somewhat modified from that used by Holland. Instead of using smoked MgO as a reflector, Kodak's White Reflectance Standard (32) has been used with excellent results. The correction table from 2500 to 6000 Å was obtained by scanning the

monochromators in tandem with the reflectance plate in the sample cell position. Five scans of this wavelength region were run, and the correction factors were output on paper tape via the teletype. Next, the rhodamine B quantum counter was replaced with a methylene blue counter and five more scans were made from 5500 to 7000 Å. The correction factors for this wavelength range were also output on paper tape. The paper tapes for each quantum counter were then input into a FORTRAN program named PMT where each set of correction factors was averaged and scaled. Mergence of the two resulting correction tables in the region between 5500 and 6000 Å, yielded the final overall correction table which resides as part of the fluorescence program. Besides extending the photomultiplier correction table to 7000 Å, the foregoing procedure eliminated much of the noise encountered by Holland in the region around 4600 Å, where xenon has some strong emission lines. Details on the use of program PMT and directions for implementing the photomultiplier correction table are contained in Appendix Three.

INSTRUMENTAL ACCURACY AND PRECISION

The accuracy and precision of the instrument used in this study is nearly the same as that which was quoted for the prototype instrument (18). The optical resolution is better than 2 Å for high resolution work and tests with a didymium filter showed better resolution than many



commercially available instruments. On the other hand, the instrumental sensitivity is low due to the slow optical speeds of the excitation and emission monochromators.

The photometric accuracy of the spectrophotometer was found to be $\pm 0.1\%$ transmittance over the range from 1 to 100% T and it seems to be limited by the accuracy of the ADC. In terms of absorbance, this error in transmittance leads to an accuracy of ± 0.001 at an absorbance of 0.10 and ± 0.04 at an absorbance of 2.0. Due to the stray light characteristics of the monochromators used in this instrument, filters may have to be used above an absorbance of 1.6 in order to maintain photometric accuracy. In addition, when fluorophore solution absorbances are near zero or close to 2.0, fluorescence emitted along the optical path of the excitation beam can sometimes present a serious problem although these effects on the photometric accuracy can be eliminated through the use of cut-off filters.

Tests of this instrument as a fluorometer indicate a relative standard deviation of less than $\pm 1\%$ can be obtained routinely for the measurement of fluorescence. The error in the emission detection system correction table relative to the quantum counters used in this instrument is about $\pm 1\%$ in the wavelength region from 2500 to 6800 Å. The precision in quantum efficiency measurements is better than $\pm 1\%$ and the accuracy over a two order of magnitude concentration range of quinine sulfate has been found to be about $\pm 5\%$. This last figure is also probably a good estimate

of the fluorometric accuracy of the instrument although this specification is difficult to determine. Tests have also shown that absorption-corrected fluorescence measurements are accurate to $\pm 3\%$ up to a solution absorbance of 2.0.



v
v
o
E
o
i
t
d

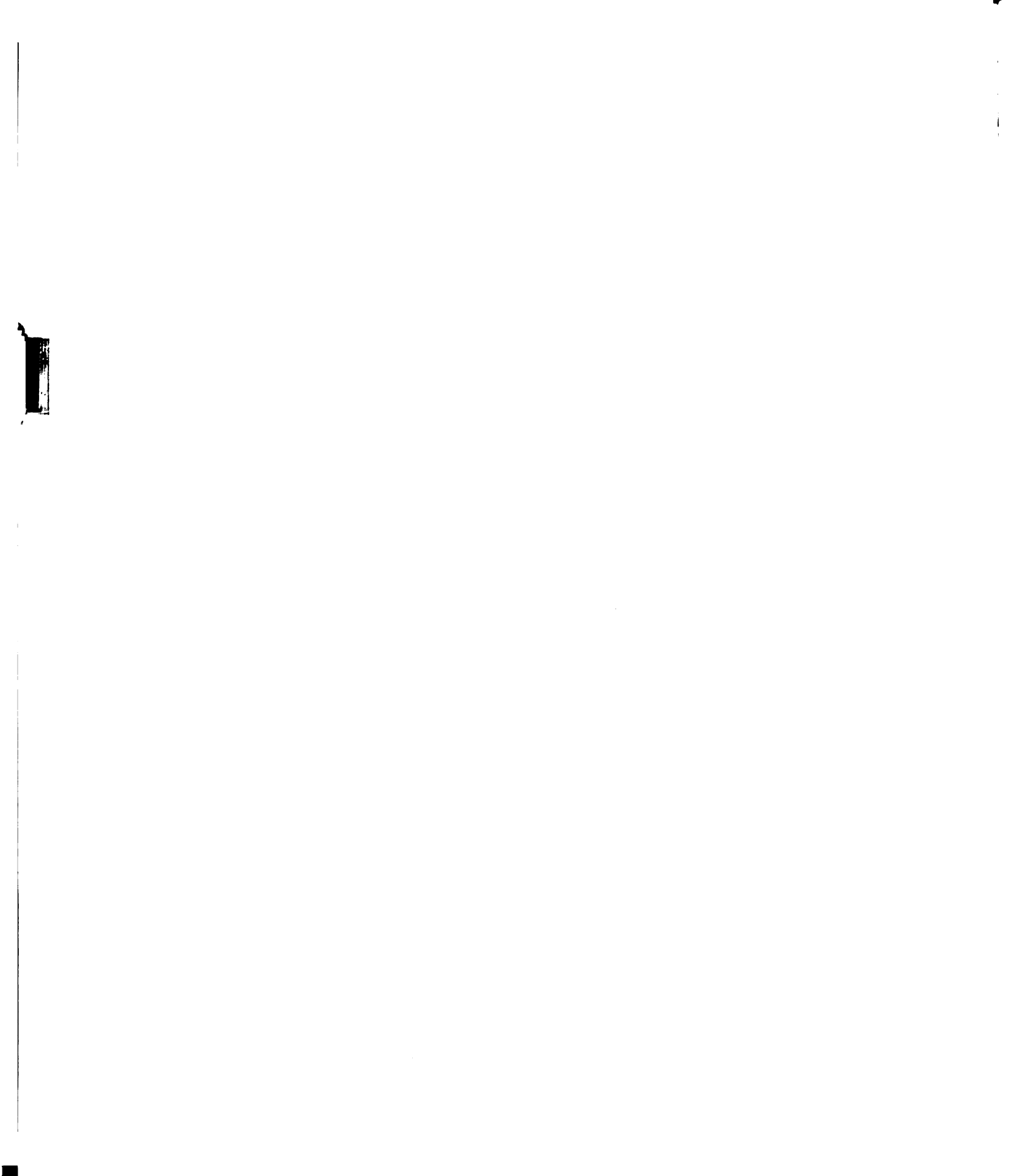
IV. EXPERIMENTAL

As noted in the theoretical chapter of this thesis, the fifth assumption for the theoretical model, which was developed for absorption-corrected fluorescence measurements, is concerned with the emission detection system and it embodies some of the most stringent requirements. In addition, the fulfillment of these requirements is of utmost importance if absorption-corrected measurements are to be made accurately. Therefore, each requirement of assumption five was carefully delineated, and the emission detection system constructed in such a way that this assumption was valid for the spectrophotofluorometer used in this study. Once this goal had been achieved, a correction scheme was developed and the accuracy of the resultant corrections determined.

EMISSION OPTICAL SYSTEM

Briefly stated, the model assumes that a fixed fraction of the fluorescence generated within the observation window is viewed by a detector with uniform sensitivity. In relation to the emission optical system, this assumption breaks down into the four following requirements:

- (1) The excitation beam must be homogeneous.
- (2) The fluorescence generated in a horizontal slice



within the observation window must reach the detector.

- (3) The observation angles for all point sources along that slice must be equal.
- (4) The detector must have a uniform sensitivity over its sensing area which is normally illuminated by the fluorescence.

The first requirement is satisfied if the excitation beam is well collimated. Since Beer's law also has this requirement, the excitation system of the fluorometer used in this study was constructed so that this requirement was met. The second requirement of the model involved a modification of the optical systems normally found in fluorometers. Since the slit height of the emission monochromator was larger than the horizontal dimension of the fluorescence observation window, either of two courses of action could have been followed. The first involves the 90° rotation of the monochromator so that its slits are in a horizontal position while the second involves the 90° rotation of the cell fluorescence image through the use of a dove prism or a set of front surface mirrors. Based on the inconvenience of monochromator rotation and the high cost of a quartz dove prism, front surface mirrors were used in this study. Furthermore, the utilization of mirrors allowed the use of conventional optical configurations. The configuration, which was chosen for this study and



c
f
d
m
c
r
r
a
s
i
o
t
w
t
t
Th
ca
re
Cu
ce
cul

is shown in Figure 5, consisted of a focusing lens positioned to give a 1:1 image ratio at the entrance slit and a field lens which was compatible with the optical speed of the emission monochromator. Note that with this optical system, the mask edges at x_1 and x_2 in conjunction with the monochromator slit width define a horizontal slice within the fluorescence observation window which is viewed by the detector. Consequently, the second requirement has been met.

The fulfillment of the third requirement, which is concerned with the observation angles, can never be totally realized; only closely approached. To help meet this requirement, a second mask with the same window dimensions as the primary mask was placed at a distance, d , from the source of fluorescence as shown in Figure 6. Preliminary investigation showed that for a constant distance, d , the observation angles ranged from a maximum at the center of the cell to a minimum at either edge of the observation window. Consequently, these two limiting angles, θ and ϕ , respectively, were used as a measure of uniformity in the observation angles across the fluorescence window. Their differences for various secondary mask distances were calculated and expressed as relative percent error. The results of these calculations are presented in Figure 7A. Curve B shows the variation in the observation angle at cell center, θ , with d . Points for these curves were calculated for a window width of 0.80 cm.

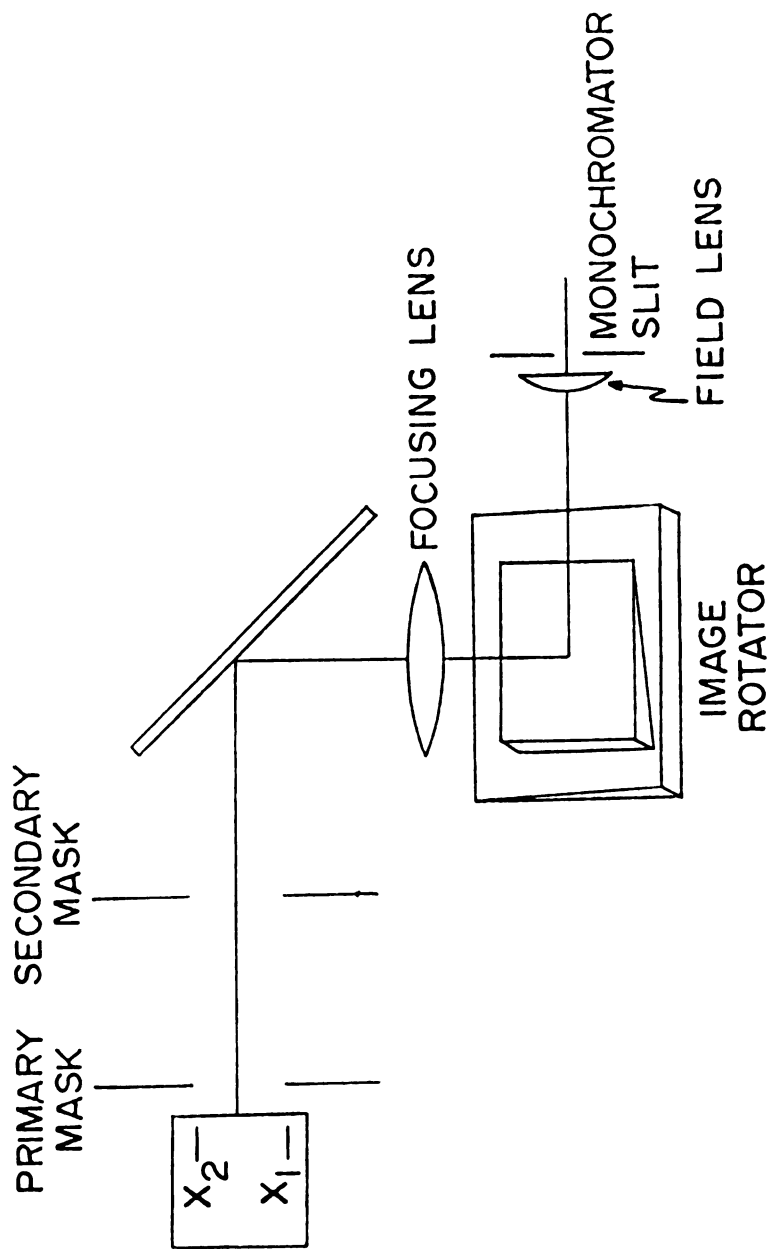
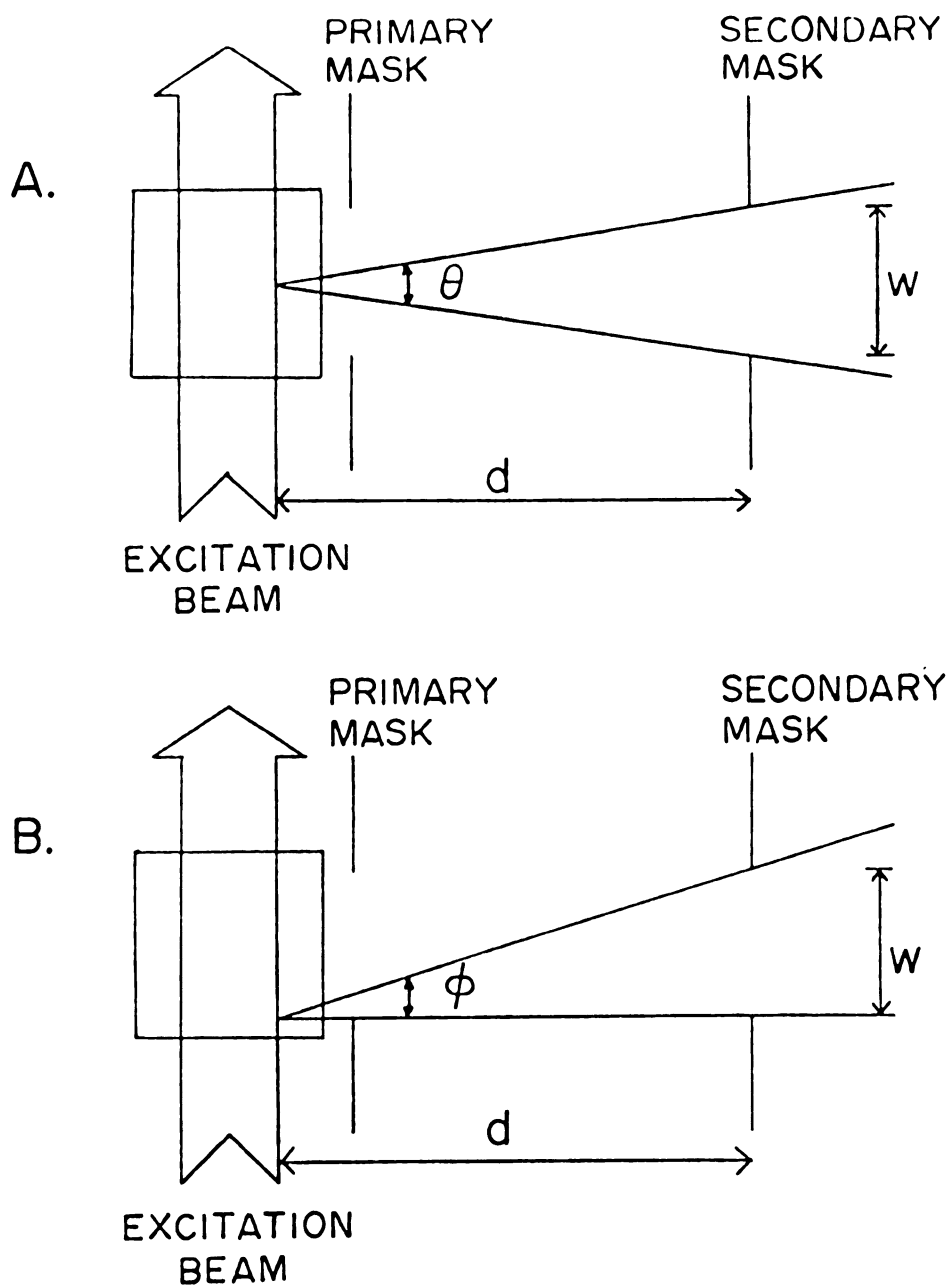


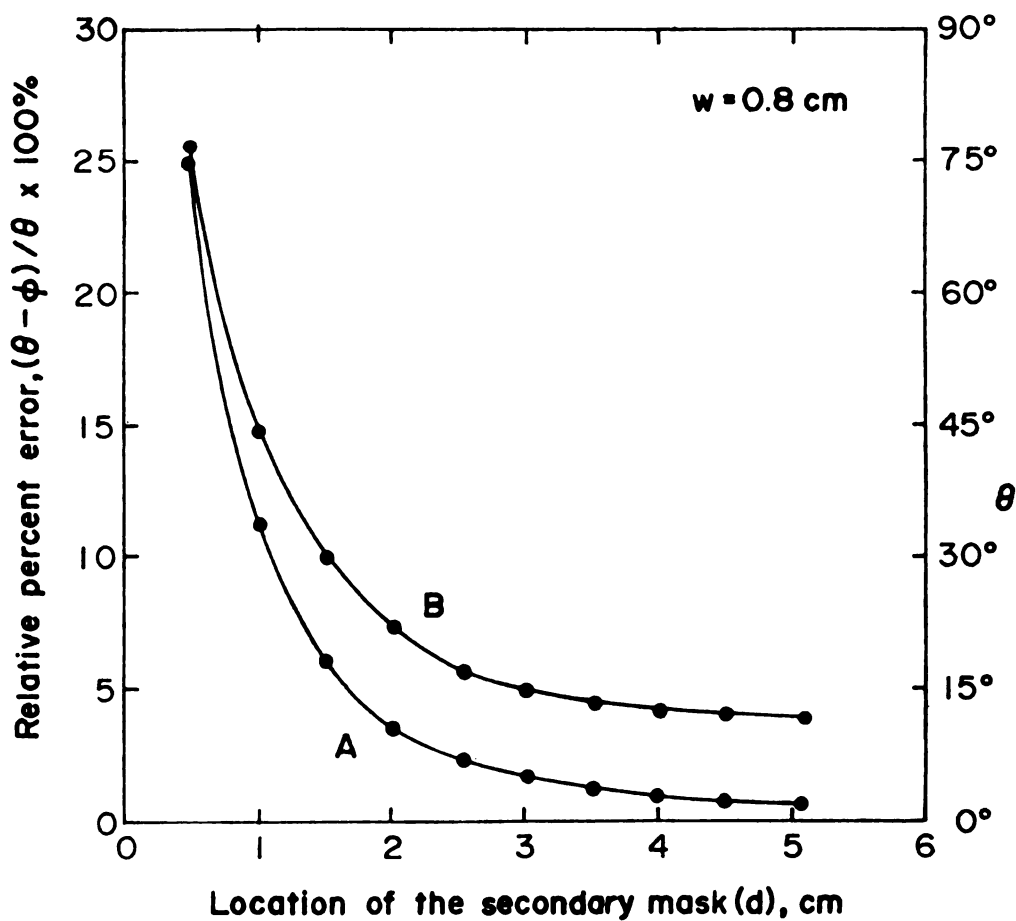
Figure 5. Geometric and Optical Configuration for the Collection of Fluorescence.



A. Maximum Observation Angle

B. Minimum Observation Angle

Figure 6. Limiting Conditions for the Fluorescence Observation Angles for Point Sources Across the Sample Cell.



A. Relative Percent Error in the Observation Angles

B. Observation Angle at Cell Center

Figure 7. Variation of Optical Parameters as a Function of Secondary Mask Distance from the Source of Fluorescence.

th
id
ra
tu
ta
ef
ch
th
pe
th
de
of
rec
was
ser
wit
vic
mea
and
dat
tra
con
uni
fluc
has

Note that as the error between θ and ϕ approaches zero, the observation angles go to zero. In other words, the ideal situation would involve the collection of only the radiation which is parallel to the optical axis. Unfortunately, this would require a large secondary mask distance and would drastically reduce the radiation collection efficiency. Consequently, a mask distance of 4.0 cm was chosen as a compromise. At this distance, the error in the observation angles across the window is less than one percent while the angles are still large enough to permit the passage of a reasonable amount of fluorescence to the detector.

The last requirement is concerned with the uniformity of the detector sensitivity. The fulfillment of this requirement by the photomultiplier tube used in this study was tested in the following way. The fluorescence from a series of quinine sulfate solutions was measured with and without a diffuser in front of the photomultiplier. Obviously, the fluorescence intensities of these two sets of measurements were not the same because of the absorption and scatter introduced by the frosted quartz but when the data were normalized, the shapes of the fluorescence-concentration curves were identical. From this result, it was concluded that the sensitivity of the photomultiplier was uniform throughout the cathode area normally illuminated by fluorescence radiation. Consequently, the last requirement has been met and the model developed for absorption-corrected

f

A

co

ha

ti

0.

th

bi

fo

fo

be

is

The

ti

a s

tic

for

of

aci

over

fluorescence measurements could then be tested.

ABSORPTION-CORRECTED FLUORESCENCE

The masks for the fluorescence collection system were constructed so that the observation windows were square and had a dimension, w , of 0.80 cm. The masks were then positioned in front of the cell so that x_1 and x_2 were 0.10 and 0.90 cm, respectively. Obviously, w_1 and w_2 should have the same values except that they are unitless. A $1\frac{1}{2}$ " quartz biconvex lens with a focal length of 2" was used as the focusing lens while a 1" quartz plano-convex lens with a 3" focal length was used as the field stop. The relationship between the focal lengths of the lenses and the monochromator is given by the general lens formula,

$$\frac{1}{2(f.l.)_{\text{focusing}}} + \frac{1}{(f.l.)_{\text{monochrom.}}} = \frac{1}{(f.l.)_{\text{field}}}$$

The front surface mirrors were obtained from Edmund Scientific Company (#591) and were resurfaced with aluminum and a soft magnesium fluoride overcoat.

Once the optical system had been constructed and positioned, experimental fluorescence curves were obtained for two series of solutions. The first series was composed of a number of quinine sulfate solutions in 1.0 N sulfuric acid. These solutions ranged in absorbance from 0.007 to over 2.0. The second was a series of solutions with a

cons.

acid

the

tior

Fig

fluc

sha

and

for

val

nea

cor

tic

pa

ce

so

Si

pa

b

o

f

s

v

h

:

h

constant quinine sulfate concentration in 0.1 N sulfuric acid but, in addition, had an increasing concentration of the chromophore, 2,5-dihydroxybenzoic acid. The first solution in this series contains only the pure fluorophore. Figures 8A and 9A show the experimental results for the pure fluorophore and the mixture, respectively. Since the shapes of these experimental curves are dependent on w_1 and w_2 , these curves were used to calculate the best values for these window parameters. In addition, the calculated values of w_1 and w_2 should be in close agreement with the measured values if the experimental emission optical system conforms to the model which was developed for making absorption-corrected fluorescence measurements.

In order to determine the best values for the window parameters, w_1 and w_2 , the absorption-corrected fluorescence for each experimental point for the pure fluorophore solution series was calculated by the following process. Since the absorption-correction factors, f_a (Equation 6, page 15), for the fluorophore solutions which have absorbances below 0.06, are close to unity and almost independent of small variations in w_1 and w_2 , the absorption-corrected fluorescence intensities for all of the pure fluorophore solutions under this absorbance limit were calculated by the use of Equation 5 and the measured observation window parameters of 0.10 and 0.90. A least-squares fitting routine was then used to determine the equation of the best straight line through these theoretical points. Once

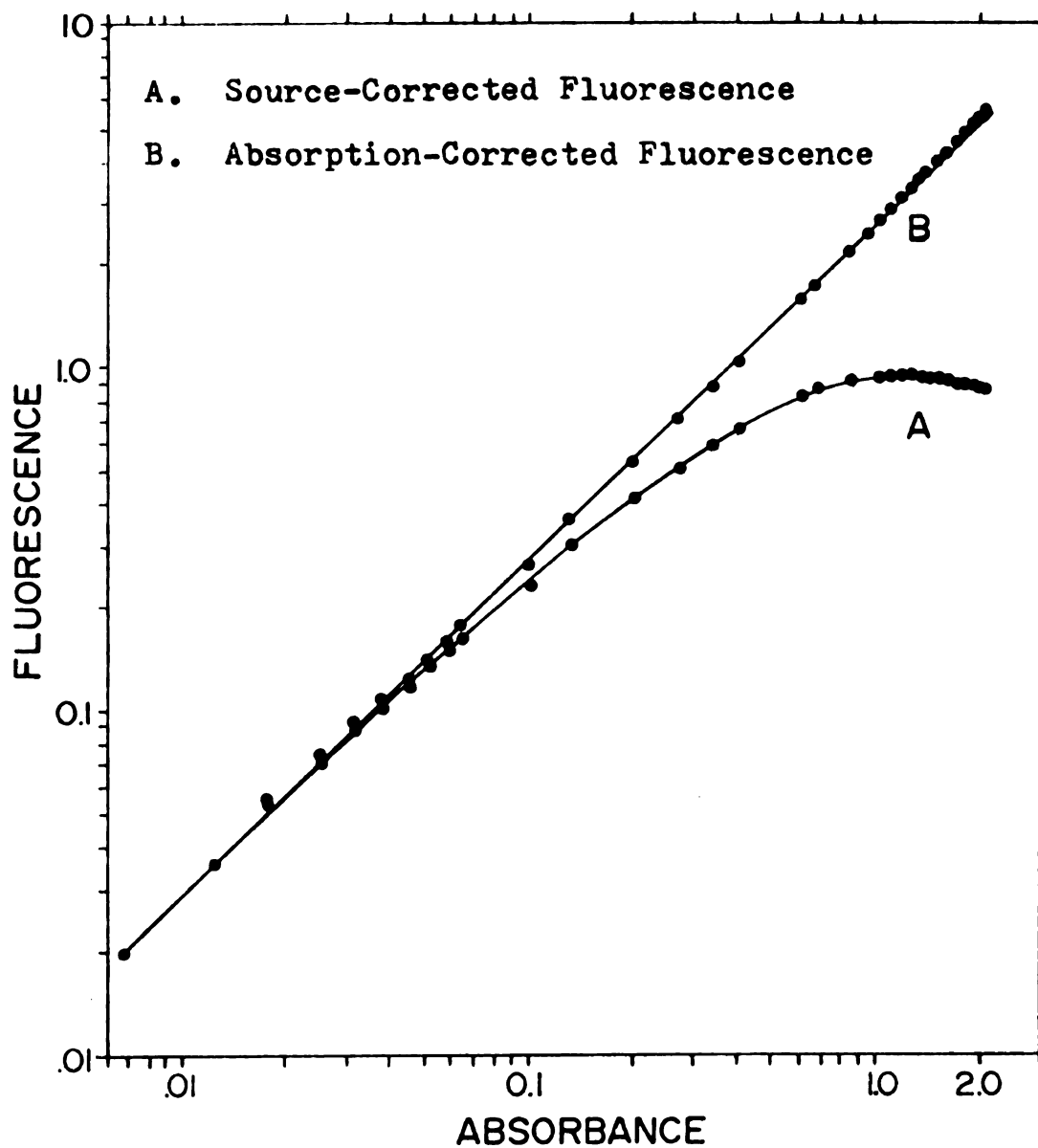


Figure 8. Fluorescence as a Function of Absorbance for Quinine Sulfate in 1.0 N Sulfuric Acid.

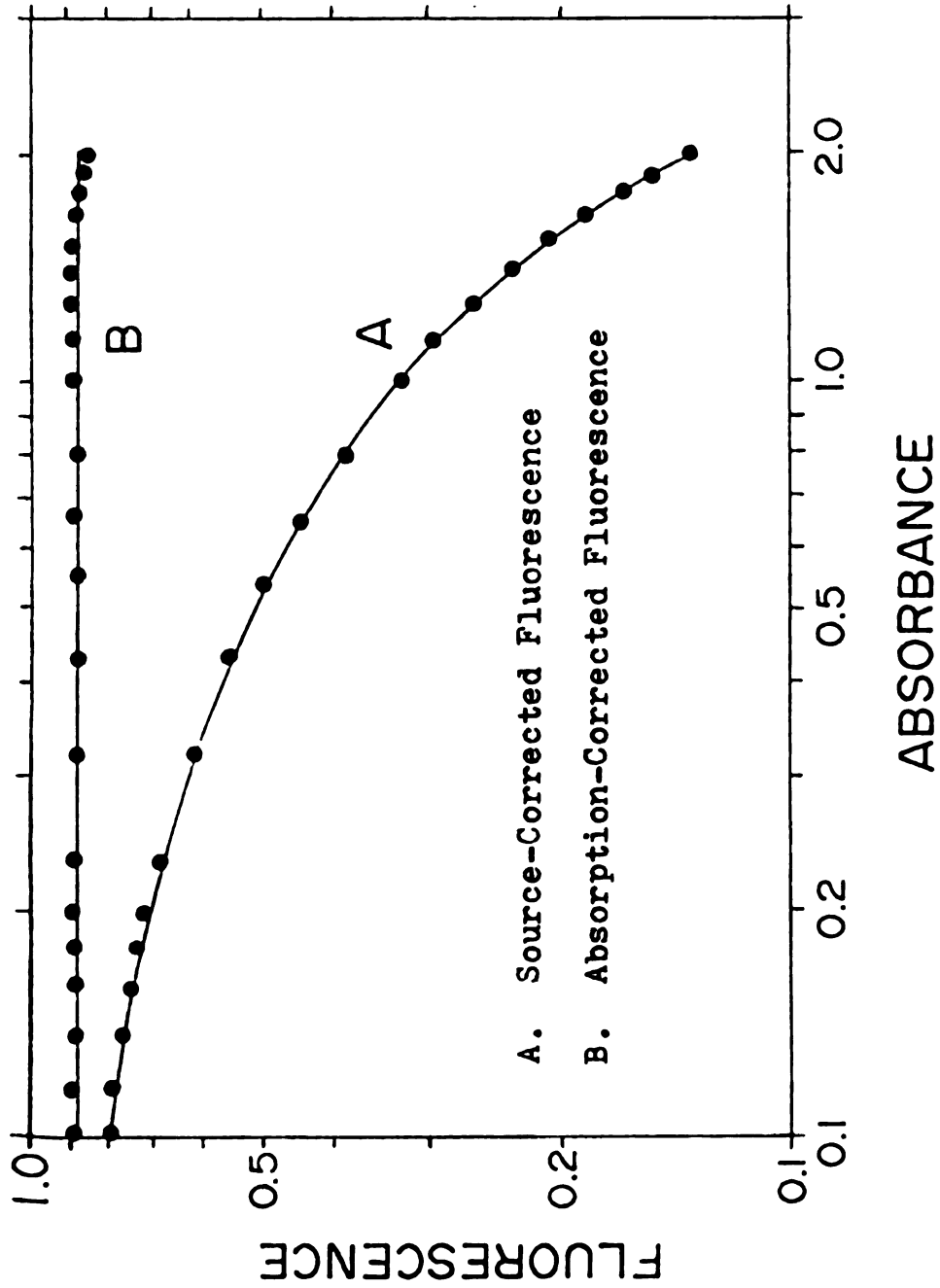


Figure 9. Fluorescence As a Function of Absorbance for Increasing Amounts of the Chromophore, 2,5-Dihydroxybenzoic Acid, in the Presence of 1×10^{-5} M Quinine Sulfate in 0.1 N Sulfuric Acid.

de
so
in
ab
na
di
ea
we
us
Ch
si
ph
Th
fo
na
or
te
a
f
e
t
c
a
a
Th

determined, this equation was used to calculate the absorption-corrected fluorescence intensities for the remaining solutions. All of the calculational processes mentioned above were performed through the use of a FORTRAN program named LSSQ. The use of this program is outlined in Appendix Four.

The absorption-corrected fluorescence intensities at each experimental point for the mixture solution series were calculated from the first experimental point by the use of Equation 5 and the measured window parameters. Obviously, all of absorption-corrected fluorescence intensities are identical since the concentration of the fluorophore was kept constant throughout the solution series. This intensity value is also utilized by program LSSQ.

The paper tape outputs from LSSQ are presented in a format which is compatible with another FORTRAN program named RTFACT. Program RTFACT is a program which is based on a modified Simplex optimization method and it is similar to the ones outlined by Deming and Morgan (33). The program accepts data from LSSQ in the form of transmittance, measured fluorescence and absorption-corrected fluorescence for each experimental point. It then uses a modified form of Equation 5 to fit the measured fluorescence to the calculated corrected fluorescence. This is accomplished by varying w_1 and w . The observation window width, w , was used because w_1 and w are independent parameters whereas w_1 and w_2 are not. The window parameters determined from the experimental

and

0.9

mea

AUT

abs

as

to

abs

pa

The

fl

fl

Eg

no

th

yi

r^w

r^w

r^w

Si

th

of

w

te

and calculated fluorescence data were found to be 0.11 and 0.91. These values are in excellent agreement with the measured values of 0.10 and 0.90.

AUTOMATED CORRECTIONS

In order to eliminate the problem of tedious manual absorption corrections, the spectrophotofluorometer program, as initially outlined in (18), has been modified by Teets to include a subroutine which automatically calculates the absorption-correction factor, f_a , from the observation window parameters and the transmittance at each experimental point. The program then applies these factors to the source-corrected fluorescence, F/R , to yield the desired absorption-corrected fluorescence. The subroutine uses a close approximation of Equation 6 to calculate the correction factors. The denominator of this equation, $(T^{w_2} - T^{w_1})$, was replaced with the first seven terms of its Taylor expansion. The expansion yielded the following expression:

$$T^{w_2} - T^{w_1} = 1 + \ln T \left[\frac{w_2^2 - w_1^2}{2!(w_2 - w_1)} \right] + (\ln T)^2 \left[\frac{w_2^3 - w_1^3}{3!(w_2 - w_1)} \right] + \dots$$

Since the quantities in brackets depend only on w_1 and w_2 , these quantities are constant and are calculated by the use of another FORTRAN program named ARTCAL. This program uses w_1 and w_2 to calculate the second through seventh bracketed terms in the Taylor expansion and then converts them into

a l

st.

sp

la

ou

Th

ex

cu

co

an

ab

a binary floating point format which can be directly substituted in the subroutine which is contained in the PAL8 spectrophotofluorometer program.

The procedure outlined above was followed. The calculated window parameters of 0.11 and 0.91 were used and the output from ARTCAL was substituted into the subroutine. The automated application of the correction factors to the experimental data yielded absorption-corrected fluorescence curves similar to the ones shown in Figures 8B and 9B.

Details for the implementation of automated absorption-corrected fluorescence measurements as well as the listings and descriptions of the various FORTRAN programs mentioned above are contained in Appendix Four.

V. RESULTS AND DISCUSSION

BASIC ASSUMPTIONS

Of the seven basic assumptions which pertain to the theoretical model for absorption-corrected fluorescence measurements, only two needed a closer examination. The first of these was concerned with the relationship between the fractional absorbance of the fluorophore and its fractional absorption of quanta. This relationship, through rigorous mathematical treatment, was shown to be,

$$\frac{A_f}{A_t} = \frac{Q_f}{Q_t}$$

The importance of this relationship is paramount since it was used to establish that absorption-corrected fluorescence measurements can be made on solutions which contain a fluorophore and several absorbing chromophores as well as solutions which contain only pure fluorophore. Consequently, Gill's question (28) about the application of the Parker and Barnes correction factor to both the case of a pure fluorophore and the case of a fluorophore and chromophore mixture has been answered.

The second and last assumption examined in this study was concerned with the observation of the fluorescence generated within the sample cell. It seems almost obvious

at

ter

ab

me

3,

Si

or

de

re

s

t

at this point that unless the measured fluorescence intensity is predictable, there would be no way to make absorption-corrected measurements. In other words, the measured fluorescence intensity must be predicted by Equation 3, which is written as

$$F_{\text{measured}} = 2.303 \frac{K A_f R}{\ln T} (T^{W2} - T^{W1})$$

Since adherence to this equation depends almost entirely on the geometric and optical configuration of the emission detection system, assumption five as listed in the Theoretical chapter was examined with respect to the detection system. As a result, this assumption was broken down into the four following requirements:

- (1) The excitation beam must be homogeneous.
- (2) The fluorescence generated in a horizontal slice within the observation window must reach the detector.
- (3) The observation angles for all of the point sources along that slice must be equal.
- (4) The detector must have a uniform sensitivity over its sensing area which is normally illuminated by the fluorescence.

In essence, the fulfillment of these requirements not only predicts Equation 3 but it also outlines the instrumental

conditions for the implementation of absorption-corrected fluorescence measurements.

IMPLEMENTATION

As noted in the preceding chapter, the emission optical system was designed and constructed so that the requirements listed above were met. Whether it actually does meet them is a point which has to be shown.

Equation 3 indicates that if all of the assumptions are met, the measured fluorescence intensity is dependent on the optical system parameters, w_1 and w_2 . Consequently, if these parameters are calculated from the measured source-corrected fluorescence intensities and corresponding transmittances, their values should agree with the values of w_1 and w_2 which were obtained by the actual measurement of these parameters when the optical system was constructed. If good agreement exists, it may be assumed that the optical system meets the requirements. Since excellent agreement has been shown to exist between the actual and calculated window parameters, it must be assumed that the emission optical system, as outlined in the Experimental chapter, meets the criteria of assumption five and subsequently, corrections have been made on solutions with total absorbances as high as 2.0.



CO

in

ap

Si

de

th

ti

in

ra

ma

ac

T.

m.

ab

th

re

as

to

ex

ti

ba

at

a

ne

CORRECTION ACCURACY

In theory, Equation 5 is an exact expression. However, in practice, the accuracy of the results obtained from its application is limited by certain instrumental factors. Since absorption-corrected fluorescence measurements are dependent on R , S and F , these measurements are limited by the accuracy of these three measured quantities. Evaluation of the measurement capabilities of the instrument used in this study should lead to a good estimate of the accuracy to which absorption-corrected measurements can be made.

As noted in the Instrumental chapter, the photometric accuracy of the instrument used in this study is $\pm 0.1\%$ T . Because this error is most prominent near zero transmittance, it is expected to have the greatest effect on the absorption-corrected measurements in this region. Indeed this is the case, the maximum predicted error in the correction factor, f_a , at an absorbance of 0.50 is .14% whereas it is 2.8% for an absorbance of 2.0. This error increases to 7.1% for an absorbance of 2.5. Obviously, the greatest error occurs in the transmittance region where the correction factors are increasing at a rapid rate. Consequently, based on the photometric accuracy of the instrument, an absorbance of 2.0 was chosen as a limiting value to ensure a reasonable accuracy in the absorption-corrected measurements.

Based on the foregoing discussion, it is expected that the correction factors should have a relative error of 2.8% or less if only the photometric accuracy of the instrument is considered. However, the accuracy of the absorption-corrected fluorescence measurements should be somewhat less since these measurements are also dependent on the accuracy of the source-corrected fluorescence, F/R . The fluorometric accuracy of a particular instrument is a difficult quantity to evaluate. Usually, the source-corrected fluorescence is ratioed to the quanta absorbed within the fluorescence observation window. This is done for a series of solutions which contain a fluorophore with a constant quantum efficiency throughout the concentration range chosen. Quinine sulfate in sulfuric acid is usually used as a standard since its quantum efficiency is believed to be constant to within 1-2%. Because the calculated ratios are directly proportional to the instrumental constant, the agreement among them over the whole series of solutions is considered to be a measure of the instrumental fluorometric accuracy. Unfortunately, this method must utilize the transmittance of each solution to calculate the number of quanta absorbed within the observation window (Equation 1). Therefore, the ratios are somewhat dependent on the photometric accuracy of the instrument, and the values obtained by this method for the fluorometric accuracy should be used only as estimates. For the instrument used in this study, the fluorometric accuracy was found to be about $\pm 5\%$. Based on

1

exp
at
in
me
it
me
th
fo
si
a
fo

li
wa
in
ar
st

experimental data, as expected, the error becomes greater at low fluorescence levels. Fortunately, the worst errors in fluorometric accuracy occur in a region where the photometric accuracy is the best and vice versa. Consequently, it is expected that the absorption-corrected fluorescence measurements should have a maximum relative error of less than $\pm 5\%$. Of course, this figure does not take into account for the errors incurred because of cell positioning, but since this source of error can be minimized by the use of a tight fitting cell chamber, it need not be considered for the purposes of this discussion.

Based on the experimental results, the error from linearity for the absorption-corrected fluorescence curves was found to be a little greater than $\pm 3\%$. This figure is in good agreement with the predicted maximum value of $\pm 5\%$ and it indicates that accurate absorption-corrected measurements are possible.



h
i
f
u
a
q
o
f
t
w
S
t
e
o
m
o
o
n
ne
ne
ou
ab

VI. SUMMARY AND CONCLUSIONS

A second computer-centered spectrophotofluorometer has been constructed. Improvements over the prototype instrument include the capability of using several different sources, computer controlled wavelength scans, the use of a reflectance standard to calibrate the emission detection system and the utilization of a methylene blue quantum counter to extend this calibration to 7000 Å.

The instrument was found to have a photometric accuracy of about $\pm 0.1\%$ T in the range from 1 to 100 % T. The fluorometric accuracy was estimated to be about $\pm 5\%$, while the fluorometric precision was found to be $\pm 1\%$.

The instrument was used to extend some of the previous work on absorption-corrected fluorescence measurements. Some of the assumptions previously used in the formulation of a theoretical model were carefully examined. This examination resulted in the construction of an emission optical system which met the criteria of the theoretical model. A scheme was then developed for the implementation of absorption-corrected fluorescence measurements based on this model. Subsequently, absorption-corrected measurements were made up to an absorbance of 2.0 and these measurements were found to be accurate to about $\pm 3\%$. Without corrections, the error due to non-linearity would be about -85% for solutions with absorbances of 2.0.

PART II
FLUOROMETRIC AND OTHER STUDIES OF THE
REACTION OF ALUMINUM (III) AND
FLAVONOL IN ABSOLUTE ETHANOL

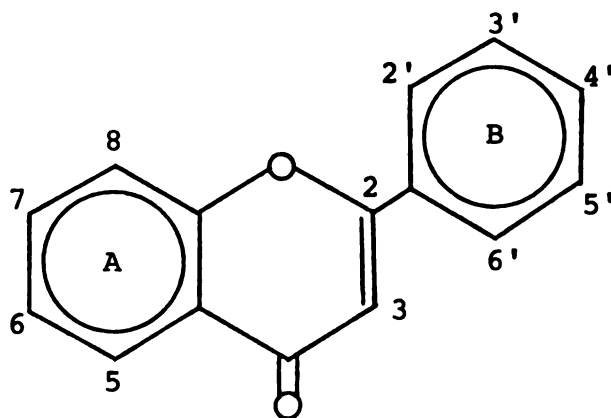


Ge
pe
In
sy
Th
re

va
at
th
ch
be
fla

I. INTRODUCTION

For years flavones have been known to exist in nature. Generally, they are found in plants as the polyhydroxy or polymethoxy derivatives of the parent flavone molecule. In recent years, however, many other flavones have been synthesized so that today well over fifty derivatives exist. The structure of the parent molecule, flavone, reveals the reason for such a myriad of derivatives. Of all the



various derivatives, those which contain hydroxy groups at the 3 and 5 positions are the most interesting. It is these derivatives which have the possibility of forming chelates with metal ions and many of these chelates have become analytically useful. As a result, the volume of flavone literature has grown immensely in the last decade.

Fortunately, there are several excellent reviews available in the literature and in all, they list well over two hundred references (34-36). In addition, they also provide an extensive list of the chemical elements which have been determined through the use of flavone derivatives.

Of all the hydroxyflavones, quercetin (3,5,7,3',4'-pentahydroxyflavone), quercetrin (3-glucoside of quercetin), rutin (5,7,3',4'-tetrahydroxy-3-rutinoside flavone) and morin (3,5,7,2',4'-pentahydroxyflavone) are probably the most important. With these four flavones, over thirty chemical elements may be determined and many of the determinations have detection limits which are well below the part per million level.

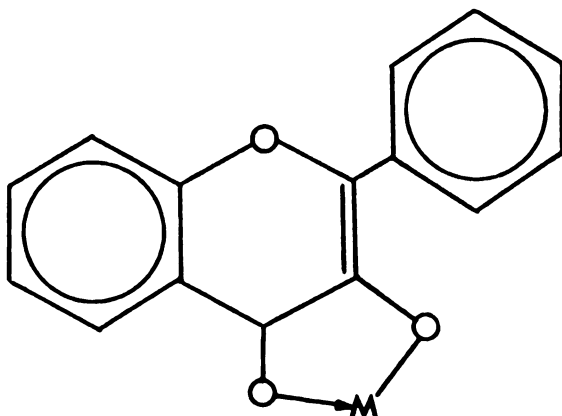
Besides elemental determinations, hydroxyflavone-metal chelates have also been used for structural determinations of the flavones themselves. Mixtures of boric acid and citric or oxalic acid have been used to identify hydroxyflavones which have hydroxy groups in the 3 or 5 position (37-41). Rutin and quercetin have been determined from their complex formations with $ZrOCl_2$, $AlCl_3$ and $TiCl_4$ (42). In addition, many other methods for the determination of flavones have been developed, and these may be found in the reviews previously referenced.

One of the simplest flavone derivatives is 3-hydroxyflavone or flavonol. Unlike many of the other flavones which are used in the formation of chelates, flavonol has only one chelation site. Consequently, it is expected



t
(
i
t
a
o
fo
ch
th
ab
th

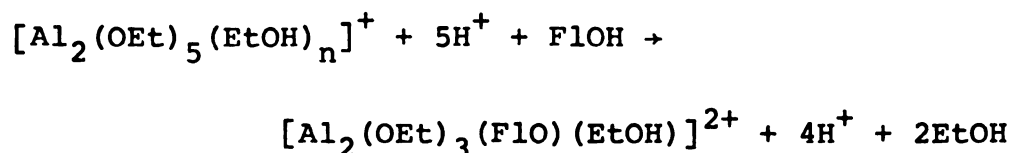
that the metallic chelates of flavonol should have the structure shown below. Chelates of this type have been used to determine quantitatively iron (43), tungsten (44,45),



tin (46), uranium (47,48), vanadium (49,50) and zirconium (51). Flavonol also forms chelates with many other metal ions, but they have not generally been used for quantitative determinations.

As a whole, flavonol chelate structures in solution are not well understood. Perhaps the most interesting of these structures are those of the chelates which are formed with aluminum (III). The first report of these chelates was made by Jurd and Geissman (52) who measured their absorption spectrum and proposed the structure shown above. Later work by Urbach and Timnick (53,54) established that a 1:1 chelate was formed in basic solutions while in

neutral solutions of absolute ethanol, three different chelates were formed. Two of the chelates were found by photometric means to have stoichiometries of 1:1 and 2:1 metal ions per ligand. The third chelate, which could only be detected fluorometrically, had a metal to ligand ratio of 6:1. In addition, from the data which were obtained from the potentiometric titrations of the chelates and from the structure of aluminum (III) in absolute ethanol, which was proposed by Ohnesorge (55), these workers were able to write an overall reaction equation for the formation of the 2:1 chelate:



where F1OH represents flavonol. Unfortunately, no attempt was made to explain why the spectra for the chelates were all identical and how a bidentate ligand forms a chelate with six aluminum ions.

In addition to work by Urbach and Timnick, Porter and Markham (56) have attempted to elucidate the structures and stoichiometries of the flavonol-aluminum (III) chelates which are formed in absolute methanol. They have found that a 2:1 metal-to-ligand chelate was formed in a 0.1 M methanolic perchloric acid solution. They also noted that the chelate fluoresced at 450 nm. However, when no acid

or base was added to the flavonol-aluminum (III) solutions, the 1:2 and 1:1 chelates were formed. Upon the addition of 0.1 M potassium acetate, two chelates were also formed. These were the 4:1 and 1:2 metal-to-ligand chelates. As noted by Urbach and Timnick and again by Porter and Markham, the presence of excess base severely inhibits chelate formation. Consequently, when Porter and Markham added 0.1 M sodium methoxide to the flavonol-aluminum (III) solutions, they found that no chelation had taken place. However, when equimolar amounts of methoxide or hydroxide and flavonol were used, the 1:2 metal-to-ligand chelate was formed. In addition, when the ratio of hydroxide to flavonol was 2.5, they found that a 1:1 chelate was the predominant species. Finally, Porter and Markham also noted that at slightly higher hydroxide or methoxide ratios, the 2:1 and 3:1 metal-to-ligand chelates were formed. In all cases, where either hydroxide or methoxide was present, the solutions did not fluoresce.

At this point, it should be fairly obvious that the systems of chelates formed between flavonol and aluminum (III) are quite complex. As a result, the data which were obtained in the two studies outlined above have raised many questions:

1. Why are the absorption and fluorescence spectra identical for all of the chelates?
2. Are the chelates structurally similar?

3. Does a 6:1 chelate actually exist in solution and if so, why?
4. What are the reasons for the vast differences in quantum efficiencies among the chelates?
5. Why do the chelates formed in methanol differ in stoichiometry from those formed in ethanol?

In an effort to answer at least some of the foregoing questions, a study was undertaken in order to re-examine the formation of flavonol-aluminum (III) chelates in absolute ethanol, and as a result, some new data have been added. This part of this thesis is a report of that re-examination, and it should serve as a stepping stone to a fuller understanding of the structure of aluminum (III) in solution as well as the chelates which are formed upon the addition of flavonol.

II. EXPERIMENTAL

INSTRUMENTATION

The following instruments were employed to make the appropriate measurements:

Beckman Expanded Scale pH meter equipped with a Sargent combination glass-saturated calomel electrode (#S-30070-10) was used to measure the apparent pH of the ethanolic chelate solutions.

Perkin Elmer Model 237B Grating Infrared Spectrophotometer was used to obtain the infrared absorption spectra.

Spex Ramalog 4 Raman Spectrometer equipped with an argon ion laser was used to obtain the Raman spectra. A double monochromator system was used for this study.

A highly modified NMRS-MP-1000 Nuclear Magnetic Resonance Spectrometer, equipped with a General Radio Model 1164-A Frequency Synthesizer, a Fabri-Tek Model 1074 Multichannel Analyzer and a super conducting magnet, was used to obtain the aluminum-27 NMR spectra.

Aminco-Bowman Spectrophotofluorometer (SPF) equipped with a rotating cam accessory and a liquid nitrogen cooling system was used to obtain the delayed fluorescence and phosphorescence spectra.

Computer-centered spectrofluorometer, as outlined in the Instrumental chapter in Part I of this thesis, was used to measure the absorption and fluorescence spectra as well as the quantum efficiencies of the chelate solutions.

Picker Copper X-ray Source and Powder Camera were used to obtain the X-ray powder diffraction patterns.



CHEMICALS

The following chemicals were used without further purification as standards or in the preparation of reagent solutions described in this study:

Aluminum Chloride	Anhydrous, Reagent Grade Matheson, Coleman and Bell
Aluminum Chloride	Reagent Grade Allied Chemical Company
Ammonium Chloride	Baker's Analyzed Reagent J. T. Baker Chemical Co.
Ammonium Hydroxide	Reagent Grade Fisher Scientific Company
Calcium Oxide	Baker's Analyzed Reagent J. T. Baker Chemical Co.
2,5-Dihydroxybenzoic acid	99% Purity Aldrich Chemical Company
Ethanol, absolute	Commercial Solvents Corp.
Ethylenediaminetetracetic acid, disodium salt, dihydrate	Baker's Analyzed Reagent J. T. Baker Chemical Co.
Hydrochloric Acid	Analytical Reagent Mallinckrodt, Inc.
Nitric Acid	Analytical Reagent Mallinckrodt, Inc.
Potassium Hydrogen Phthalate	Reagent Grade (ACS) Matheson, Coleman & Bell
Potassium Permanganate	Baker's Analyzed Reagent J. T. Baker Chemical Co.
Quinine Sulfate, dihydrate	Baker Grade J. T. Baker Chemical Co.
Silver Nitrate	Baker's Analyzed Reagent J. T. Baker Chemical Co.

Sodium Hydroxide	Analytical Reagent Matheson, Coleman & Bell
Sulfuric Acid	Baker's Analyzed Reagent J. T. Baker Chemical Co.
2-Thiouracil	97% Purity Aldrich Chemical Company
Zinc Sulfate	Reagent Grade Allied Chemical Company

PURIFICATION OF FLAVONOL

Flavonol obtained from the Eastman Kodak Company was purified by the following process. The impure flavonol (yellow) was dissolved in a minimum amount of hot absolute ethanol. About ten milliliters of dilute sulfuric acid was added to this solution. The solution immediately turned from a dark yellow to a very pale yellow. Water was added to the hot ethanolic solution until obvious crystal formation had started. The solution was left to stand until it had cooled to room temperature. The solution and crystals were then cooled in an ice bath until complete crystallization had taken place. The crystals were filtered and then washed with cold water. The melting point range of the fine pale yellow needle-like crystals was 167.8 - 169.7 C. The literature melting point range is given as 168 - 170 C. The ultraviolet absorption spectrum of the product matched that of flavonol.

PREPARATION OF STOCK SOLUTIONS

A standard aqueous solution of ethylenediaminetetraacetic acid was prepared by the direct weighing of the disodium salt, dihydrate.

This standard EDTA solution was then used to standardize an aqueous solution of zinc sulfate. Erichrome Black T was used as the indicator.

Aluminum solutions were prepared by dissolving anhydrous aluminum chloride in absolute ethanol. The dissolutions were carried out in a dry ice and acetone bath to prevent the formation of impurities due to the reactive nature of the anhydrous salt. The solutions were then made up to be about 0.01 M in aluminum chloride. Aliquots of these solutions were taken to dryness on a hot plate and the solid was dissolved in a small amount of concentrated hydrochloric acid. Upon dilution, a small excess of the standard EDTA solution was added, and the pH of each solution was adjusted to between 7 and 8. A few drops of Eriochrome Black T were added, and the excess EDTA was immediately titrated with the standardized zinc sulfate solution. The endpoint was reached when the solutions turned from a pure blue to a wine red color. The concentrations of the aluminum chloride solutions were calculated, and the 0.01 M solutions were diluted to make 1.00×10^{-3} M stock solutions. Various concentrated aluminum chloride solutions were standardized in a similar manner, and these solutions were used when

high concentrations of aluminum were required.

Standard ethanolic stock solutions of flavonol were prepared by the direct weighing of the solid.

Stock solutions of sodium hydroxide in absolute ethanol were prepared by dissolving the pellets in water to yield a 50% solution. This solution was allowed to stand for three days to allow any carbonate to settle out. Three milliliters of this solution were then diluted to 500 ml with boiled absolute ethanol. This ethanolic solution was then standardized against potassium hydrogen phthalate. This solution was then diluted further to obtain 1.00×10^{-3} M stock sodium hydroxide solutions.

Stock solutions of hydrochloric acid were prepared by diluting five milliliters of 37% hydrochloric acid to 500 ml with absolute ethanol. This solution was standardized against a standard solution of sodium hydroxide and diluted further to obtain the 1.00×10^{-3} M stock solutions.

EXPERIMENTAL PROCEDURES

Spectrofluorometer

All of the absorption and fluorescence spectra were measured on the computer-centered spectrofluorometer. These measurements were made with a 150 watt Xenon arc lamp as the source and a 4.0 nm bandpass for both the excitation and emission monochromators. All spectra were background

corrected, and in addition, the emission spectra were corrected for all instrumental variables.

The quantum efficiency measurements were made with the same monochromator bandpasses and were relative to quinine sulfate. The instrument was calibrated by the use of either a 1.00×10^{-4} or 5.00×10^{-5} M quinine sulfate solution in 1.0 N sulfuric acid. The calibration was carried out at an excitation wavelength of 365.3 nm, and the emission monochromator was scanned from 370 to 620 nm. The generally accepted quantum efficiency of 0.546 for quinine sulfate in sulfuric acid was used. All quantum efficiency measurements on the unknown chelate solutions were made at an excitation wavelength of 404.6 nm. The emission wavelength range was changed slightly from the range used for the standard in order to eliminate any Rayleigh scattering.

Photometric and Fluorometric Titrations

Aliquots of the titrant and the reagent to be titrated were placed in a series of volumetric flasks. In all cases, flavonol was added to the aluminum aliquot. Acid or base was then added, if necessary, and the contents of the flasks were diluted to volume with ethanol. After a waiting period of at least three hours, the appropriate measurements were made. No corrections for dilution were necessary with this procedure.

Apparent pH Measurements

The apparent pH measurements were made by calibrating the meter at a pH of 7.0 with the use of an aqueous buffer. The electrode was then allowed to equilibrate for thirty minutes in absolute ethanol before any test measurements were made. The test solutions were stirred between readings and no temperature control was employed.

Emission Measurements

All delayed fluorescence and phosphorescence measurements were made on samples contained in 5 mm quartz tubes. The samples were deoxygenated by the bubbling of nitrogen through the solutions for at least 15 minutes before being frozen to 77 K. All the spectra were scanned on the Aminco-Bowman Spectrophotofluorometer which used a 150 watt Xenon arc lamp as the source and had a bandpass of 20 nm for both monochromators. The period of the rotating cam was not determined since the delayed fluorescence and phosphorescence lifetimes were quite long. All spectra were recorded at a medium scan speed.

Concentrated Chelate Solutions

Concentrated chelate solutions could not be prepared in the normal manner since flavonol is soluble only to the extent of about 0.05 M in absolute ethanol. However, the chelates themselves were found to be extremely soluble

in ethanol, and this characteristic was utilized in the preparation of concentrated chelate solutions.

An appropriate amount of a concentrated aluminum chloride solution was placed in a volumetric flask, and the required weighed amount of solid flavonol was dissolved in it. The solution was then diluted to volume with absolute ethanol. Solutions prepared in this fashion were used in the aluminum-27 NMR and Raman studies. In addition, these concentrated chelate solutions were also used in the preparation of the solid samples which were used in the infrared and X-ray powder diffraction studies.

Raman Spectra Measurements

All liquid and solid samples were sealed in 1.8 mm glass capillary tubes. The spectrum of flavonol was obtained on a solid sample because of its limited solubility in ethanol. The spectra were run by the use of the argon ion line at 5145 \AA as the source. The laser was operated at 30.5 amperes and the spectra were measured at a scan rate of 20 cm^{-1} per minute. The sensitivity, filtering and slits were adjusted to meet the requirements of the samples.

Infrared Spectra Measurements

Solid chelate samples were obtained by the evaporation of the solvent from solutions which contained the appropriate stoichiometric ratios of aluminum and flavonol.

The evaporations were carried out on sodium chloride plates and yielded thin solid films. All of the spectra were obtained at a slit setting of normal, a slow scan speed and with air as the reference.

X-ray Powder Diffraction Measurements

Again, solid samples were prepared by the evaporation of the solvent from liquid samples. Small amounts of the solids were then placed on cellophane tape to hold them in place. Finely powdered platinum metal was added to each sample as a reference. The tape was then placed on a metal disc so that the sample was positioned over a small hole in the center. The sample was then placed in the target chamber along with a camera and irradiated with the copper K_{α_1} line at 1.541 Å. The source was run at 35 kilovolts and 18 milliamperes and the film was exposed for a period of six hours at these settings. Subsequent development of the film yielded the desired diffraction patterns.

Aluminum-27 NMR Measurements

All measurements were made on concentrated chelate solutions which were contained in 5 mm sample tubes. Aqueous aluminum chloride was used as a reference for all the measurements. The resonance frequency for the reference was at 59,133,015 Hz for a magnetic field strength of 53 kilogauss. All shifts for the chelates were to the low

field or high frequency side of the reference signal. The number of scans per spectrum was varied and depended on the concentrations of the samples but in all cases, the dwell time was four milliseconds and the sweep width was 1684 Hz. In addition, all measurements were performed on spinning samples and at room temperature.

III. RESULTS AND DISCUSSION

ABSORPTION AND FLUORESCENCE SPECTRA OF FLAVONOL

The absorption and fluorescence spectra of flavonol in absolute ethanol are presented in Figure 10. The maxima of the major bands in the absorption spectrum occur at 306 and 344 nm, and they can be attributed to carbonyl (π, π^*) transitions, since the molar absorptivities are quite large ($\epsilon_{306} = 10,600$ and $\epsilon_{344} = 16,500$). The fluorescence spectrum also consists of two major bands with the maxima located at 410 and 535 nm. These bands almost certainly result from the deactivation of a (π, π^*) excited state. However, the fluorescence spectrum is a little unusual from the standpoint that it is not the true mirror image of the absorption spectrum as would be expected for an ideal fluorophore. In fact, the intensity of the high energy band is quite low compared to that of the band at 535 nm. In addition, the wavelength region between the two maxima is nearly void of fluorescence. These characteristics seem to suggest that flavonol may have some unusual absorption and emission features.

EMISSION SPECTRUM OF FLAVONOL AT 77 K

The emission spectrum of flavonol at liquid nitrogen temperatures is presented in Figure 11. The spectrum

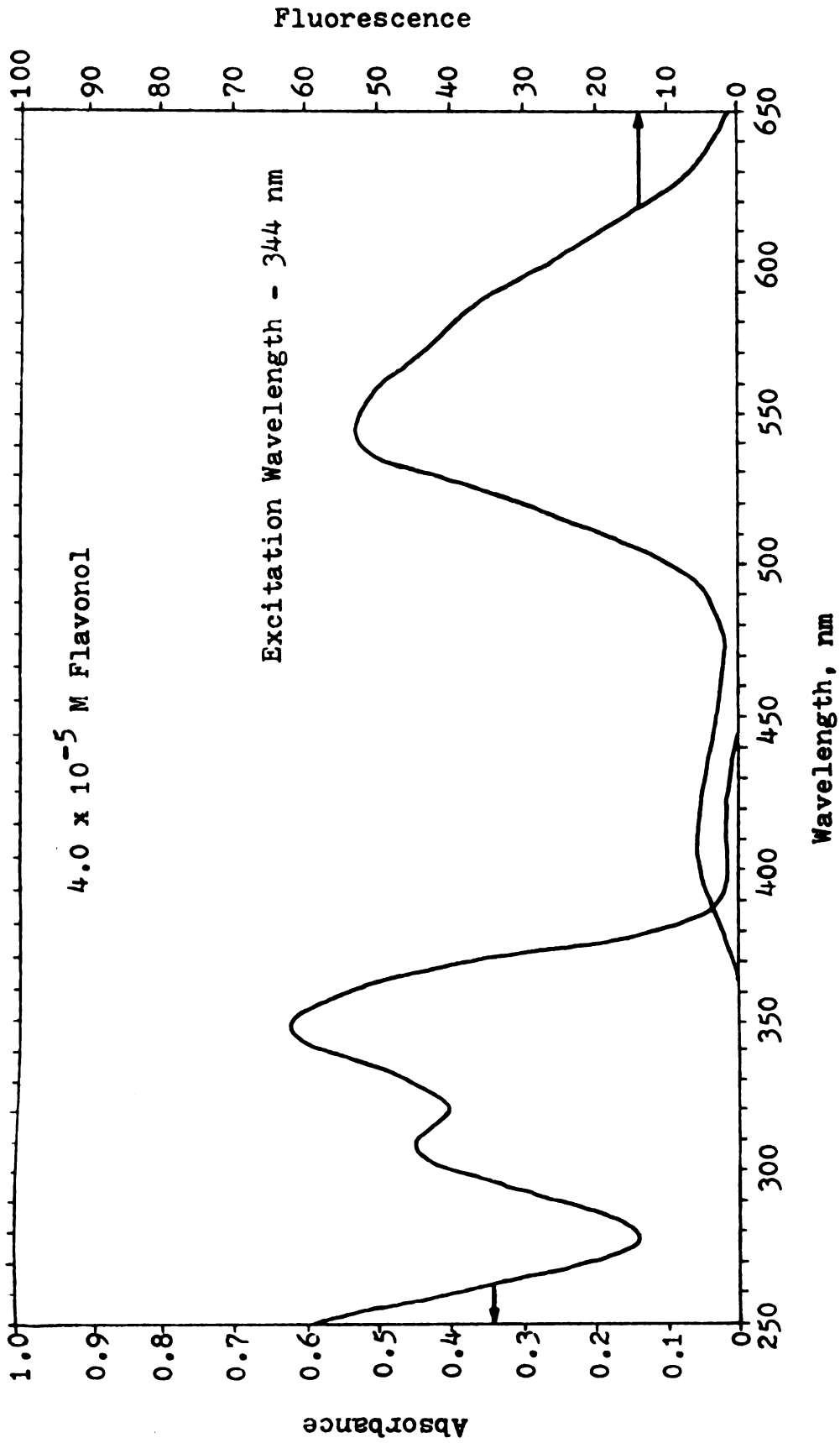


Figure 10. Absorption and Fluorescence Spectra of Flavonol in Absolute Ethanol.

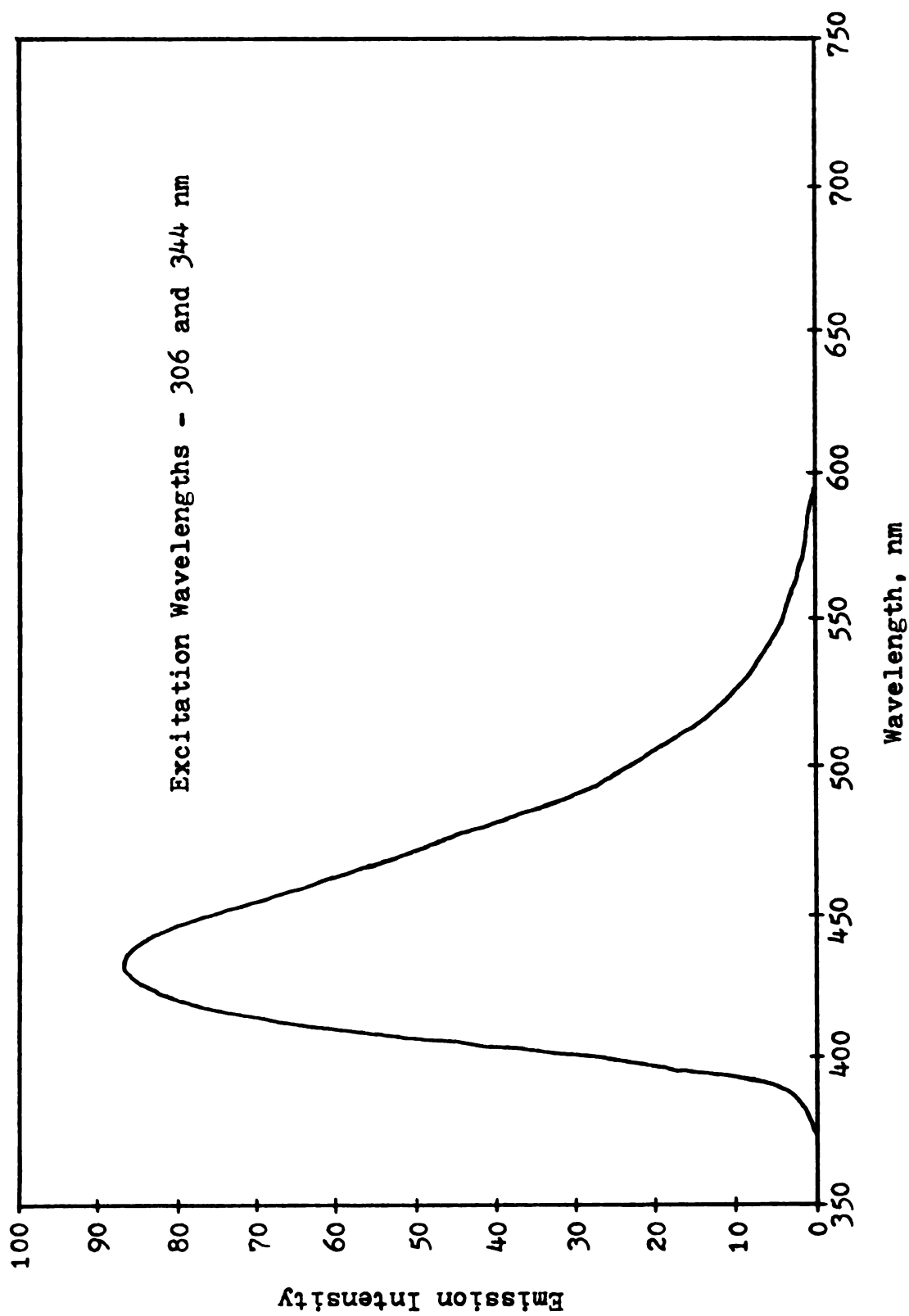


Figure 11. Emission Spectrum at 77 K for Flavonol in Absolute Ethanol.

consists of a single band which is attributed to delayed fluorescence, since it is located on the high energy side of the main prompt fluorescence band and has a fairly long lifetime. The location and intensity of this band is dependent upon the wavelength of excitation and somewhat on the presence of oxygen. Table II summarizes these dependencies. The data contained therein have not been corrected

Table II

Dependence of the Delayed Fluorescence of Flavonol
on Excitation Wavelength and the Presence of Oxygen

Excitation Wavelength	Emission Maximum	Emission Intensity	Dissolved Oxygen
306	435	1000	Present
344	462	55	Present
306	440	714	Absent
344	456	59	Absent

for inner-filter effects or for variations in the signals due to sample positioning. However, it is quite apparent that the production of delayed fluorescence is much more efficient when flavonol is excited into its second electronic state. This phenomenon may be rationalized through the following explanation.

Excitation at 306 nm would produce an excited singlet

state with sufficient energy so that intersystem crossing results in a triplet state with a large excess of vibrational energy. The second intersystem crossing to an excited state then occurs before the lowest vibrational level of the triplet state is reached. Since in this case no additional energy is required for the second intersystem crossing to occur, the production of delayed fluorescence would be fairly efficient. On the other hand, excitation at 344 nm would produce a less energetic singlet state. Intersystem crossing would then result in a triplet state which was much lower in vibrational energy than that produced by excitation at 304 nm. Presumably, in this case, the dissipation of this excess vibrational energy to the lowest vibrational level would occur before a second intersystem crossing to an excited singlet state would be achieved. Since after this dissipation, the energy of the triplet state would now be lower than that of the lowest vibrational level of the first excited singlet state, a second intersystem crossing could only occur with an increase in vibrational energy. Consequently, the production of delayed fluorescence by excitation at 344 nm would be relatively inefficient.

At this point, it is interesting to note that the data contained in Table II show that the delayed fluorescence occurs in a spectral region where very little prompt fluorescence is observed. This seems to indicate that

the delayed fluorescence originates from an excited state other than the ones which give rise to prompt fluorescence.

(n, π^*) EXCITED STATE OF FLAVONOL

In the ultraviolet absorption spectrum of flavonol, shown in Figure 10, the absorption tails off in an unusual manner in the region between 390 and 450 nm. The excitation spectrum of flavonol, which is presented in Figure 12, was obtained by monitoring the fluorescence generated at 535 nm. It is apparent that the tailing in the 390 to 450 nm region is missing. Consequently, it must be concluded that absorption in this region does not result in the generation of fluorescence at 535 nm. However, as is shown in Figure 13, excitation at 410 nm does generate a single fluorescence band with a maximum located at 484 nm. The partial quantum efficiency plot presented in Figure 14, shows definitively that a previously undiscovered electronic excited state is formed when flavonol is excited by radiation within the tailing region.

At this time, it is believed that this new absorption band arises from a (n, π^*) transition, although the experimental evidence is somewhat ambiguous. The molar absorptivity of this band based on the concentration of flavonol is small ($\epsilon_{410} \approx 250$) and is indicative of a (n, π^*) transition. On the other hand, the spectral studies of flavonol in different solvents by Urbach (53), show no correlation

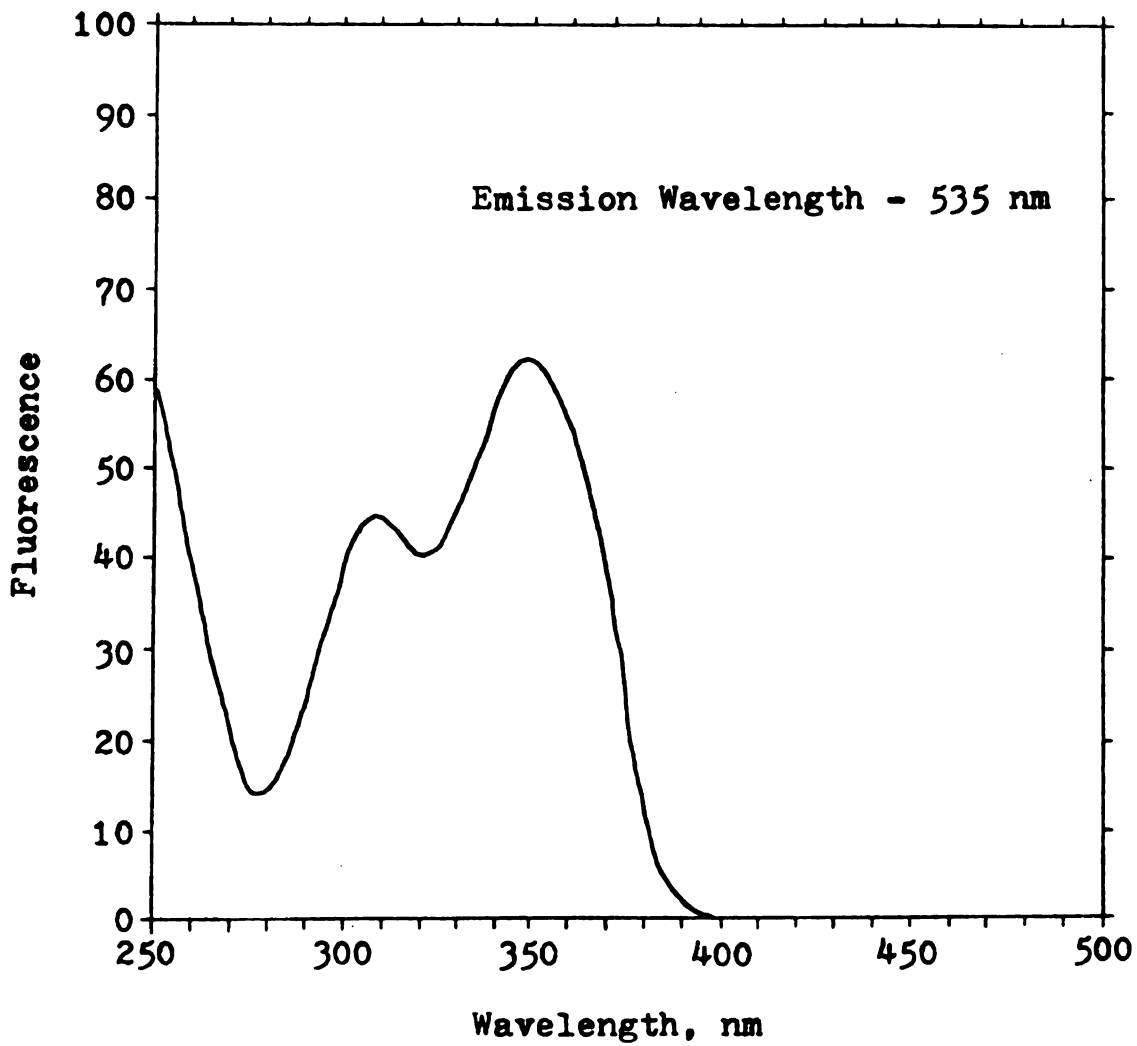


Figure 12. Excitation Spectrum of Flavonol in Absolute Ethanol.

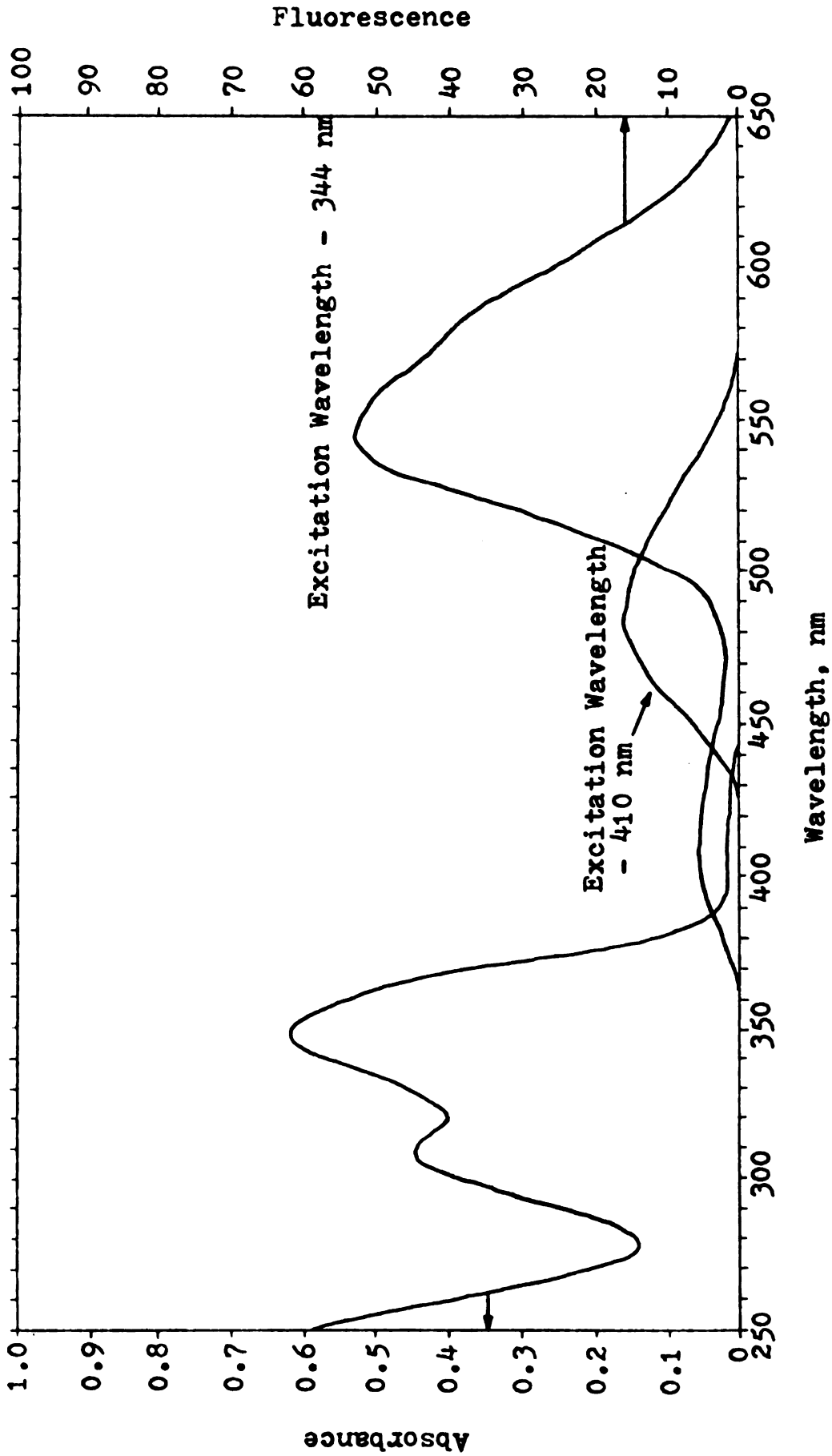


Figure 13. Absorption and Fluorescence Spectra of Flavonol in Absolute Ethanol.

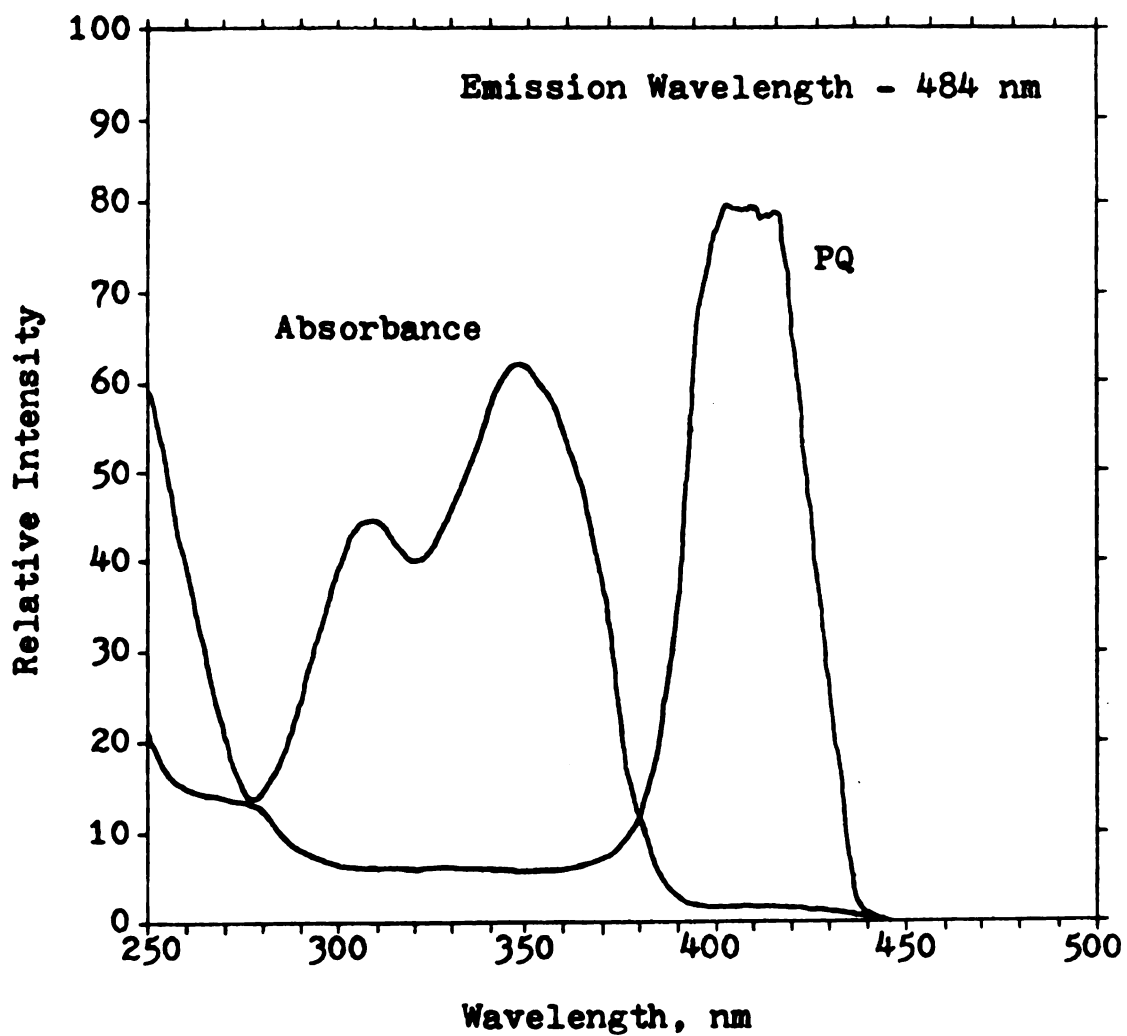


Figure 14. Plot of Partial Quantum Efficiency (PQ) as a Function of Wavelength for Flavonol in Absolute Ethanol.

between band position and solvent polarity. In his studies, the new absorption band was absent when flavonol was dissolved in chloroform, carbon tetrachloride or acetone and present when dissolved in isooctane, methanol or ethanol. In cases where the band was observed, no apparent shift in wavelength was noticed. If indeed the transition in question were a (n, π^*) transition, it should undergo a hypsochromic shift as the solvent polarity was increased. Since this is not the case, a transition assignment cannot be made. The absence of the absorption band in non-polar solvents could be explained by the fact that (π, π^*) transitions undergo a bathochromic shift as solvent polarity is increased. In this case, the absence of the band indicates that it is located under the other major absorption bands when non-polar solvents are used. However, this argument is extremely weak since the band is present for flavonol solutions in isooctane and absent for acetone solutions. Consequently, it would appear that the solvent studies on flavonol are quite inconclusive and assignment, as to the type of transition involved, is not possible.

Further spectral studies of flavonol in absolute ethanol have indicated that the presence of acid affects the position of the absorption band and its associated fluorescence. This effect is shown in Figure 15. Upon the addition of ethanolic hydrochloric acid, the absorption band undergoes a slight blue shift, which may be indicative of a (n, π^*)

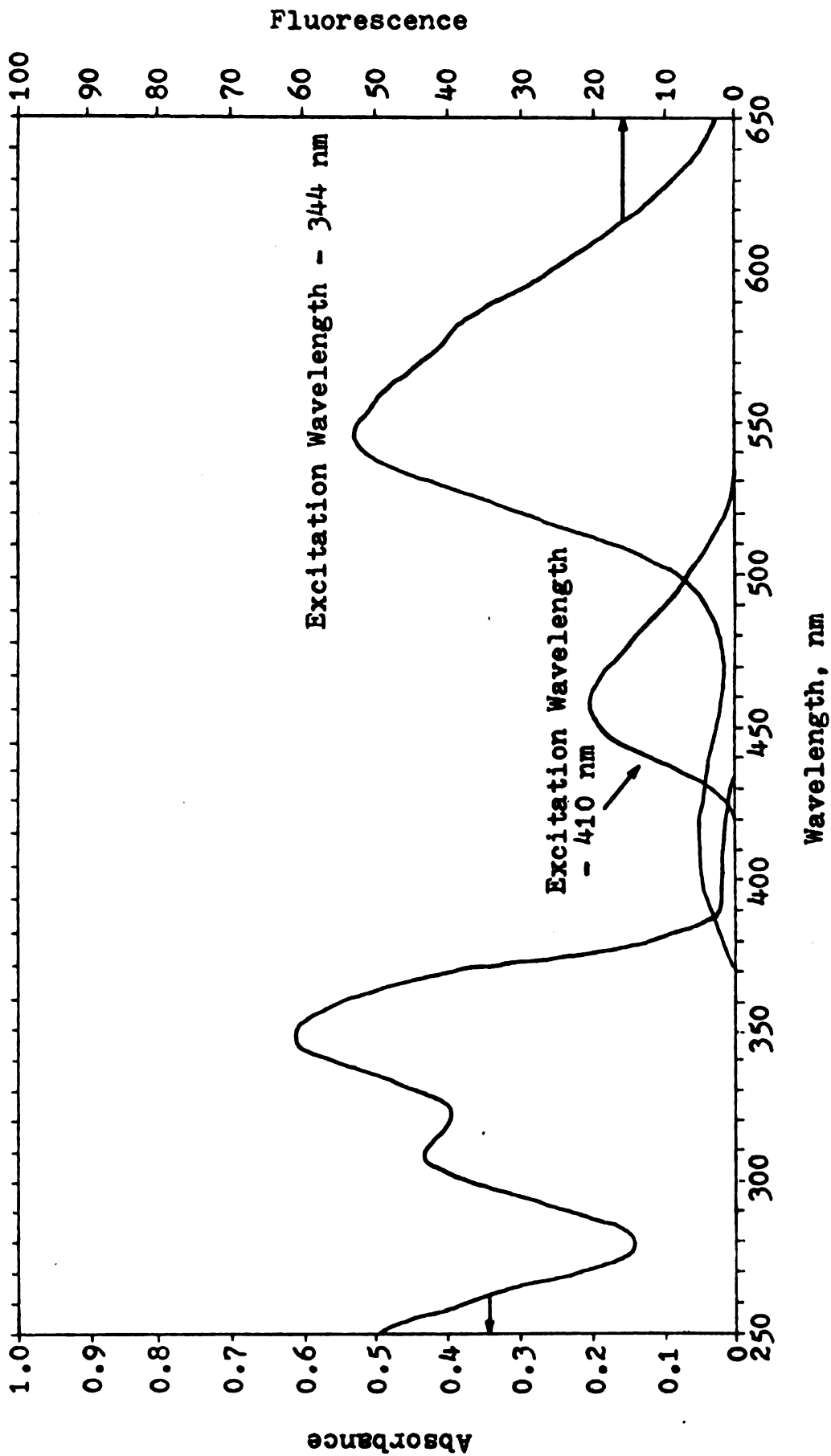


Figure 15. Absorption and Fluorescence Spectra of Flavonol in Acidic Absolute Ethanol.

transition. In addition, the fluorescence band also undergoes a hypsochromic shift and its maximum is moved from 484 to 455 nm. The magnitude of this shift is larger than that which would normally be expected for a change from a non-polar to a polar solvent, but in this case, the change in polarity is quite drastic.

At this point, it would seem that the evidence favors the likelihood that the tail in the spectrum of flavonol in absolute ethanol is actually a (n, π^*) transition. However, one more possibility should be considered. Since flavonol is an α -hydroxy ketone, there exists a possibility for the formation of a keto tautomer. If a small amount of the keto form does exist, it is then possible that the newly discovered band is actually a (π, π^*) transition for the isomer. If this were the case, the previously evaluated molar absorptivity for this band would be in error since the concentration of the keto form would be much smaller than the concentration of flavonol. Reconsideration on this basis would indicate that the band is a (π, π^*) transition.

Unfortunately, the results of the solvent studies by Urbach are once again inconclusive. Since the enol form is normally favored in non-polar solvents for reasons of solubility (57), it is expected that the intensity of the band in question would be depressed for these types of solvents. Obviously, the presence of the band for flavonol

in isooctane and its absence for acetone solutions does not support the existence of the keto tautomer.

Upon the addition of acid to flavonol, it is expected that the fluorescence, which is emitted from the newly discovered excited state, would decrease in intensity, since the enol form is now favored because of the formation of the enolic oxonium cation (57). In fact, the fluorescence intensities before and after the addition of acid are just about equal. This result also seems to indicate that the new absorption band does not originate from the presence of a keto tautomer. In addition, since it is believed that the delayed fluorescence occurs via a radiational deactivation of this excited state, it is highly unlikely that excitation of the enol form at 344 nm would result in the emission of delayed fluorescence from an excited state which is supposedly associated with the keto form. Based on the foregoing arguments, there seems to be little doubt that the newly discovered absorption band is not caused by the existence of a keto form. However, the existence of a (n, π^*) transition in the wavelength region of 400 nm is quite unusual.

Normally, the (n, π^*) transitions for aromatic carbonyl compounds occur between 300 and 350 nm and are usually the lowest energy electronic transitions. The efficiency of intersystem crossing to the triplet state is ordinarily quite high in these types of molecules and generally, they will not exhibit much fluorescence. However, flavonol

is unusual in that the molecule contains a very highly conjugated π system. In fact, the whole molecule is involved in this system. As a result, it is expected that the lowest energy transitions for flavonol would be of a (π, π^*) nature. Indeed, this statement would probably be true if it were not for the fact that flavonol is also an oxygen heterocyclic molecule. In this case, conjugation across the pyrone ring causes the energy of the (n, π^*) state to be lowered to a point where it is actually the lowest energy transition. It has been found that conjugation in unsaturated ketones has lowered the energy of the (n, π^*) state to such an extent that in molecules such as p-benzoquinone, the (n, π^*) transition occurs at 435 nm. Presumably, this same type of conjugation is responsible for the low energy (n, π^*) transition in flavonol.

ABSORPTION AND FLUORESCENCE SPECTRA OF THE CHELATES

The absorption and fluorescence spectra of the flavonol-aluminum (III) chelates are presented in Figure 16. All of the chelates, no matter what the stoichiometry, have the same spectra. The absorption spectrum consists of two major transitions above 250 nm. The maxima of these absorption bands are located at 326 and 405 nm and are identical to the ones described by Urbach (53). It is also apparent from the molar absorptivities of these bands that (π, π^*) transitions are involved. The fluorescence

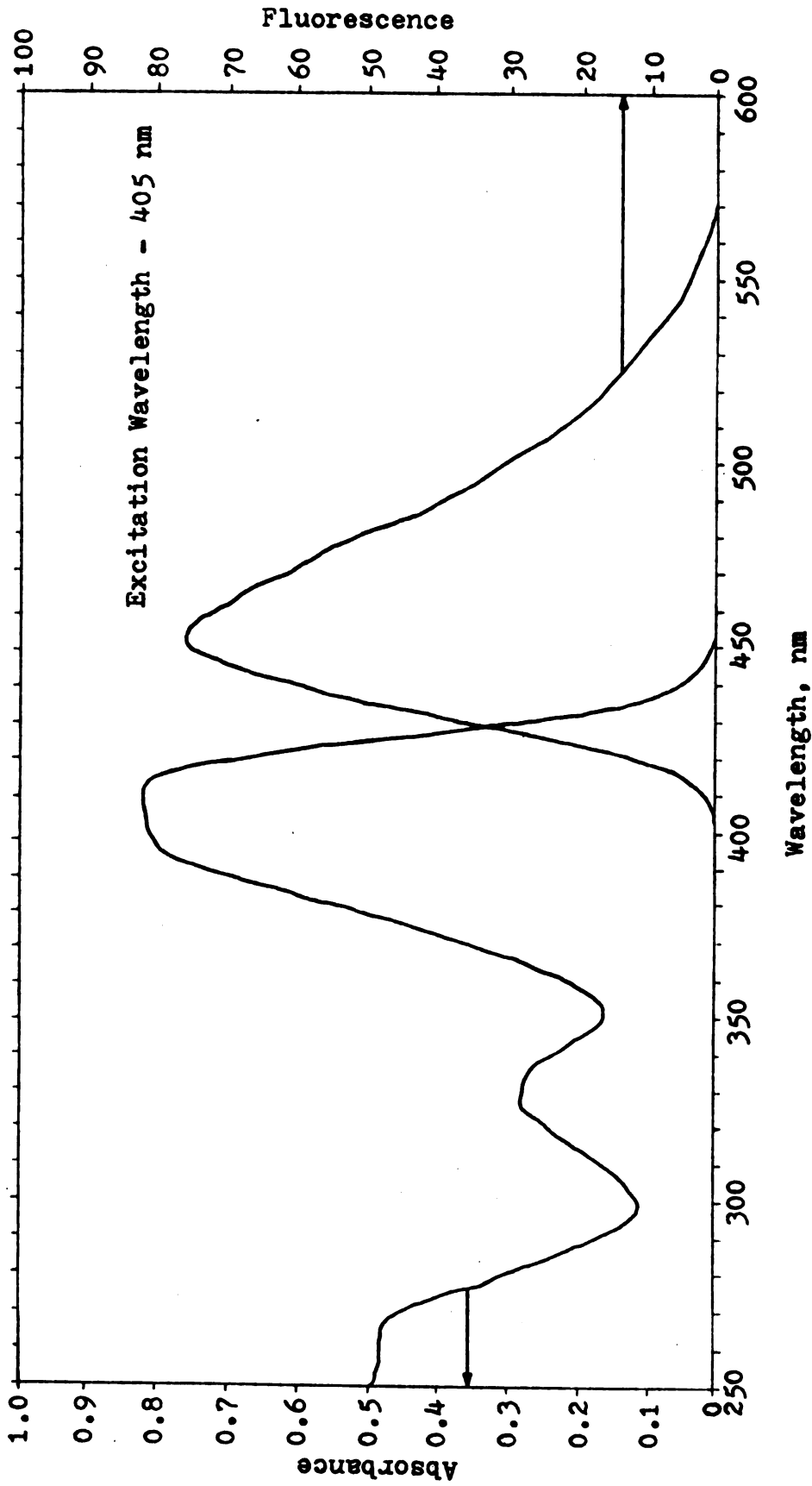


Figure 16. Absorption and Fluorescence Spectra of the Aluminum-Flavonol Chelates in Absolute Ethanol.

spectrum for the chelates consists of a single band with its maximum located at 450 nm. It also appears that the fluorescence originates from a (π, π^*) transition.

EMISSION SPECTRA OF THE CHELATES AT 77 K

The emission spectra for the 2:1 and 6:1 metal-to-ligand chelates are presented in Figure 17. The spectra consist of two major bands. The band at 672 nm has been attributed to the emission of phosphorescence, while the band near 460 nm has been attributed to delayed fluorescence. The location and intensity of the delayed fluorescence band is dependent on the stoichiometry of the chelate, the wavelength of excitation and the presence of oxygen. Table III summarizes these dependencies. The data contained in this table have not been corrected for inner-filter effects or for variations in the emission signals due to sample positioning.

As was the case for flavonol, the excitation of the chelates to the second excited state (326 nm) is more efficient in the production of delayed fluorescence in most instances. The only exception to this phenomenon is the 6:1 chelate in the presence of oxygen. In addition, it is also apparent that there are some major differences in the emission characteristics of the two chelates. The presence of oxygen with the 2:1 chelate seems to have little effect on the intensity of the emitted delayed fluorescence. On

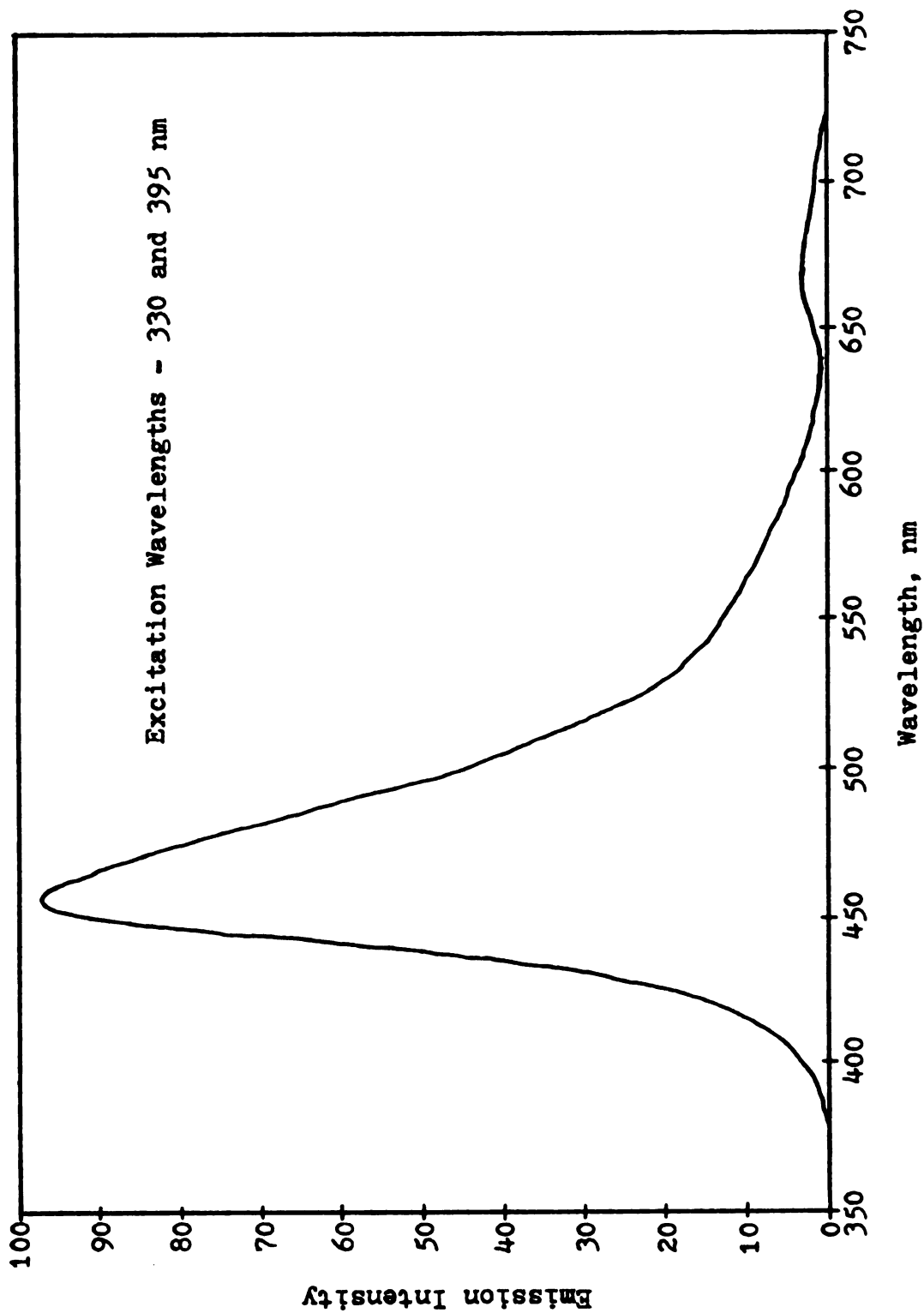


Figure 17. Emission Spectrum at 77 K for the 2:1 and 6:1 Aluminum to Flavonol Chelates in Absolute Ethanol.

Table III

Dependence of Delayed Fluorescence on Chelate Stoichiometry,
Excitation Wavelength and the Presence of Oxygen

Chelate Al:Flavonol	Excitation Wavelength	Emission Maximum	Emission Intensity	$\frac{I(330 \text{ nm})}{I(395 \text{ nm})}$	Dissolved Oxygen
2:1 ^a	330	460	1000	2.96	Present
	395	460	338		Present
2:1 ^a	330	460	738	2.88	Absent
	395	460	256		Absent
6:1 ^b	330	450	200	1.00	Present
	395	450	200		Present
6:1 ^b	330	455	385	2.28	Absent
	395	455	169		Absent

^aFlavonol concentration - 3.2×10^{-4} M

^bFlavonol concentration - 1.2×10^{-4} M

the other hand, the presence of oxygen has a marked effect on the 6:1 chelate. In this case, the production of delayed fluorescence from excitation at 330 nm is greatly decreased. In fact, the fluorescence intensity is the same for both excitation wavelengths. Upon the removal of oxygen, the production of delayed fluorescence from excitation at 330 nm increases although the efficiency is not as high as for the 2:1 chelate. This phenomenon may be explained by the following argument.

If the mechanism for the production of delayed fluorescence in the chelates is similar to the one proposed for flavonol, then the emission could occur in the following fashion. Figure 18 shows the energy level diagrams for the proposed mechanism. Figure 18A shows excitation to the second excited singlet state (326 nm). A slight amount of energy is lost to internal conversion before the intersystem crossing occurs. The triplet state is then formed, and some dissipation of the excess vibrational energy occurs before a second intersystem crossing takes place. Note that the loss of the vibrational energy does not result in a triplet state of lowest vibrational energy. During the second intersystem crossing, energy is again lost which results in a singlet state from which the delayed fluorescence originates.

Figure 18B shows excitation to the first excited singlet state (405 nm). Again, a slight amount of energy is lost before the intersystem crossing can occur. Upon crossing,

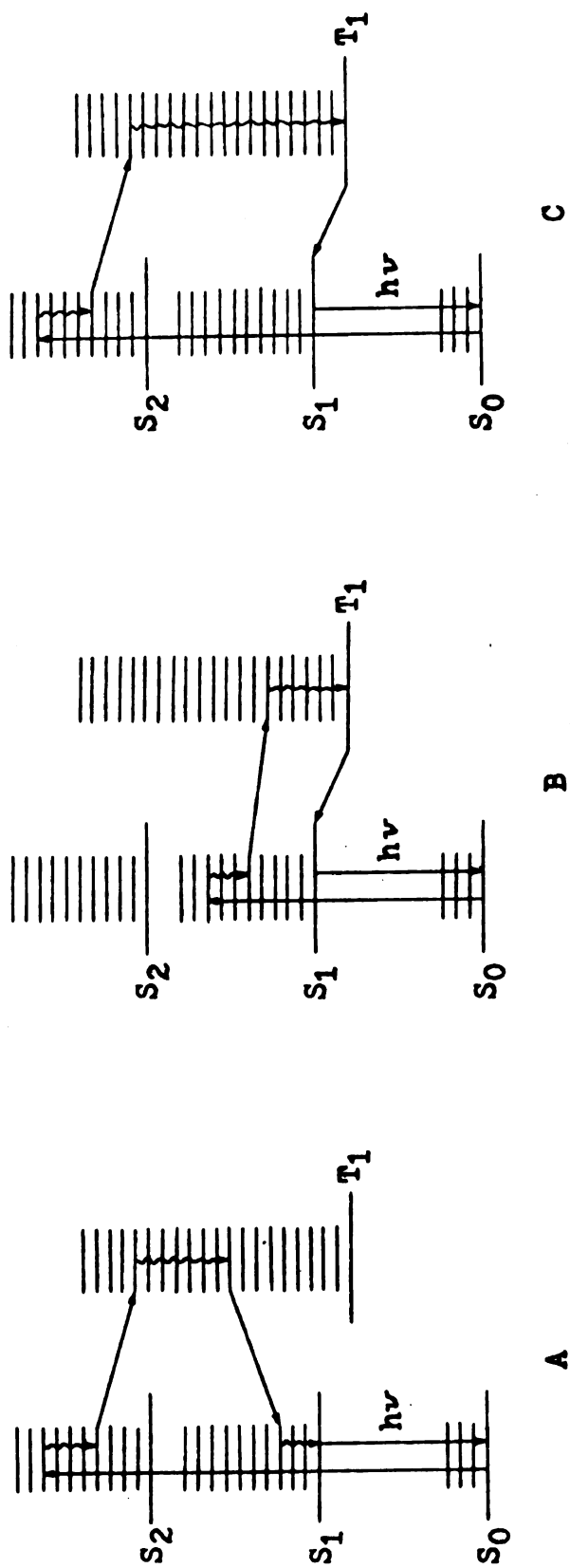
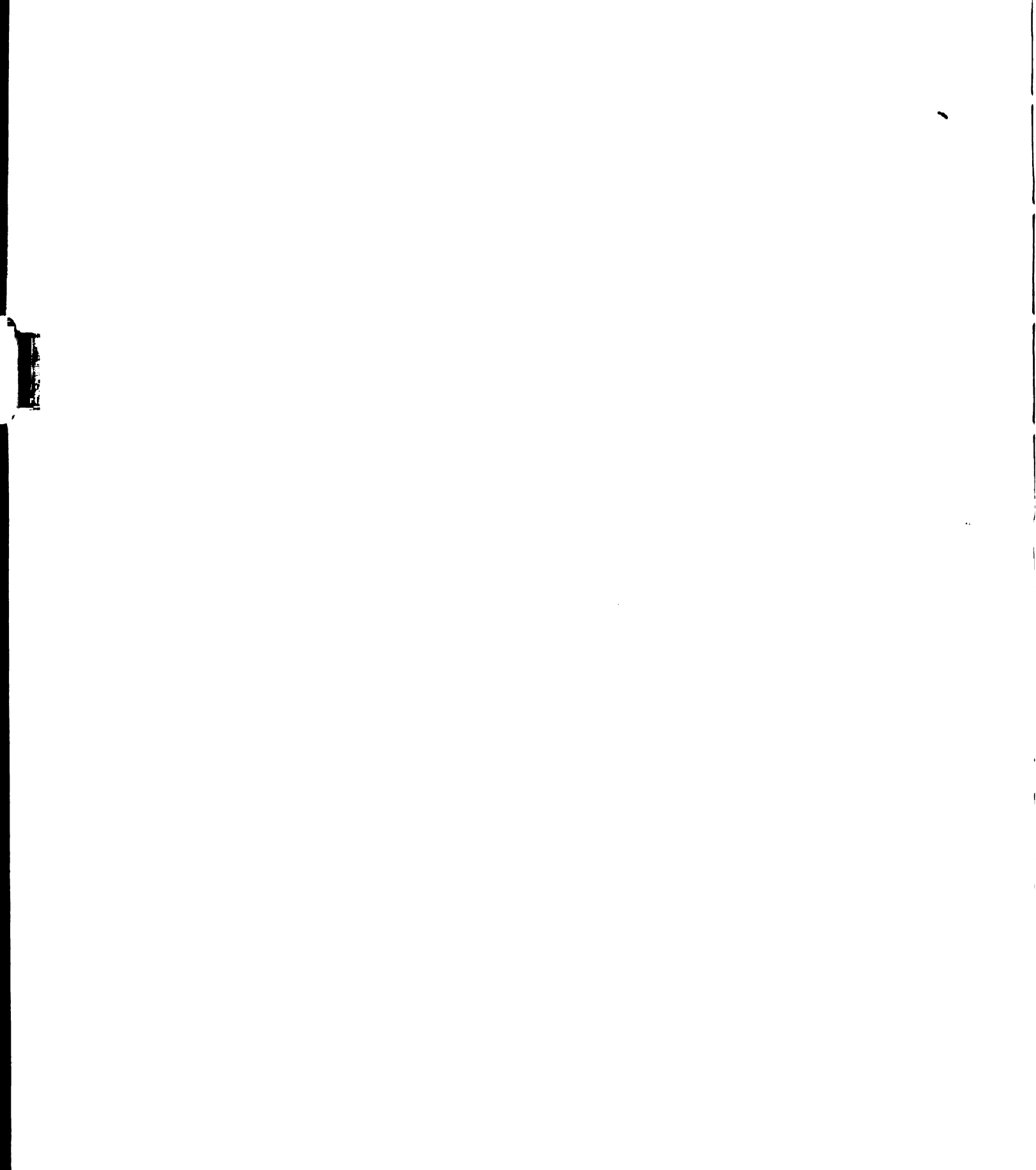


Figure 18. Energy Level Diagrams for the 2:1 and 6:1 Aluminum to Flavonol Chelates in Absolute Ethanol at 77 K.

the resultant triplet state is formed with a relatively little excess of vibrational energy. Consequently, before a second crossing can occur, the molecule loses almost all of this excess energy, and the second crossing must occur with an increase in energy. Note that this was not the case when the molecule was excited to the second electronic state. As a result, the production of delayed fluorescence in this second case is much less efficient. Since this mechanism was used for flavonol to explain this phenomenon, it seems likely that the emission mechanism for the 2:1 chelate would be similar, since the data are nearly the same. On the other hand, it would not explain the data which were obtained for the 6:1 chelate.

Apparently, the presence of oxygen has a serious effect on the production of delayed fluorescence from this chelate. Note that the production is fairly inefficient even though the fluorescence is excited at the 326 nm band. This phenomenon may be explained by the energy level diagram in Figure 18C. This figure shows that the amount of vibrational energy which is lost to internal conversion in the triplet state is increased by the presence of oxygen, and a low energy level is reached before the second intersystem crossing can occur. Consequently, it is expected that the production efficiency of delayed fluorescence for this mechanism would be the same as for the mechanism shown in Figure 18B where the molecule is excited only to the first



electronic state. On the other hand, upon the removal of oxygen from the system, excitation at 326 nm now results in a more efficient production of delayed fluorescence, since the mechanism shown in Figure 18A is now in operation.

At this point, an important question arises. Why does the presence of oxygen affect the 6:1 and not the 2:1 chelate? Perhaps the answer to this question lies in the structural differences between the two chelates. Since it is believed that the 6:1 chelate is much larger than the 2:1 chelate, it is likely that the quenching of the larger molecule by oxygen is much more efficient. Other evidence also seems to support this argument. Note that even in the absence of oxygen, the intensity ratio (I_{330}/I_{395}) for the delayed fluorescence from the 6:1 chelate is not as large as it is for the 2:1 chelate. Apparently, internal conversion of the triplet state for the 6:1 chelate is more efficient even without the presence of molecular oxygen. Consequently, it is logical to assume that oxygen would have a greater effect on the internal conversion processes of the 6:1 chelate, and as a result, the production of delayed fluorescence is decreased.

Unlike flavonol, the delayed fluorescence for the two chelates occurs at nearly the same wavelength as the prompt fluorescence. Since it is fairly certain that the prompt fluorescence originates from a (π, π^*) excited state, it then follows that the delayed fluorescence emanates from that same state. However, for flavonol, the delayed

fluorescence seems to originate from a (n, π^*) excited state. Consequently, it appears that upon chelation, the lowest lying (π, π^*) transition of flavonol (344 nm) undergoes a bathochromic shift to 405 nm. On the other hand, the low lying (n, π^*) transition of flavonol (410 nm) would be expected to undergo a hypsochromic shift and as a result, it is lost under the (π, π^*) manifolds of the chelate absorption spectrum. Therefore, the (π, π^*) transition at 405 nm is now the lowest energy singlet transition, and the delayed fluorescence is expected to originate from this excited state.

CHELATE STOICHIOMETRIES

Basic Solutions

As noted by Urbach (53), two chelates are formed under mildly basic conditions. When the hydroxide to aluminum (III) ratio was one, a chelate with an aluminum to flavonol ratio of 2:1 was formed. Upon standing, further chelation occurs, and a 1:1 chelate is formed. When the hydroxide to aluminum (III) ratio was raised to 2.5, only the 1:1 chelate was formed. In solutions where the hydroxide to aluminum (III) ratio exceeded 2.5, no chelate formation was indicated.

Neutral Solutions

The term "neutral" in this case indicates that no acid or base has been added to the test solutions. As noted by Urbach, the existence of two chelates is indicated by photometric studies. In freshly prepared solutions, the existence of a chelate with a metal-to-ligand ratio of 2:1 was indicated. Upon standing for two weeks, further chelation resulted in the formation of a 1:1 chelate in addition to the 2:1 species. A 6:1 metal-to-ligand chelate has also been found to exist, but this chelate could only be detected with fluorometric methods.

Acidic Solutions

Present studies indicate that two chelates are formed in the presence of acid when the acid to aluminum (III) ratio was 5:1. A 1:1 chelate can be detected by either a photometric or fluorometric titration of aluminum (III) with flavonol as shown in Figure 19. The other chelate which has a metal-to-ligand ratio of 2:1 can only be detected by a fluorometric titration. No significant stoichiometric changes occur with time except that the break for the 2:1 chelate becomes better defined.

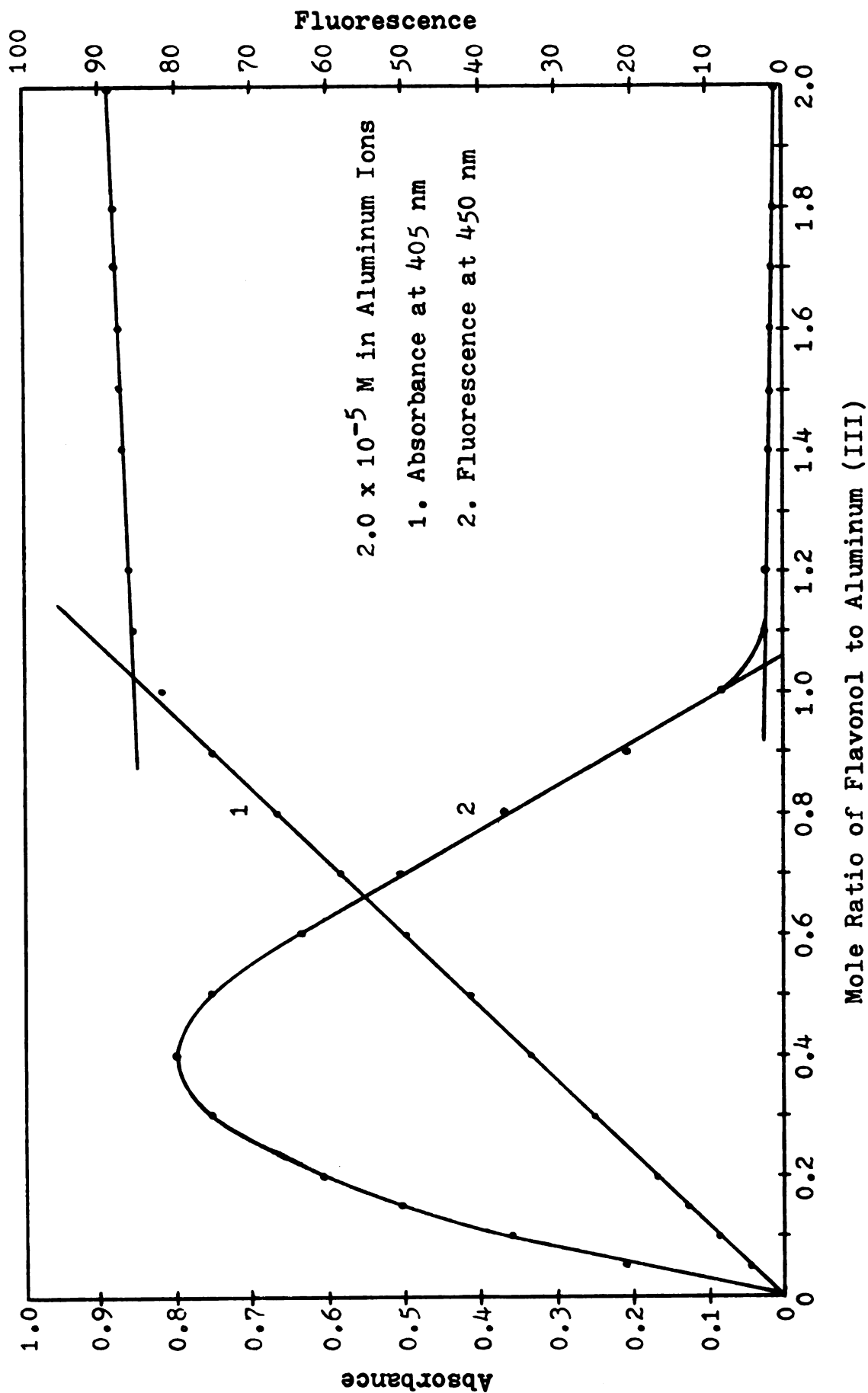


Figure 19. Spectrophotometric and Spectrofluorometric Titration Curves for Aluminum (III) Titrated with Flavonol with the Proton to Metal Ion Ratio 5:1.

RAMAN SPECTRA

Of all the chelates, perhaps the most interesting are the 2:1 and 6:1 chelates which are formed in "neutral" solutions of absolute ethanol. Urbach (53) has noted that the 6:1 species is much more fluorescent than the 2:1 chelate. Since an increase in structural rigidity can be responsible for an increase in quantum efficiency, it was suspected that the 6:1 chelate might have an unusually rigid structure, which might account for the large increase in fluorescence efficiency. If this were the case, Raman and infrared spectroscopy should give an indication of the nature of this structure. Consequently, samples of flavonol and the two chelates were subjected to analysis by these techniques.

The Raman spectra for these sample have been tabulated in Table IV. The Raman spectrum of flavonol was obtained with a solid sample since the solubility of flavonol in absolute ethanol was not large enough to obtain reasonably intense scattering peaks. The 2:1 and 6:1 chelate spectra were obtained with ethanolic solutions which were 0.245 and 0.048 molar in flavonol, respectively.

It is apparent from the data contained in Table IV that there is structurally little difference in the chelates as far as flavonol is concerned. Since the reading error is about $\pm 3 \text{ cm}^{-1}$, apparently there are no significant shifts in the spectral features in either spectrum. There is only one scattering peak which is not common to both of the

Table IV
Raman Spectra of Flavonol, 2:1 and 6:1
Metal-to-Ligand Chelates

Flavonol		2:1 Chelate		6:1 Chelate	
cm ⁻¹	Intensity	cm ⁻¹	Intensity	cm ⁻¹	Intensity
198	3	275	1	278	1
263	3	402	1	402	1
297	3	432*	1	430*	5
332	1	490	2	492	5
378	1	520	1	520	1
433	4	578	15	578	46
438	3	617	1	617	1
510	7	667	3	667	8
579	9	683	6	683	17
618	3	844	6	843	14
624	3	881*	2	881*	36
672	9	997	12	997	32
777	3	1044*	1	1052*	7
836	8	1097*	1	1097*	9
988	18	1152	7	1153	22
997	13	1168	3	1169	3
1032	3	1187	6	1188	17
1148	4	1235	14	1235	46
1187	11	1278*	--	1278*	5
1210	1	1327	9	1328	29
1225	3	1357	2	1358	9
1245	3	1427	10	1428	39
1277	3	1443	12	1444	55
1307	23	1459	7	1458	30
1318	9	1492	2	1492	3
1350	8	1497	1	1498	1
1410	7	1529	12	1530	47
1443	11	1557	9	1558	37
1468	14	1573	1	1573	2
1480	1	1595	24	1597	94
1489	4	1614	15	1615	57
1565	98	2875*	54	2876*	58
1594	79	2925*	100	2927*	100
1618	100	2969*	40	2971*	43
3070	3	3073	1	3073	--
3077	2				

* Ethanol Bands

chelate spectra and it appears at 3073 cm^{-1} for the 2:1 chelate. Since a vibrational peak in this spectral region is normally associated with the -OH stretch of alcohols, it may indicate that some free flavonol is present in solution. Unfortunately, the concentration of flavonol in the 6:1 chelate solution could not be increased because of the large scattering background which was encountered. Consequently, this peak in the spectrum of the 6:1 chelate may not be intense enough to be detected, and as a result, no conclusions can be drawn.

The only other interesting spectral features in the chelate spectra are the scattering peaks which are located in the region near 280 cm^{-1} . These peaks are due to aluminum (III) in solution. When no flavonol is present, this scattering peak occurs at 282 cm^{-1} . There is a shift to 278 cm^{-1} for the 6:1 species and to 275 cm^{-1} for the 2:1 chelate. These shifts may indicate that the aluminum (III) structure in the 6:1 chelate is fairly similar to the structure of normally solvated aluminum ions even though chelation has occurred. Unfortunately, these scattering peaks are extremely weak, even under conditions of high spectrometer sensitivity. As a result, no additional conclusions can be drawn.

INFRARED SPECTRA

The infrared spectra for flavonol, the 2:1 and 6:1 chelates are presented in Figures 20, 21 and 22, respectively. The flavonol spectrum was obtained from a potassium bromide pellet of the sample. The chelate samples were prepared as indicated in the Experimental chapter.

As was the case for the Raman spectra of the chelates, no apparent shifts were found between the chelate spectra. Again, there seems to be little structural difference in the two chelates as far as flavonol is concerned. However, one interesting piece of information was obtained from this study. Figure 23 presents the spectrum of the dry residue formed by the evaporation of ethanol from a solution of aluminum chloride. The sample for this spectrum was prepared in the same way as the chelates. Note that this spectrum is markedly different from that of absolute ethanol which is presented in Figure 24. This difference is explained by the fact that the residue actually contains very little free ethanol. Since this sample was evaporated to dryness, the spectrum is really that of the ethoxide ions and ethanol associated with aluminum (III). Upon re-inspection of the chelate spectra, it is evident that the spectral features found in the residue spectrum are quite prominent in the 6:1 chelate spectrum, but not in the 2:1 spectrum. In fact, parts of the 6:1 spectrum are almost obliterated by the presence of these features. Based on these

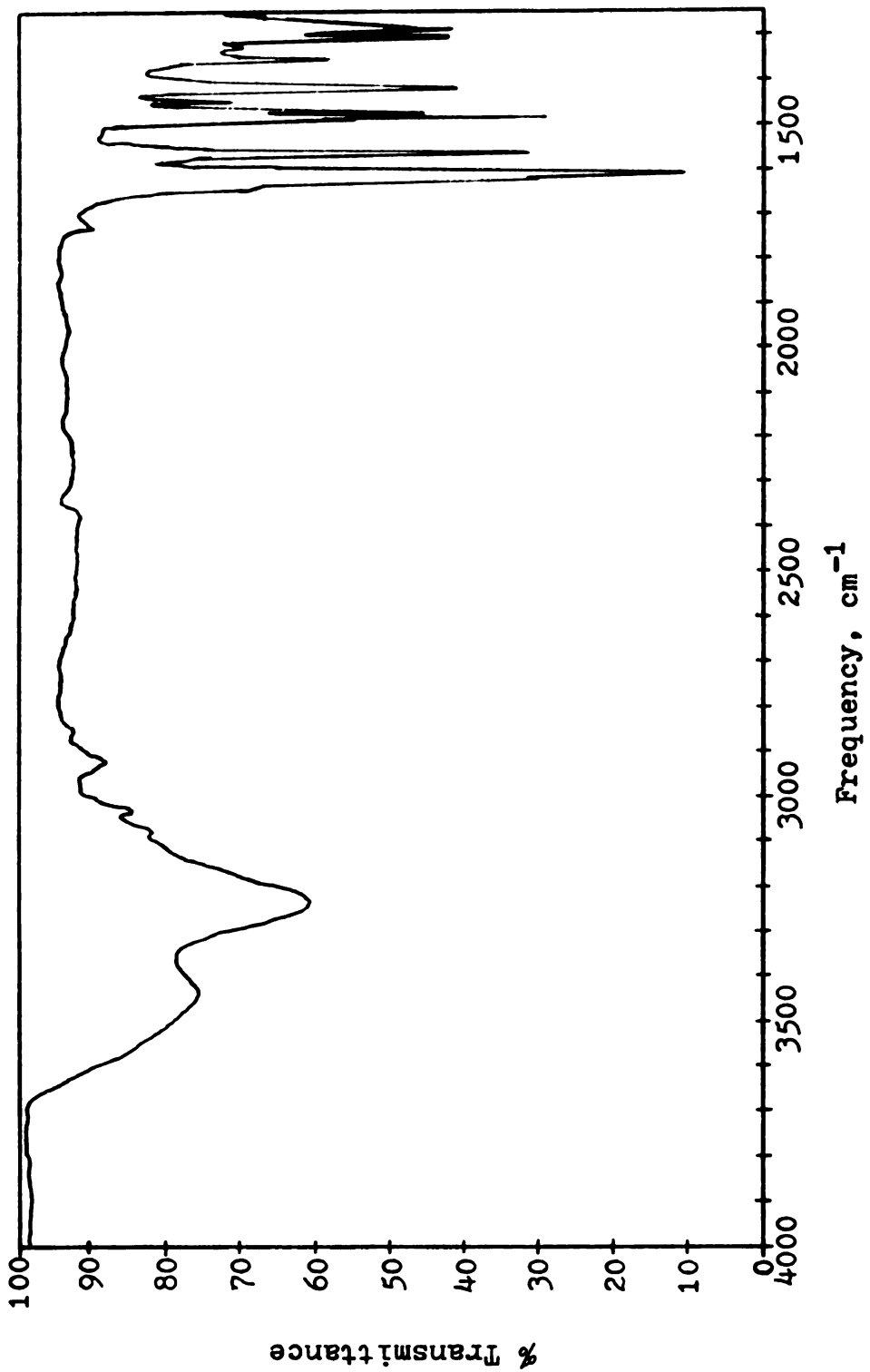
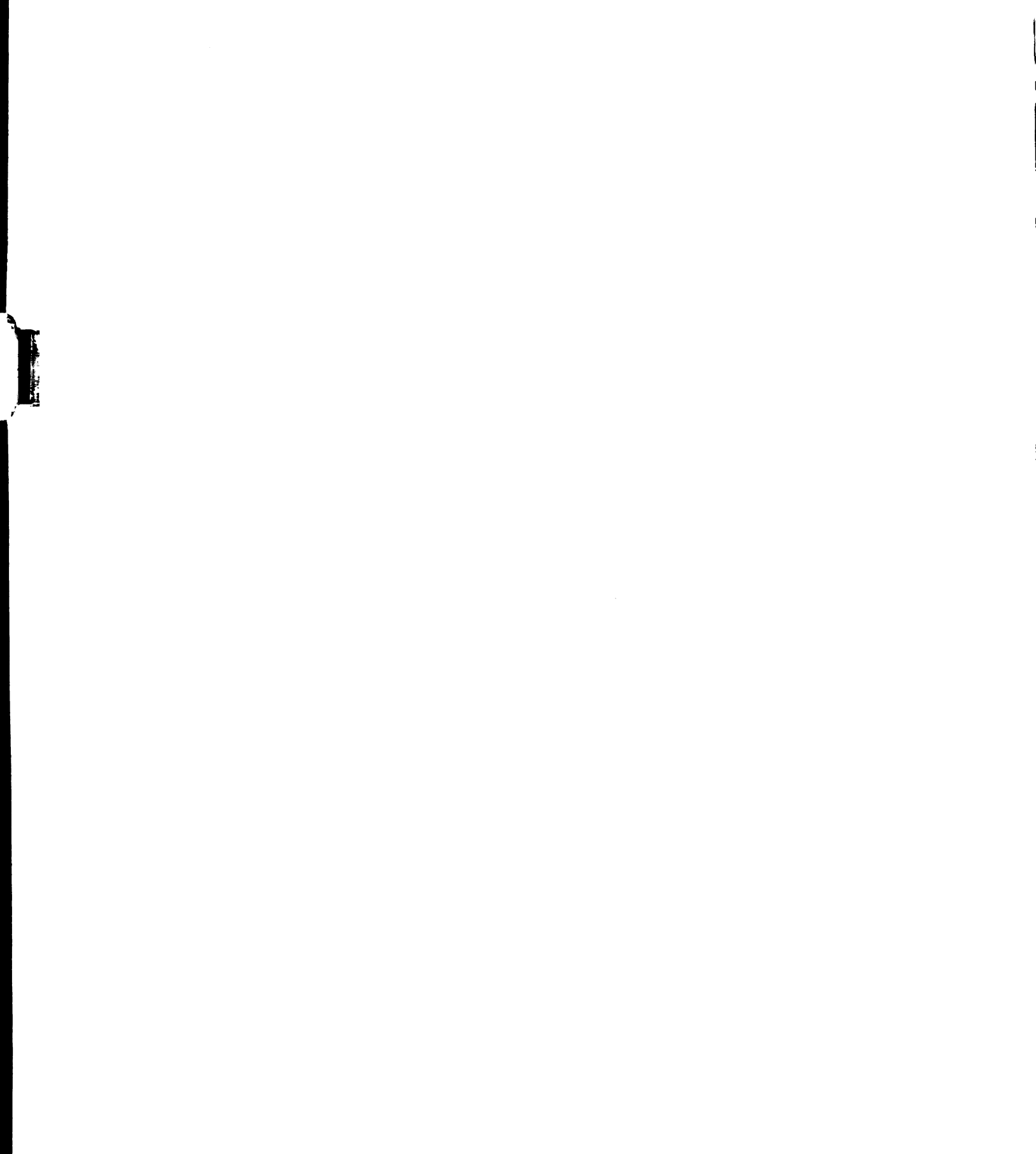


Figure 20A. Infrared Absorption Spectrum of Flavonol.



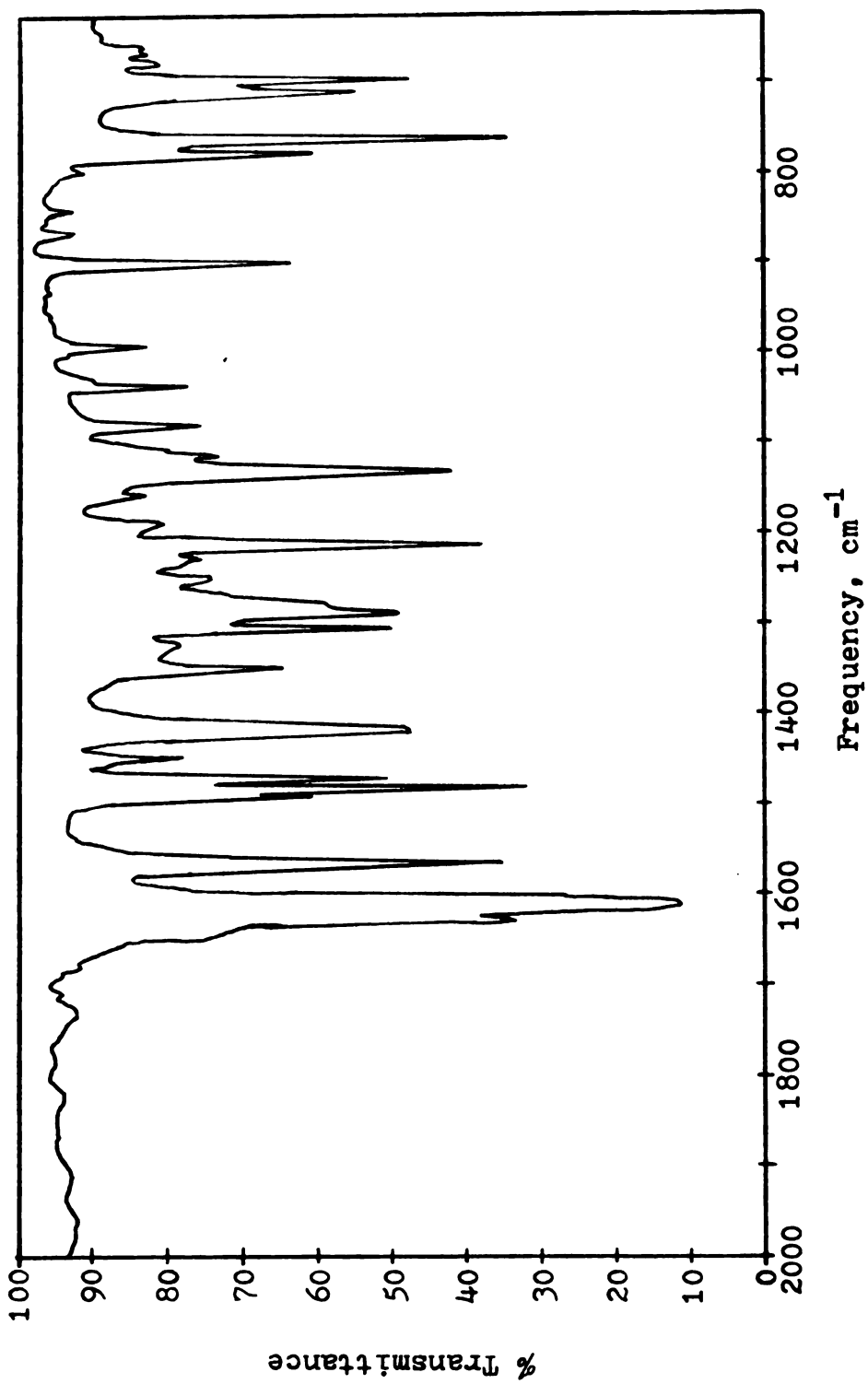


Figure 20B. Infrared Absorption Spectrum of Flavonol.

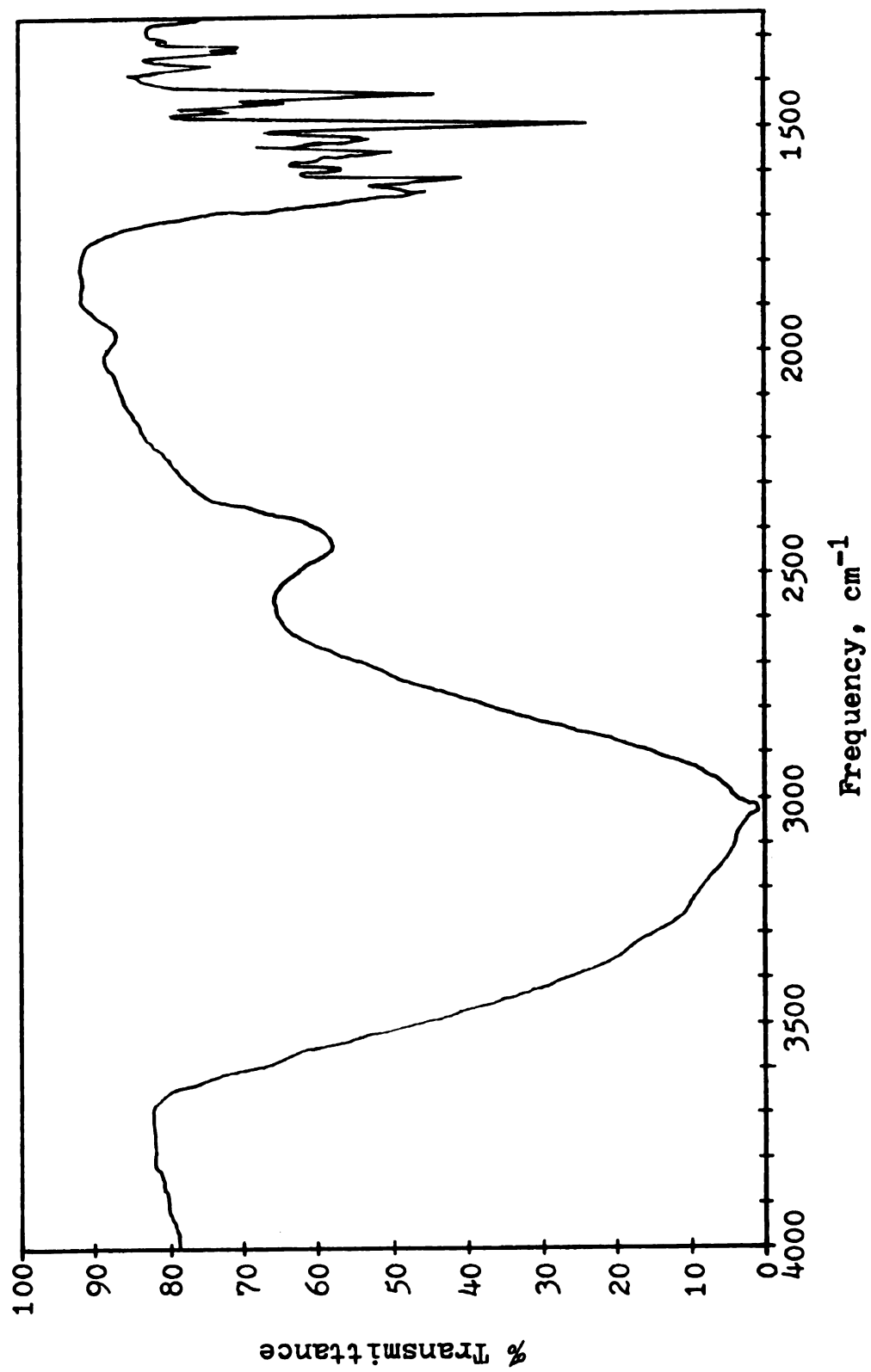


Figure 21A. Infrared Absorption Spectrum of the 2:1 Aluminum to Flavonol Chelate.

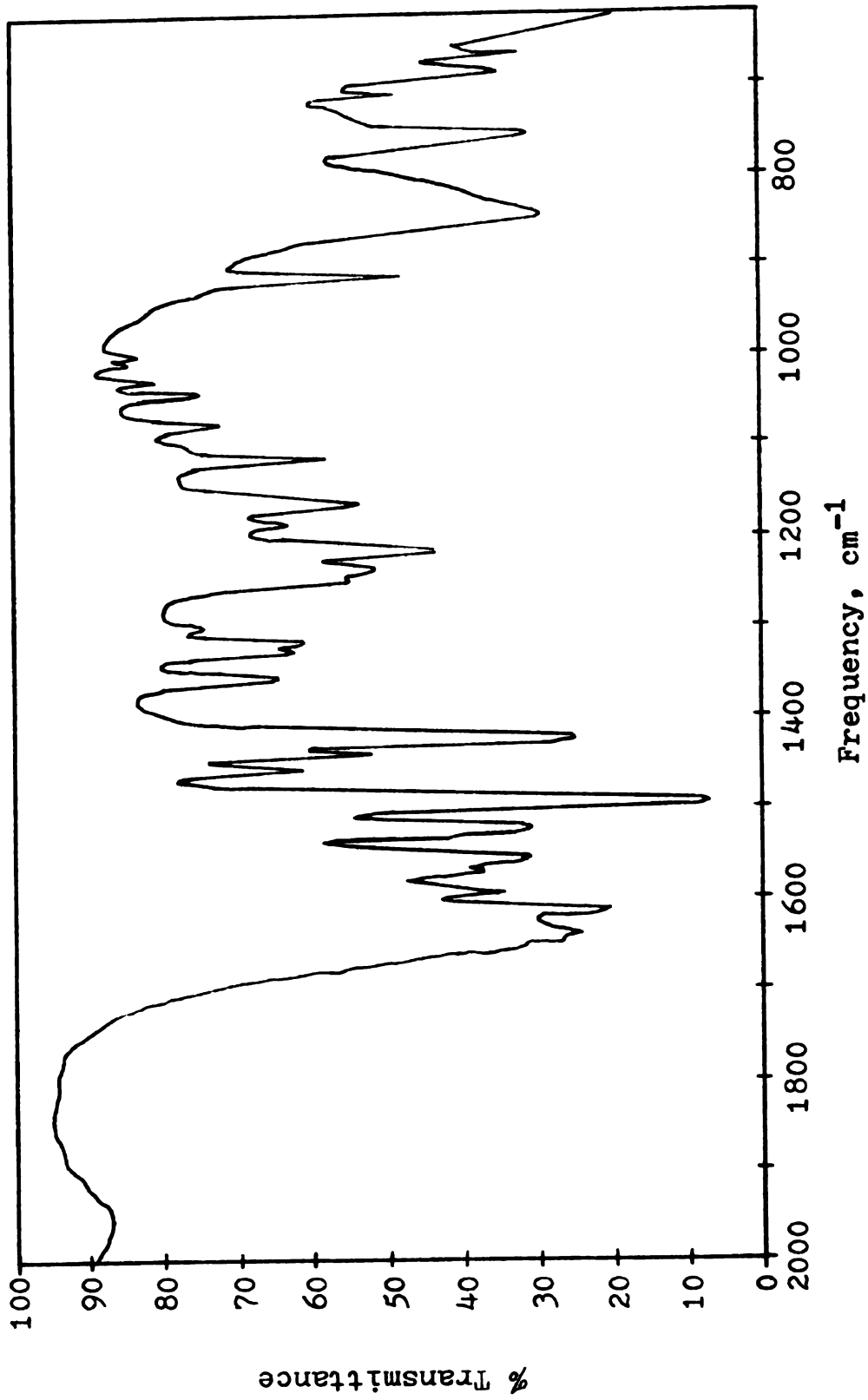


Figure 21B. Infrared Absorption Spectrum of the 2:1 Aluminum to Flavonol Chelate.

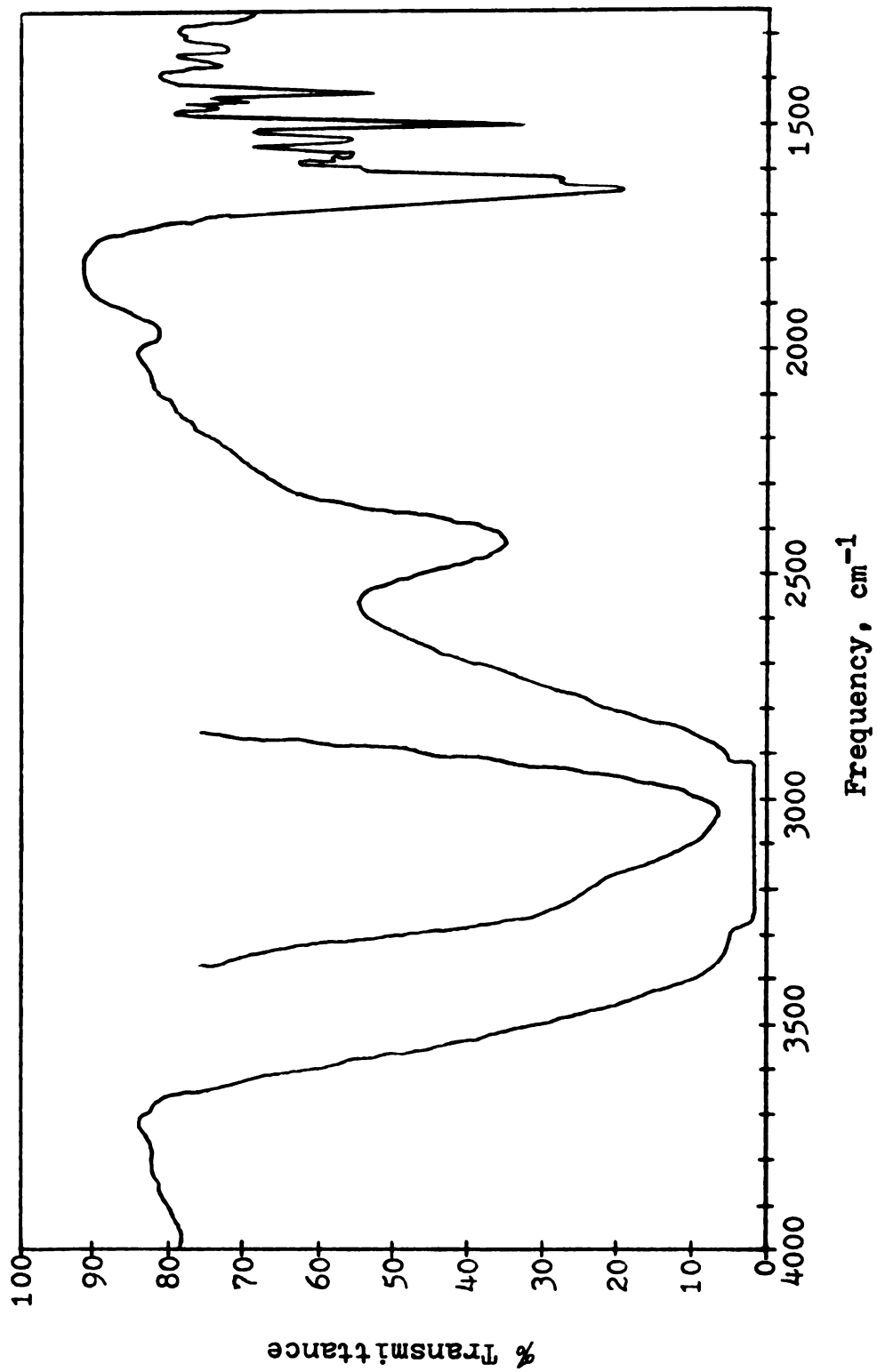


Figure 22A. Infrared Absorption Spectrum of the 6:1 Aluminum to Flavonol Chelate.

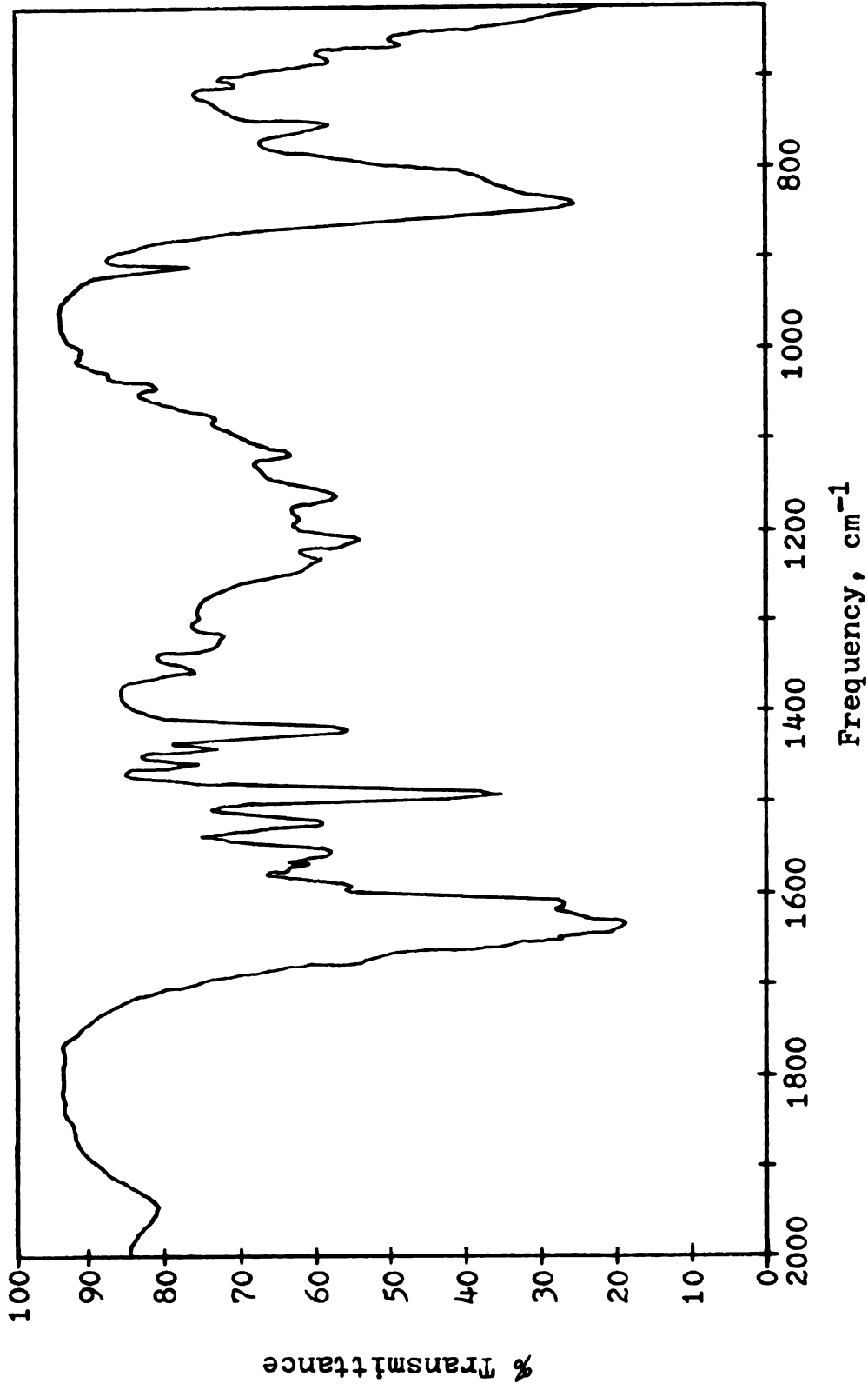


Figure 22B. Infrared Absorption Spectrum of the 6:1 Aluminum to Flavonol Chelate.

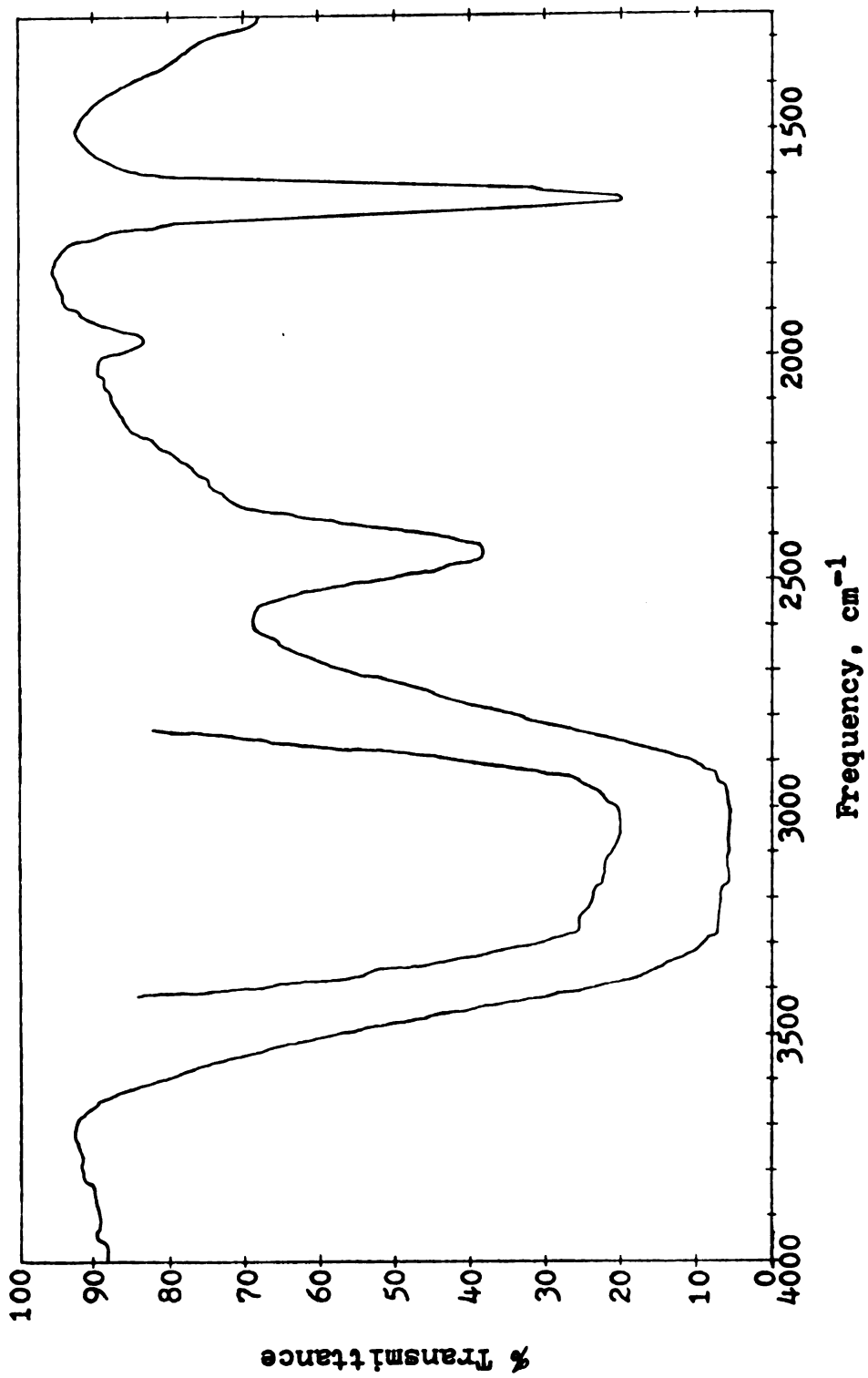


Figure 23A. Infrared Absorption Spectrum of the Residue Formed When the Solvent from an Alcoholic Solution of Aluminum Chloride is Evaporated.

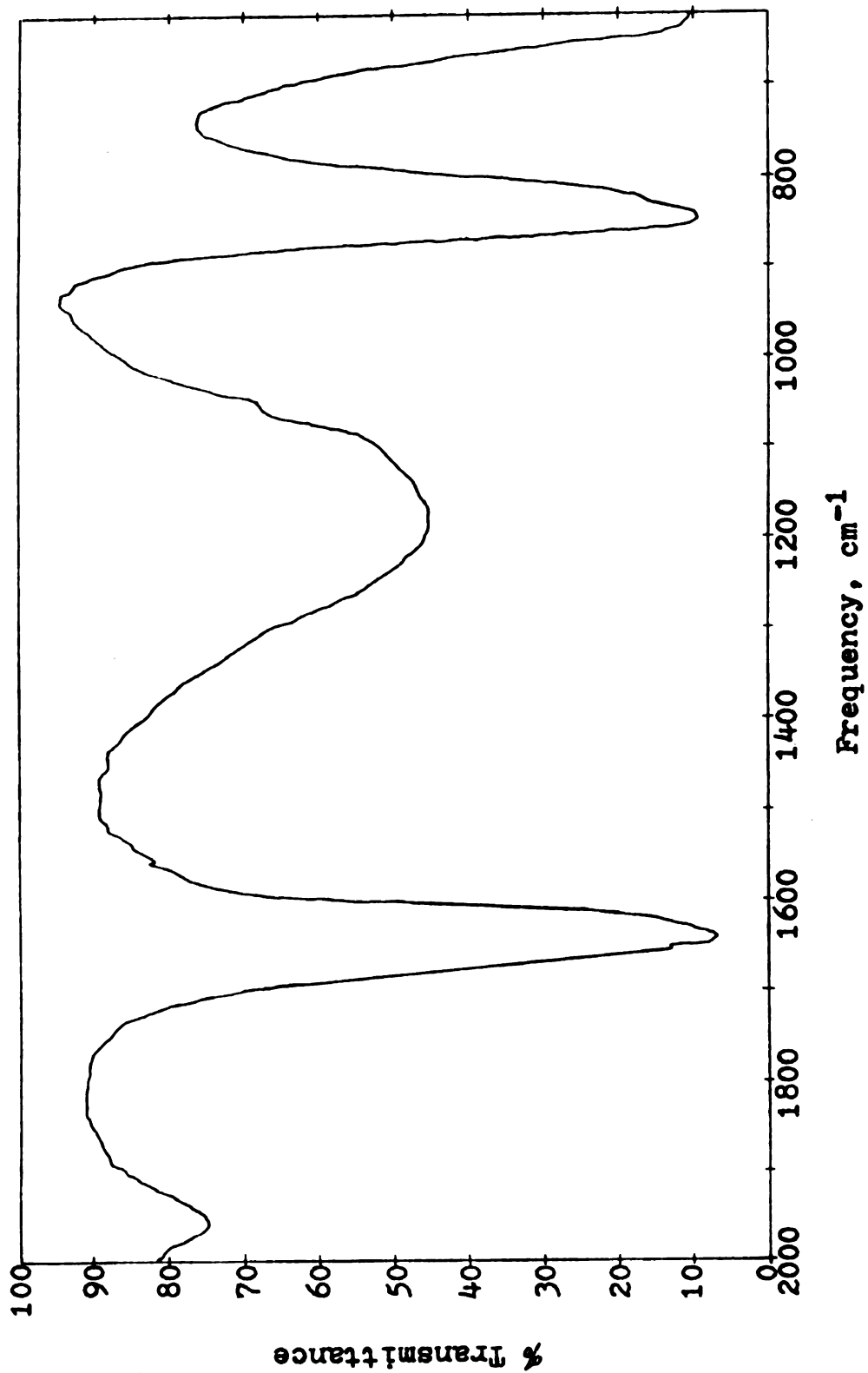


Figure 23B. Infrared Absorption Spectrum of the Residue Formed When the Solvent from an Alcoholic Solution of Aluminum Chloride is Evaporated.

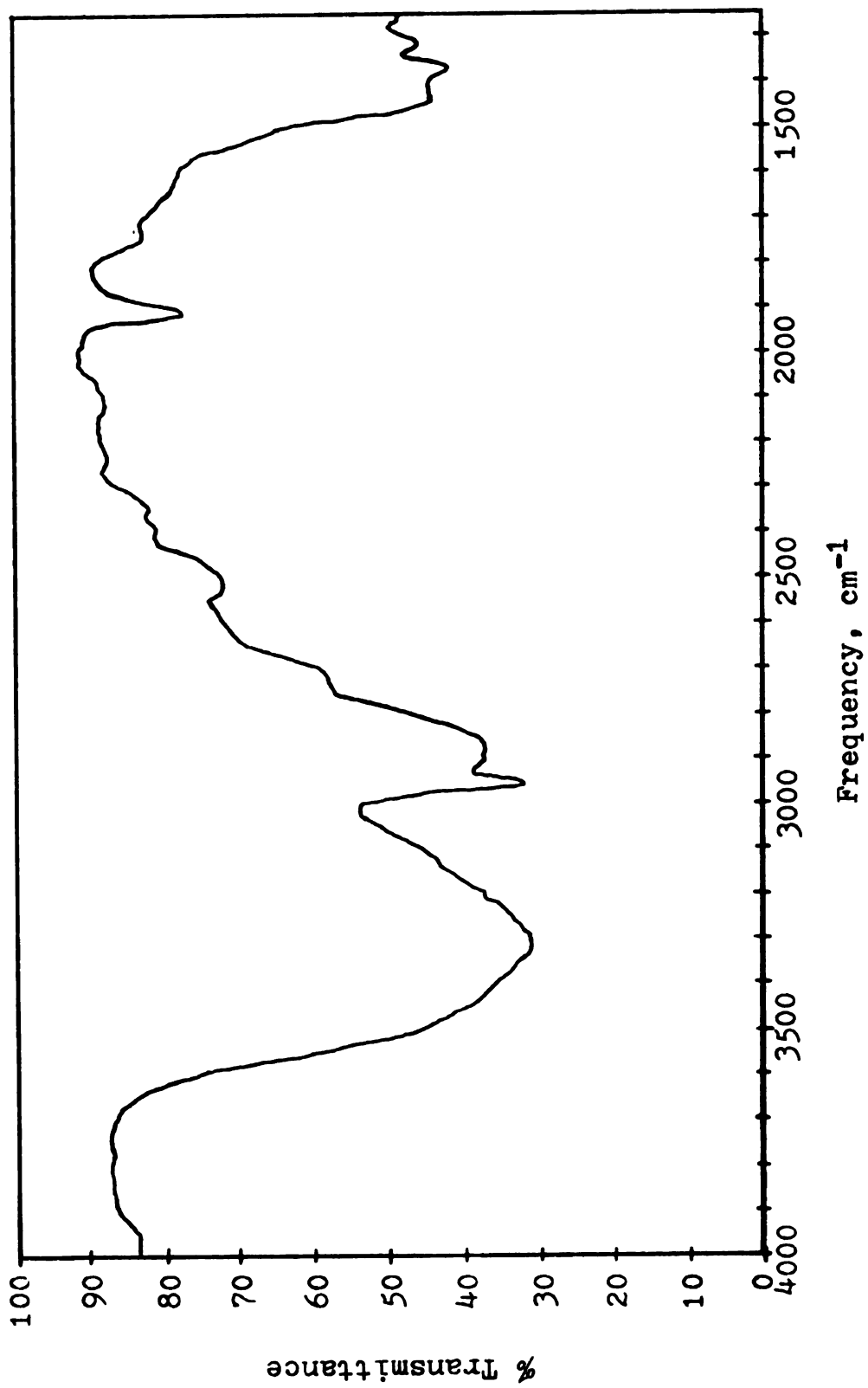


Figure 24A. Infrared Absorption Spectrum of Absolute Ethanol.

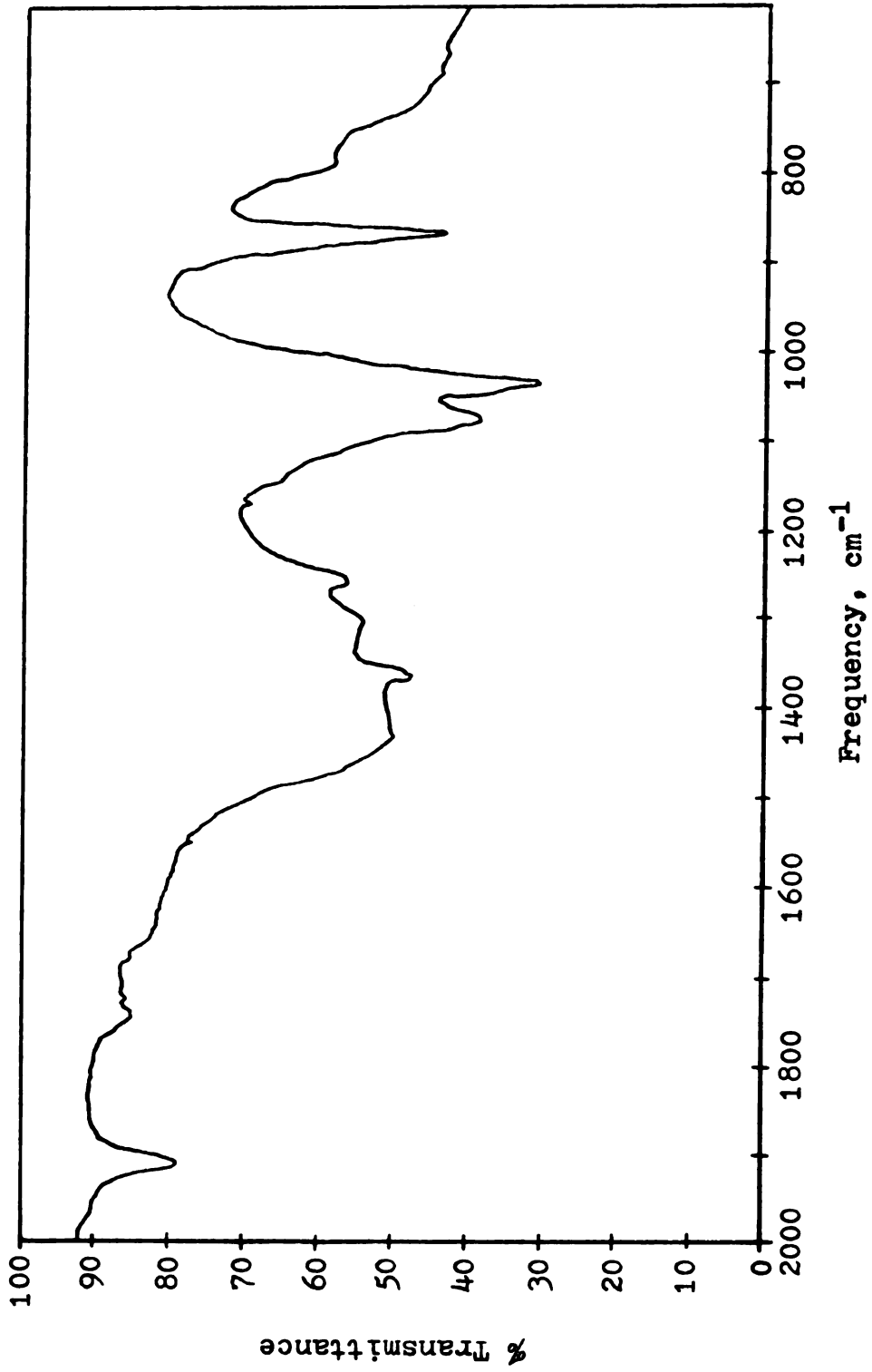


Figure 24B. Infrared Absorption Spectrum of Absolute Ethanol.

observations, it would appear that the 6:1 chelate is somewhat similar in structure to aluminum (III) in absolute ethanol.

ALUMINUM-27 NMR

Since very little information about the chelates was obtained from the Raman and infrared studies, aluminum-27 nmr spectroscopy was employed. A typical nmr spectrum for the chelates is shown in Figure 25. The chelate resonance peak lies to the high frequency side of the reference signal. The widths at half height for the reference signals were about 45 Hz, while for the chelate peaks, they ranged from about 350 Hz to a little greater than 400 Hz.

Figure 26 presents the shifts for the two chelates as a function of aluminum concentration, and it indicates that a concentration dependency exists. Since the concentrations used in this study are about one thousand times larger than those normally used in fluorescence studies, there is a good possibility that the chelate structures change with increasing concentration. It is interesting to note that as the concentration of aluminum (III) increases, the difference in the shifts decreases. This may indicate that at high concentrations, only one chelate exists in solution. This phenomenon may explain why the Raman and infrared spectra were identical for the two chelates.

Figure 27 shows the shift of the aluminum (III)

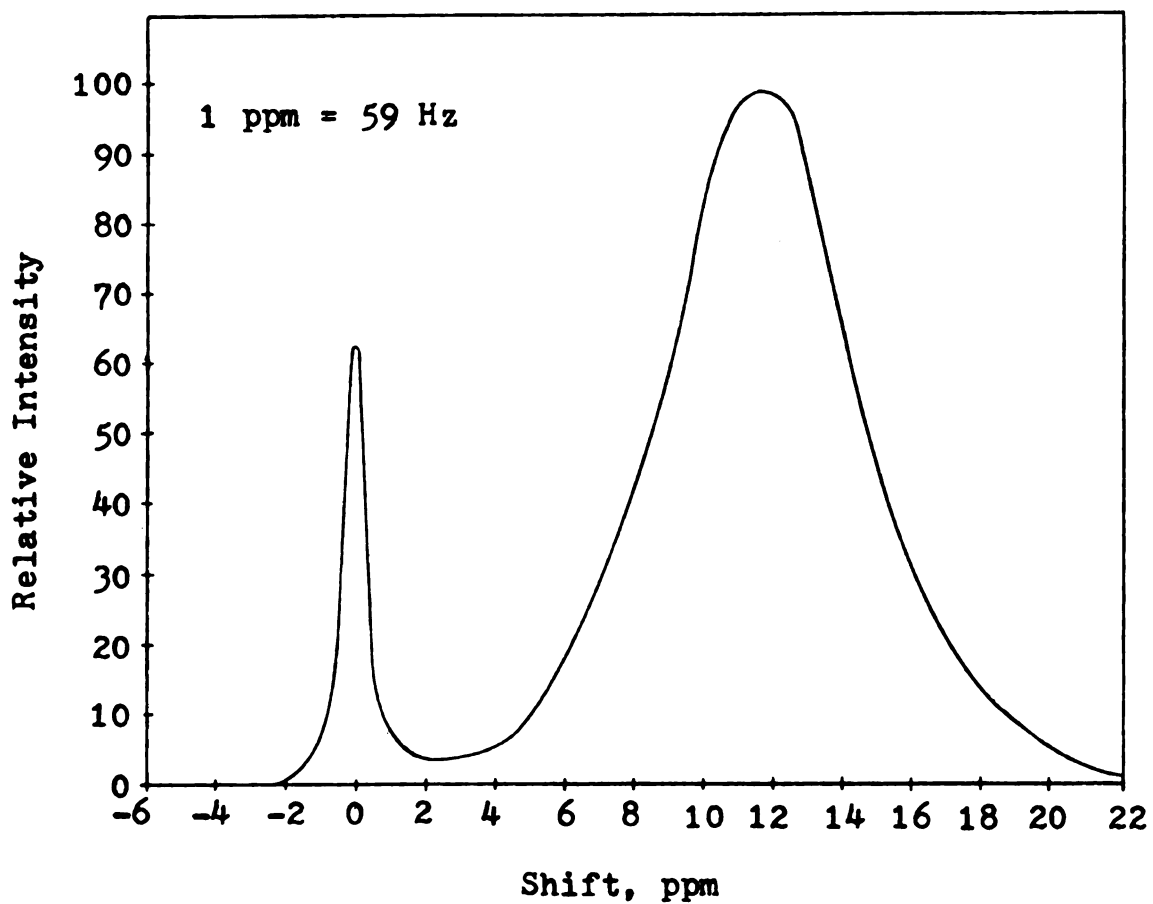


Figure 25. Typical Aluminum-27 NMR Spectrum for the Aluminum-Flavonol Chelates Formed in Absolute Ethanol.

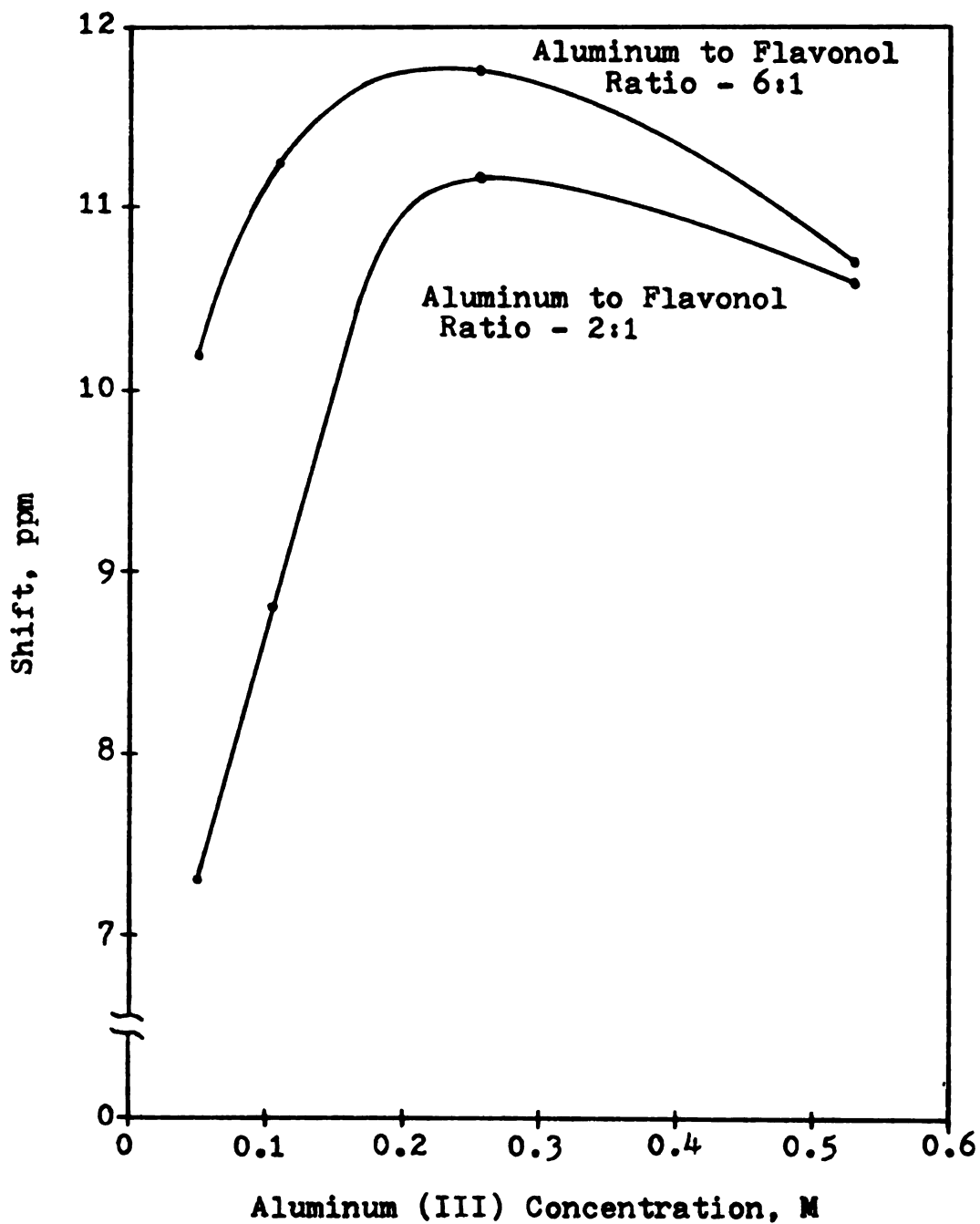


Figure 26. Aluminum-27 NMR Shift as a Function of Aluminum (III) Concentration for Solutions with 2:1 and 6:1 Aluminum to Flavonol Ratios in Absolute Ethanol.

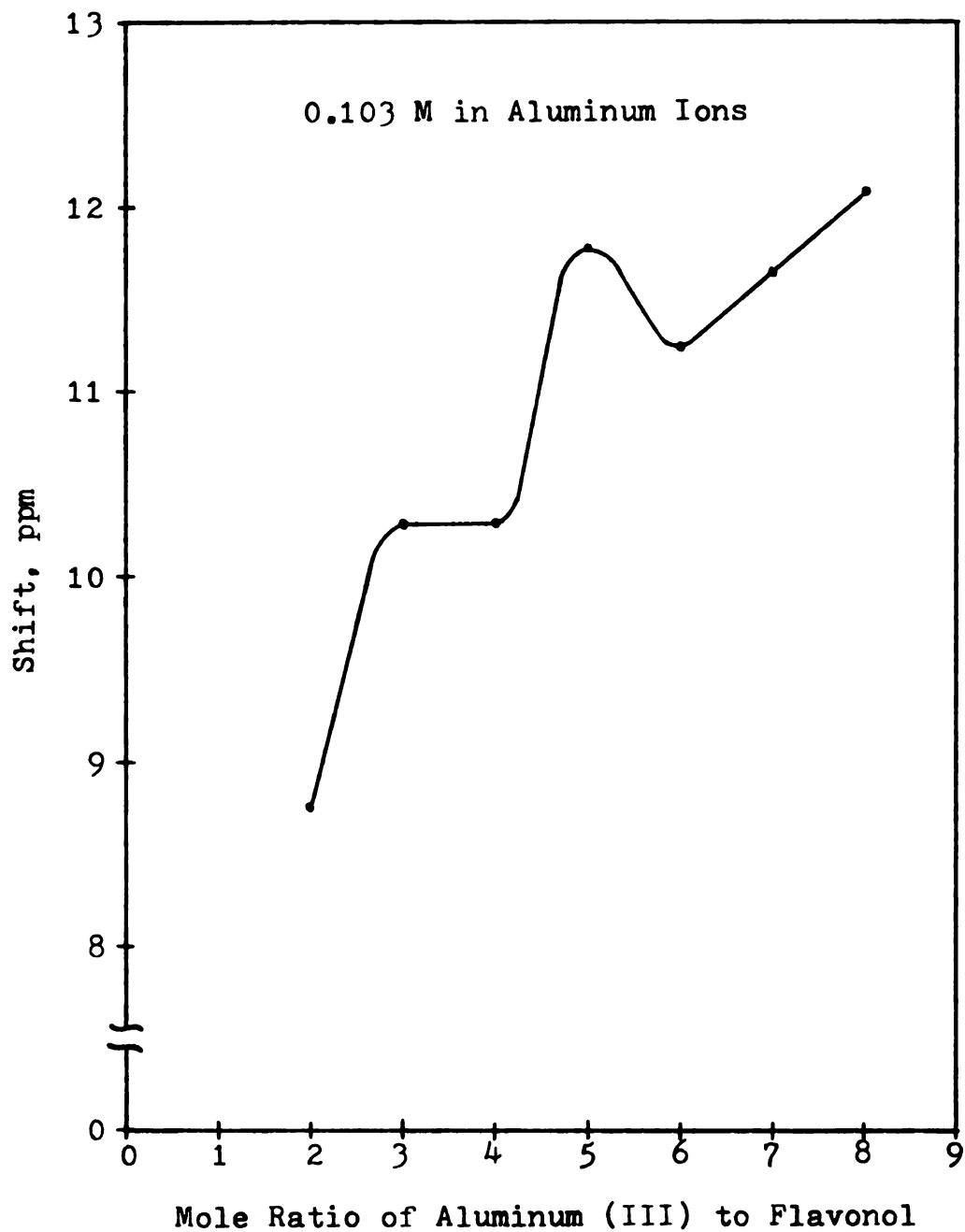


Figure 27. Aluminum-27 NMR Shift as a Function of the Aluminum to Flavonol Mole Ratio in Absolute Ethanol.

resonance signal as a function of the mole ratio of aluminum to flavonol for a constant aluminum (III) concentration of 0.103 M. The shape of this plot was quite unexpected and is difficult to explain. Apparently, some unknown significant structural change occurs at a mole ratio of five aluminum ions to one flavonol. The results of this aluminum-27 nmr study as well as the Raman and infrared studies indicate that the chelate(s) formed at high aluminum (III)-flavonol concentrations may be different from those formed at the concentration levels normally used in fluorescence studies.

POTENTIOMETRIC TITRATIONS

When aluminum salts are dissolved in protic solvents, the resultant solutions are acidic. Based on this characteristic, much useful information has been gained from the titration of these solutions with sodium hydroxide. Ohnesorge (55) determined from potentiometric titrations that five protons are released for every two aluminum ions which are solvated in absolute ethanol. In addition, he also found that with the presence of small amounts of water, the normal titration curve for aluminum chloride in absolute ethanol shows a shift toward higher proton to aluminum ratios. Figure 28 shows the potentiometric titration curve of anhydrous aluminum chloride in absolute ethanol. The inflection point of this curve occurs at a hydroxide to

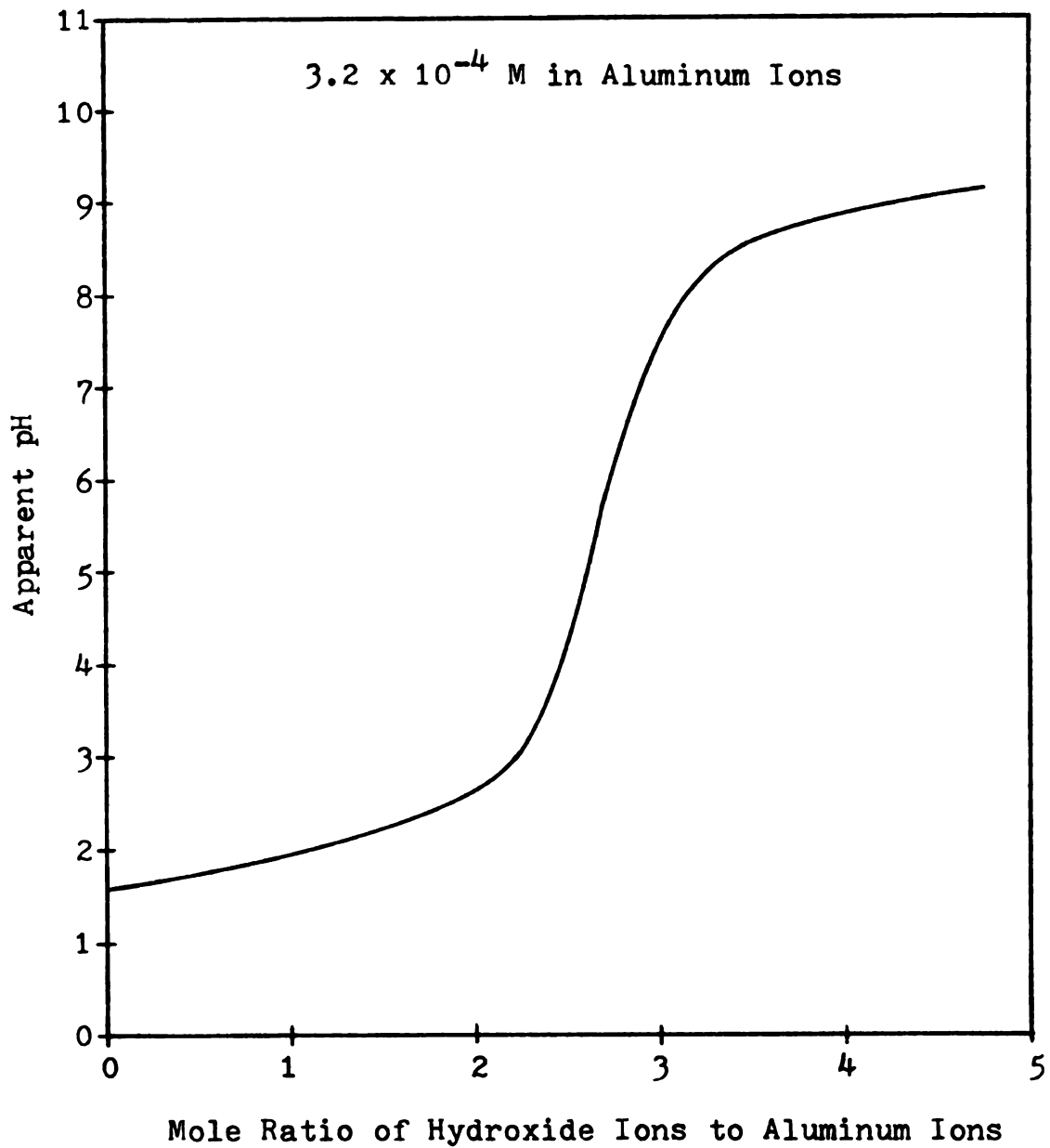
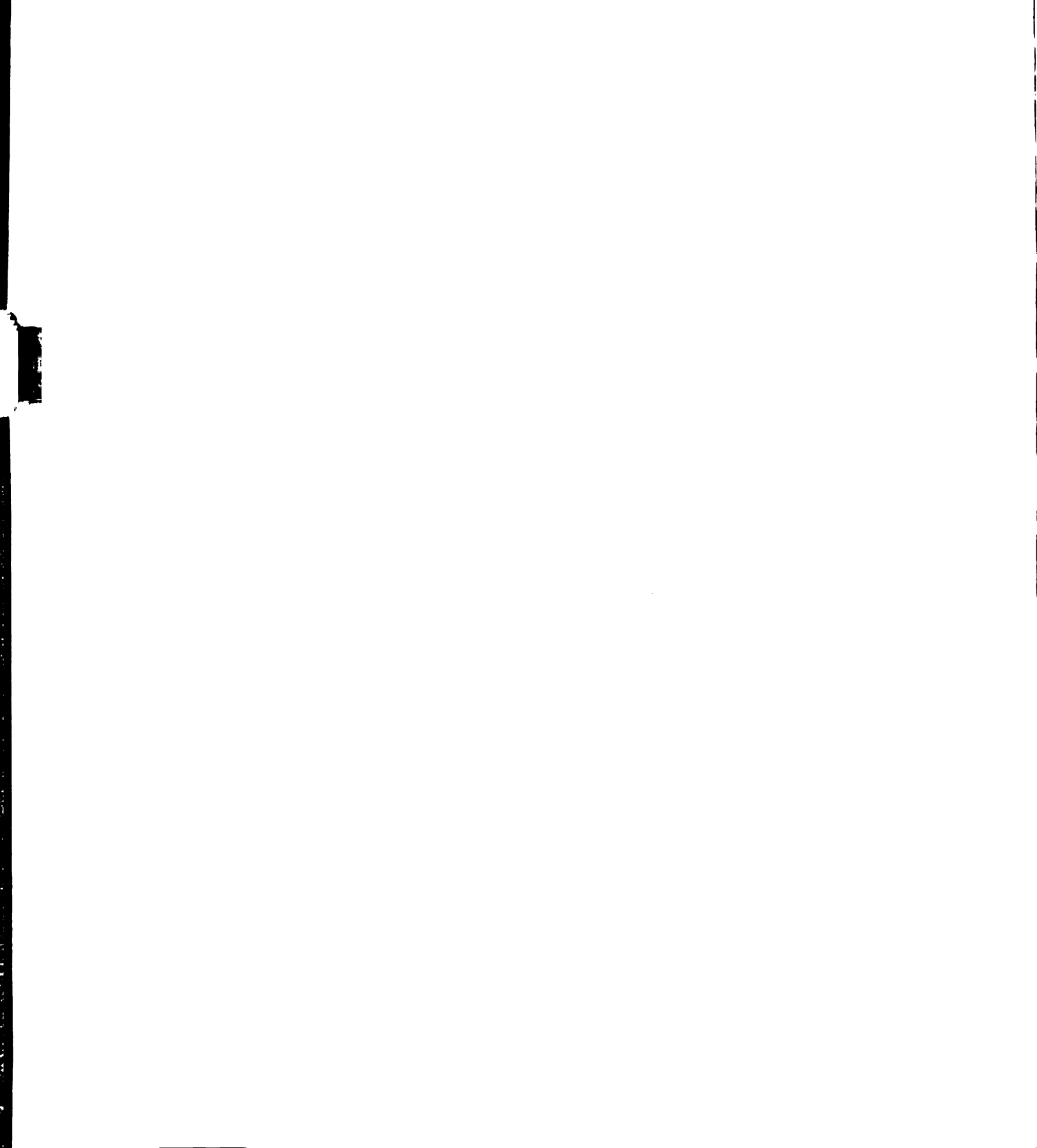


Figure 28. Potentiometric Titration Curve for Aluminum (III) Titrated with Hydroxide Ions in Absolute Ethanol.

aluminum (III) ratio of 2.7 and is identical to the curve which was obtained by Urbach (53). Apparently, even minute traces of water in the ethanol result in a shift from the 2.5 ratio which was found by Ohnesorge. This shift was not expected since anhydrous aluminum chloride was used in this study whereas Urbach used the nonanhydrate. In any case, Ohnesorge's results have been fairly well confirmed.

In a similar manner, a number of solutions, with varying mole ratios of aluminum to flavonol, have also been titrated with sodium hydroxide and some interesting results have been obtained. Urbach demonstrated that with freshly prepared aluminum-flavonol solutions, the titration curves show two breaks which occur at hydroxide to aluminum ratios of 2.2 and 2.7. Since it is assumed that water should also affect the positions of these breaks, these ratios actually indicate a 2.0 and 2.5 hydroxide to aluminum relationship. Urbach also noted that as the ratio of aluminum to flavonol was increased, the first break became less well defined. Unfortunately, he did not go higher than a ratio of four metal ions per flavonol. In addition, all of the titrations which he performed were on freshly prepared solutions. Consequently, there is no information available on the 1:1 chelate which is formed upon aging.

To obtain this desired information, similar potentiometric titrations have been performed on a series of solutions with varying aluminum to flavonol ratios which were aged for two weeks. The results of this study are shown



in Figures 29 through 32. It is apparent from these curves that except for the solution with a 2:1 metal-to-chelate ratio, two breaks appear. As noted by Urbach, the first break becomes ill defined as the mole ratio increases. This indicates that the predominant species, which should be the 6:1 chelate, is responsible for the liberation of five protons for every two aluminum ions upon its formation. On the other hand, the formation of the 2:1 chelate, as proposed by Urbach (54), liberates two different sets of protons. The first set consists of four protons and accounts for the first break in the curve. The second set consists of one additional proton which is titrated for every two aluminum ions and accounts for the second break. Supposedly, this one additional proton is the result of an abstraction from one of the ethanol molecules within the coordination spheres of the aluminum ions.

Upon aging the 2:1 chelate, it is known that it is transformed into a chelate with a 1:1 stoichiometry. The potentiometric titration of this 1:1 chelate is shown in Figure 33. Curve A is the titration curve for the 2:1 chelate while curve B is for the 1:1 species. Note that the curve for the 1:1 chelate essentially exhibits one break at a hydroxide to aluminum ratio of two. This indicates that this chelate is formed with the liberation of four protons for every two aluminum ions and that the structure is significantly different from that of its predecessor, the 2:1 chelate.

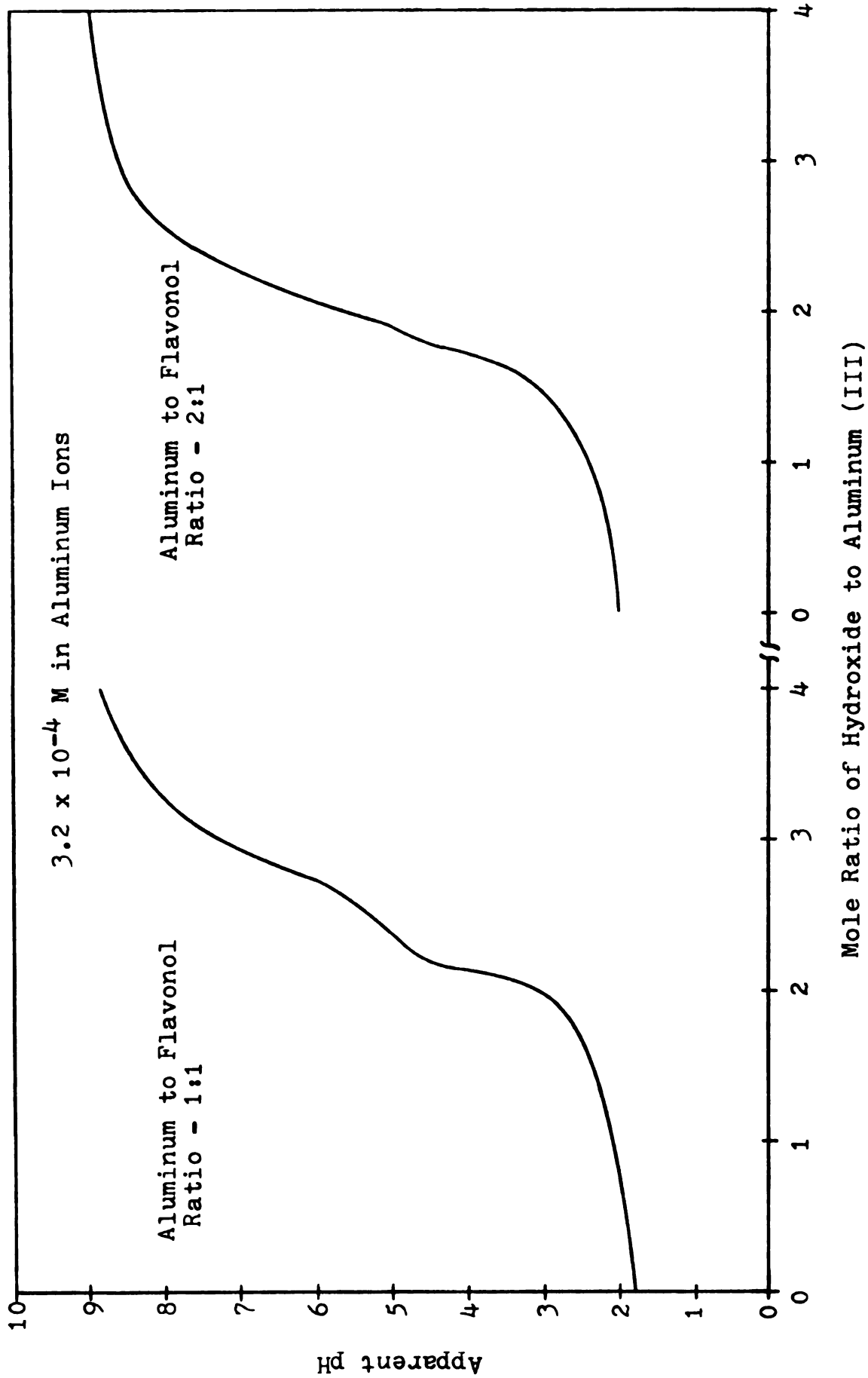


Figure 29. Potentiometric Titration Curves for the Titrations of Various Aluminum to Flavonol Ratios with Hydroxide Ions in Absolute Ethanol.

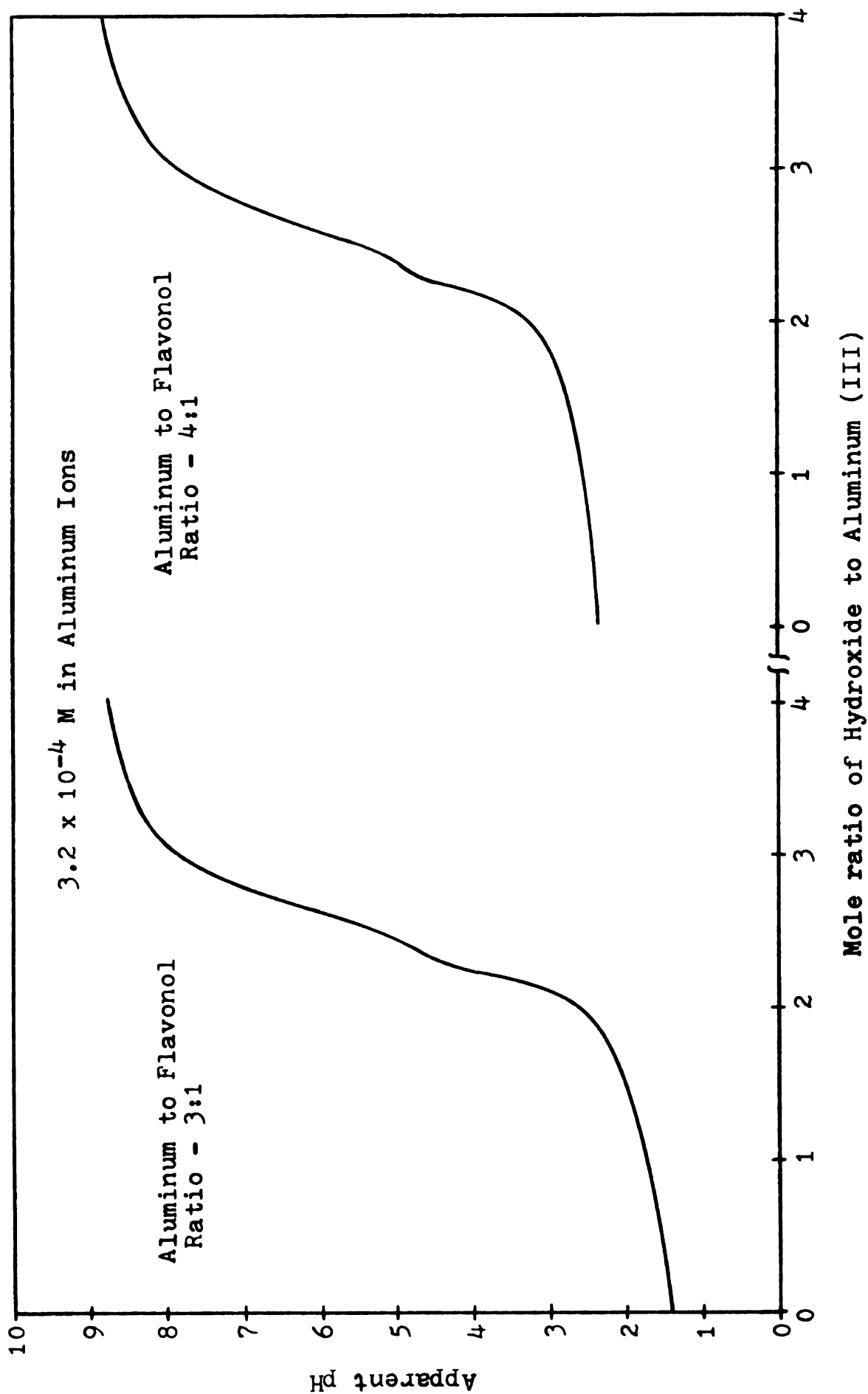


Figure 30. Potentiometric Titration Curves for the Titration of Various Aluminum to Flavonol Ratios with Hydroxide Ions in Absolute Ethanol.

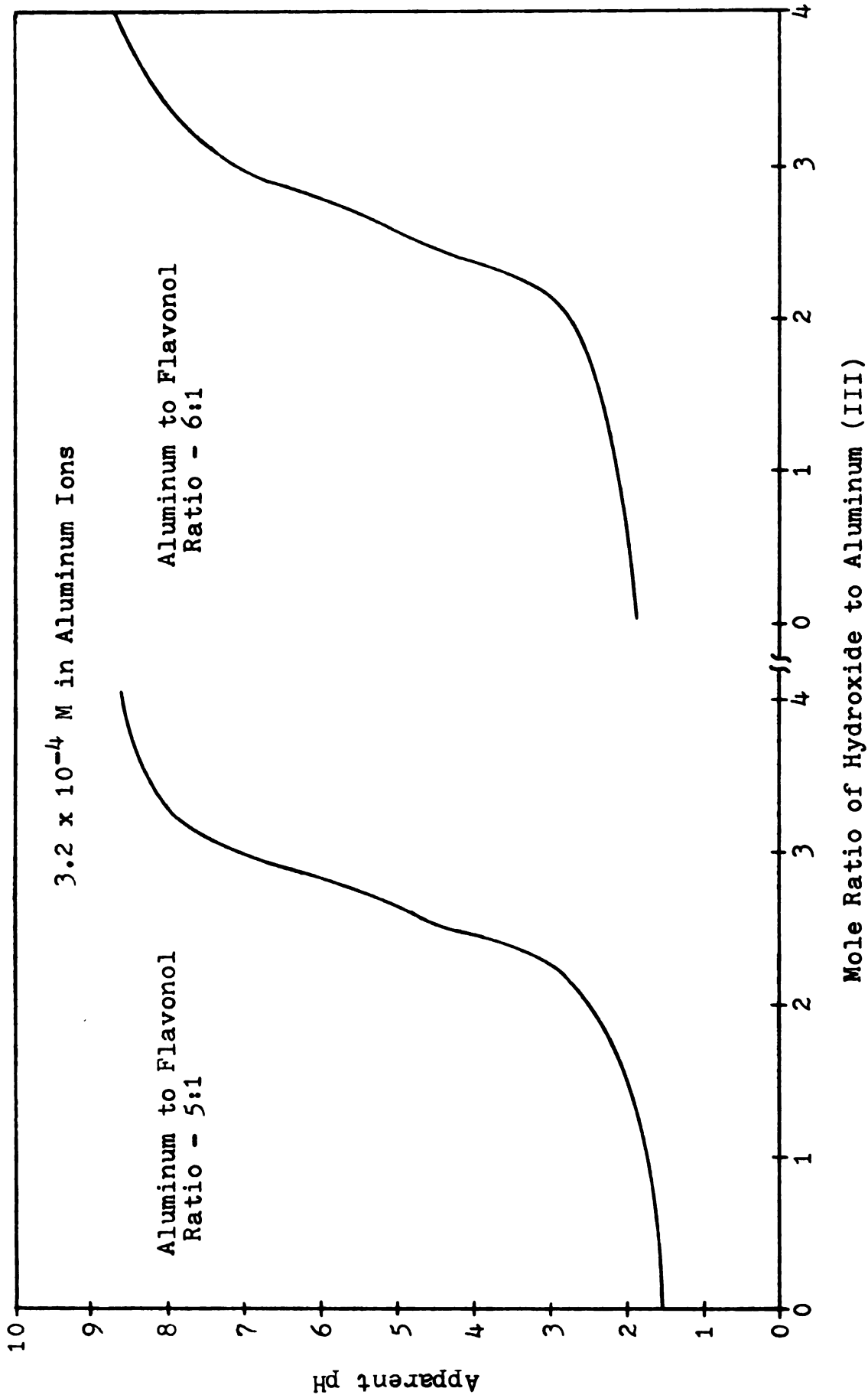


Figure 31. Potentiometric Titration Curves for the Titration of Various Aluminum to Flavonol Ratios with Hydroxide Ions in Absolute Ethanol.

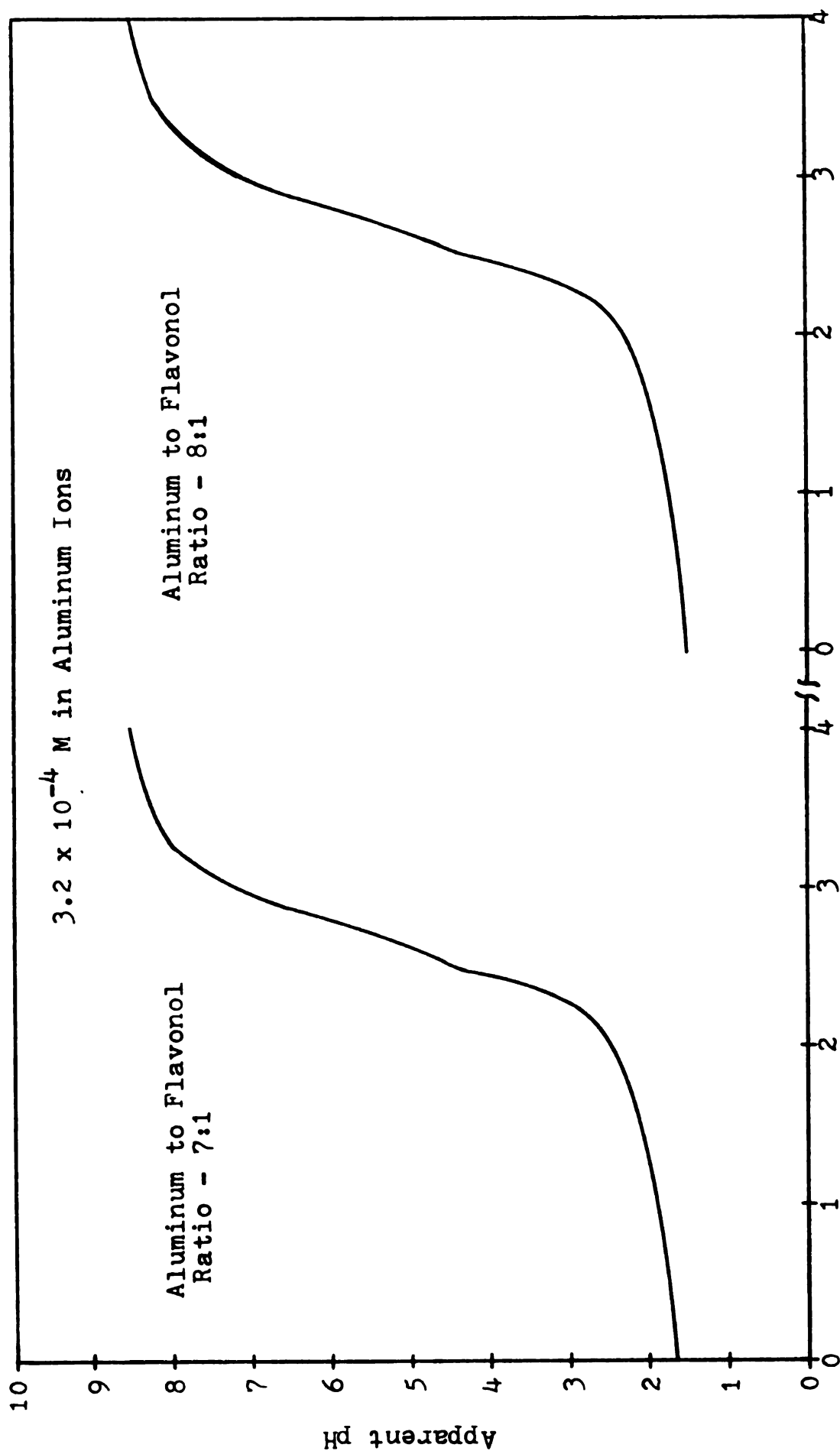


Figure 32. Potentiometric Titration Curves for the Titration of Various Aluminum to Flavonol Ratios with Hydroxide Ions in Absolute Ethanol.

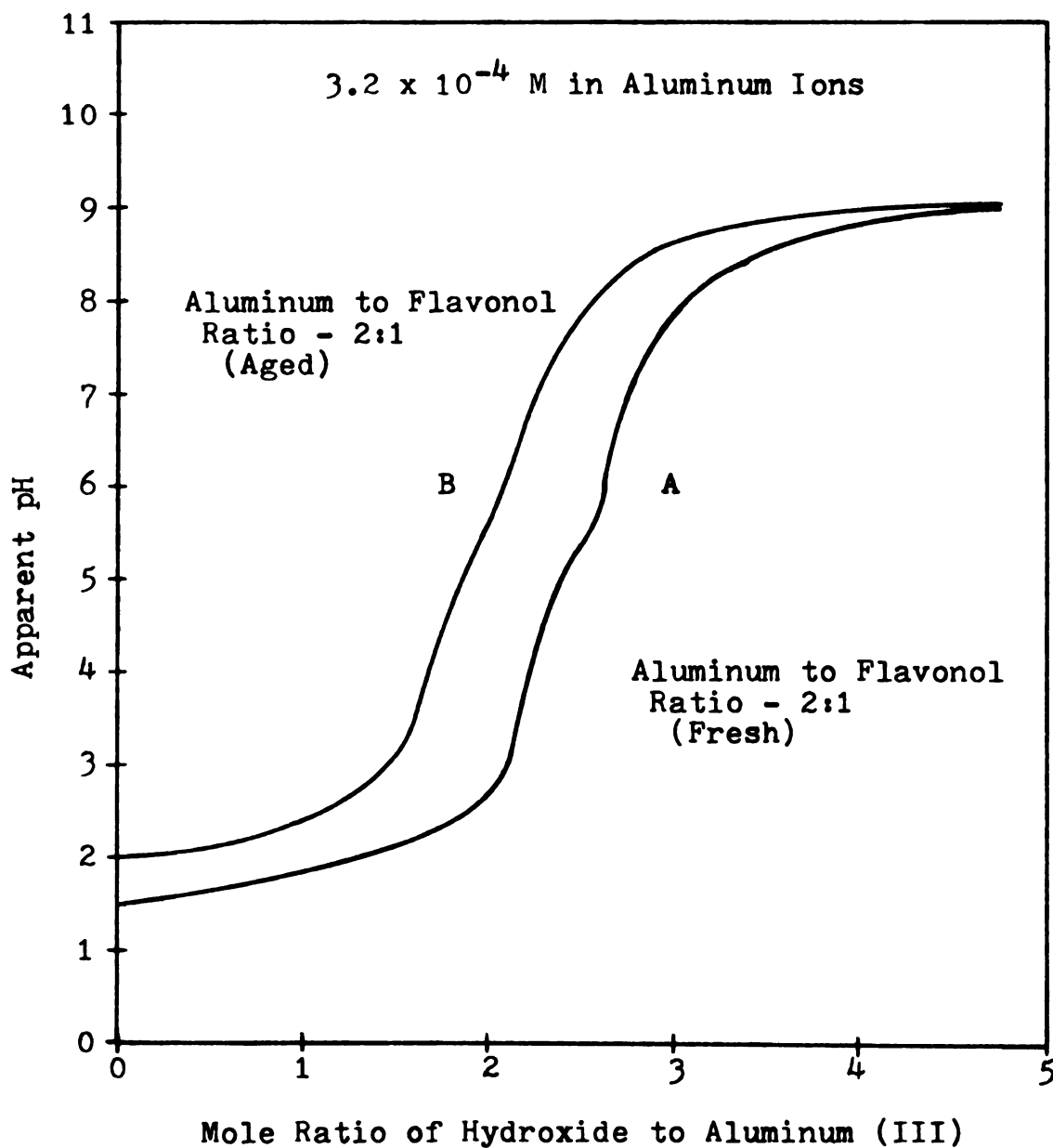


Figure 33. Potentiometric Titration Curves for Fresh and Aged Solutions with an Aluminum to Flavonol Ratio of 2:1 Titrated with Hydroxide Ions in Absolute Ethanol.

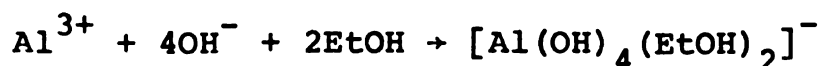
In the following sections of this chapter, all of the information, which was obtained from this and several other studies, will be used to arrive at a proposal for the structures of the various aluminum-flavonol chelates in absolute ethanol.

ALUMINUM (III) SPECIES STRUCTURES IN ABSOLUTE ETHANOL

Since the structure of aluminum (III) species in solution is certainly responsible for the large variety of chelate stoichiometries, it is appropriate at this point to begin with a discussion of these structural properties.

Basic Solutions

In basic aqueous solutions, aluminum salts dissolve to give aluminate ions. The same reaction almost certainly occurs in basic absolute ethanol solutions. In addition,

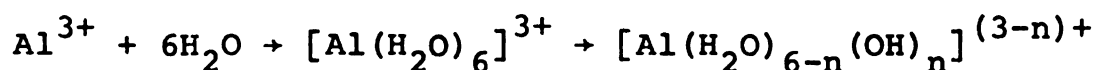


these aluminate ions are believed to be monomeric in nature and consequently, any chelates which are formed in basic solutions should also be of a monomeric nature.

"Neutral" Solutions

In "neutral" aqueous solutions, the structure of solvated aluminum ions appears to be quite complex. Since

aluminum salts undergo extensive hydrolysis upon dissolution, the solutions which result are quite acidic. In addition, the aluminum ions in solution are considered to

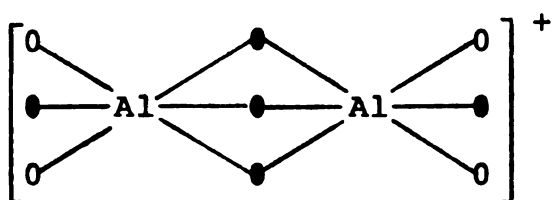


be octohedrally coordinated and polymeric in nature. Unfortunately, very little is known about the extent of polymerization. Studies by Aveston (58) suggest that the predominant ionic species in aqueous solutions may be $[\text{Al}_2(\text{OH})_2]^{4+}$ and $[\text{Al}_{13}(\text{OH})_{32}]^{7+}$. On the other hand, Brosset, et al., concluded that the predominant species may be $[\text{Al}_6(\text{OH})_{15}]^{3+}$ and they have suggested that a ring structure may be involved (59). In addition, cryoscopic measurements by Kohlschütter and Hantelmann (60) tend to support a hexameric species.

In "neutral" solutions of absolute ethanol, the stoichiometry of the ionic aluminum species is believed to be similar to the one proposed by Brosset and others. Since Ohnesorge has shown that the ratio of ethoxide to aluminum ions is 2.5, the simplest polymeric species would have to be at least a dimer. However, since a 6:1 chelate has been shown to exist, it would appear that aluminum ions in ethanol have a hexameric structure. Therefore, it would appear that the ionic species formed in absolute ethanol is $[\text{Al}_6(\text{OEt})_{15}(\text{EtOH})_n]^{3+}$.

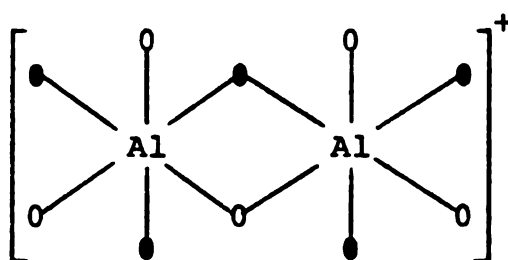
From aluminum-27 nmr studies, it has been found that

anhydrous aluminum chloride in ethanol gives only one resonance signal. This indicates that the aluminum ions, which are involved in the structure of the ionic species in solution, have similar or identical environments. To meet this criterion, it is quite obvious that the aluminum ions must be a part of a ring or cyclic structure. Of



A

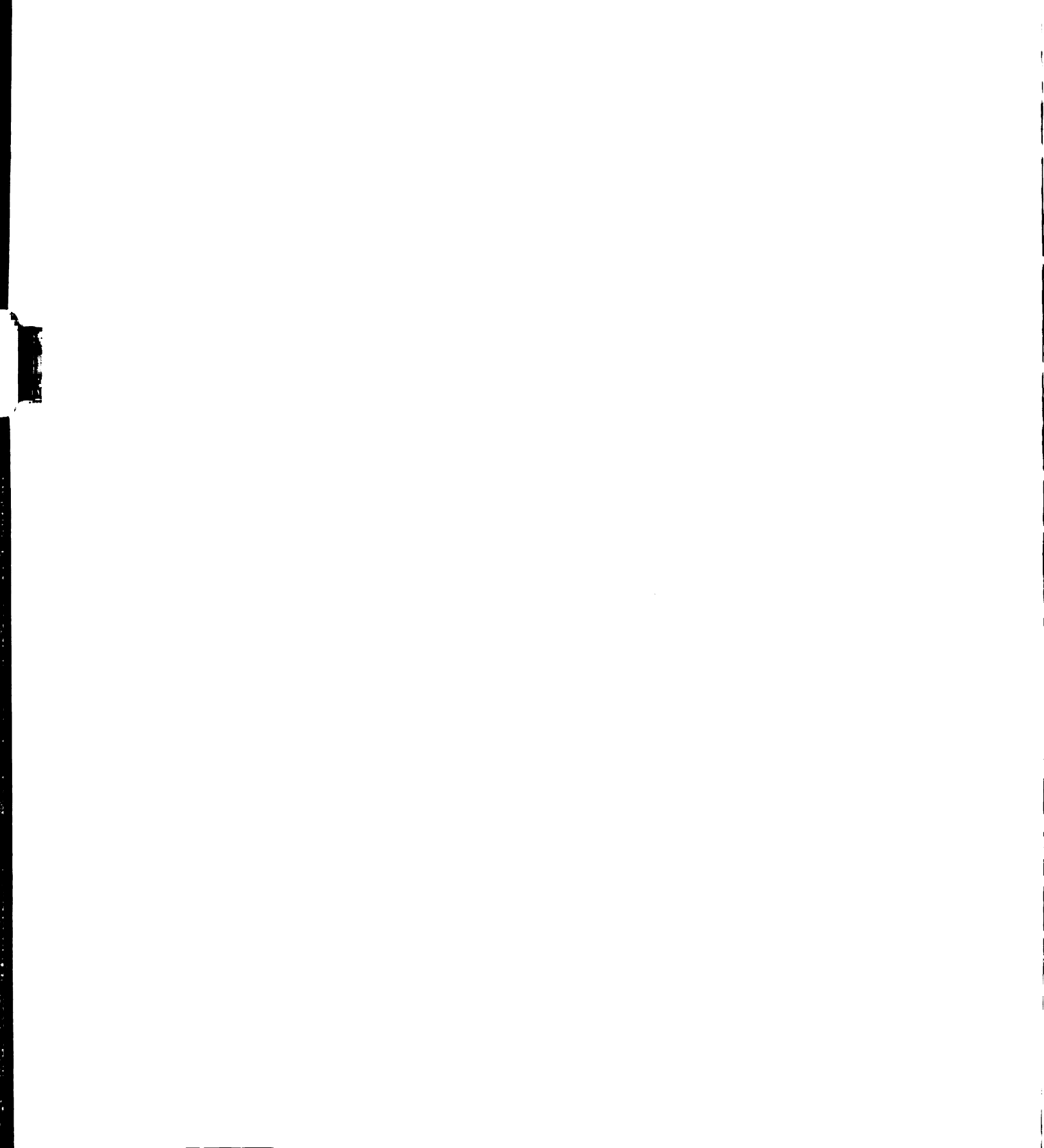
O = Ethanol

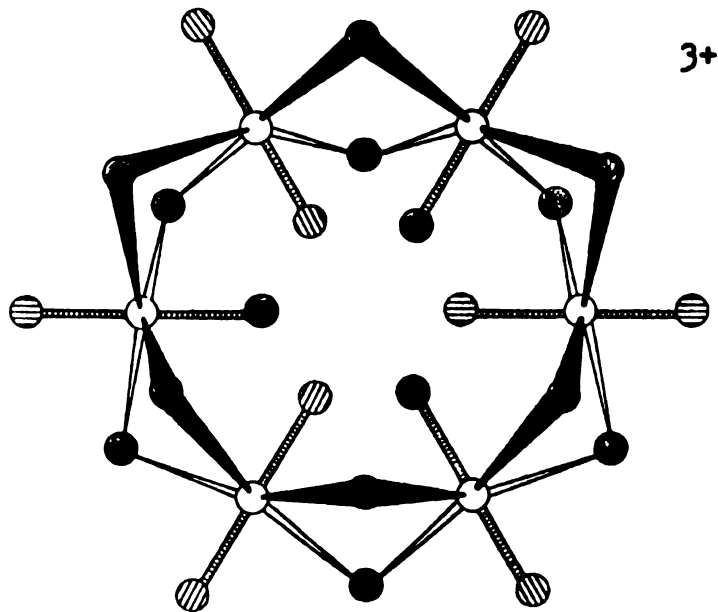
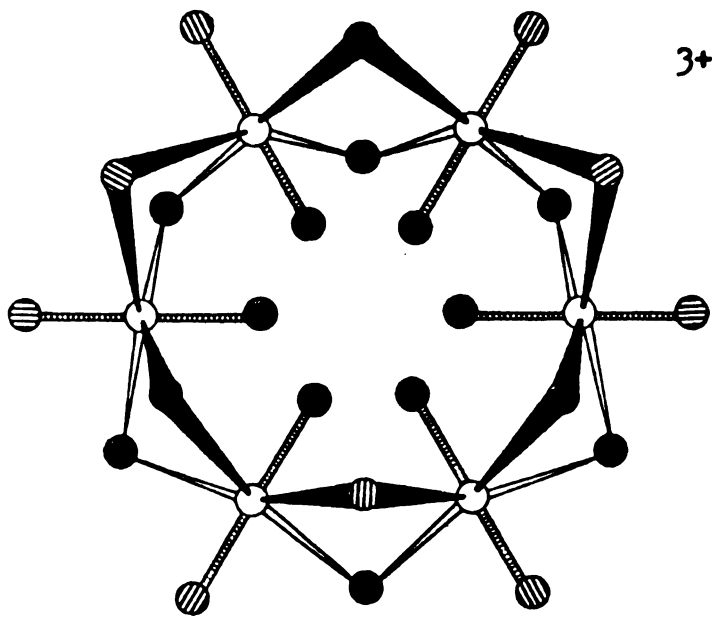


B

● = Ethoxide

the two simple structures shown above, which have been used by Ohnesorge (55,61) in the explanation of some of his work with aluminum-8-hydroxyquinolates, neither A or B are adequate building blocks for the construction of a six membered aluminum ring. However, slight modifications of these structures do result in the three possible structures which are shown in Figure 34. In structure A, the aluminum ions are not quite equivalent since the coordination sites within the ring are occupied by alternating ethoxide and ethanol molecules. On the other hand, they may appear equivalent on the nmr time scale since proton exchange should be quite rapid in this ionic molecule.



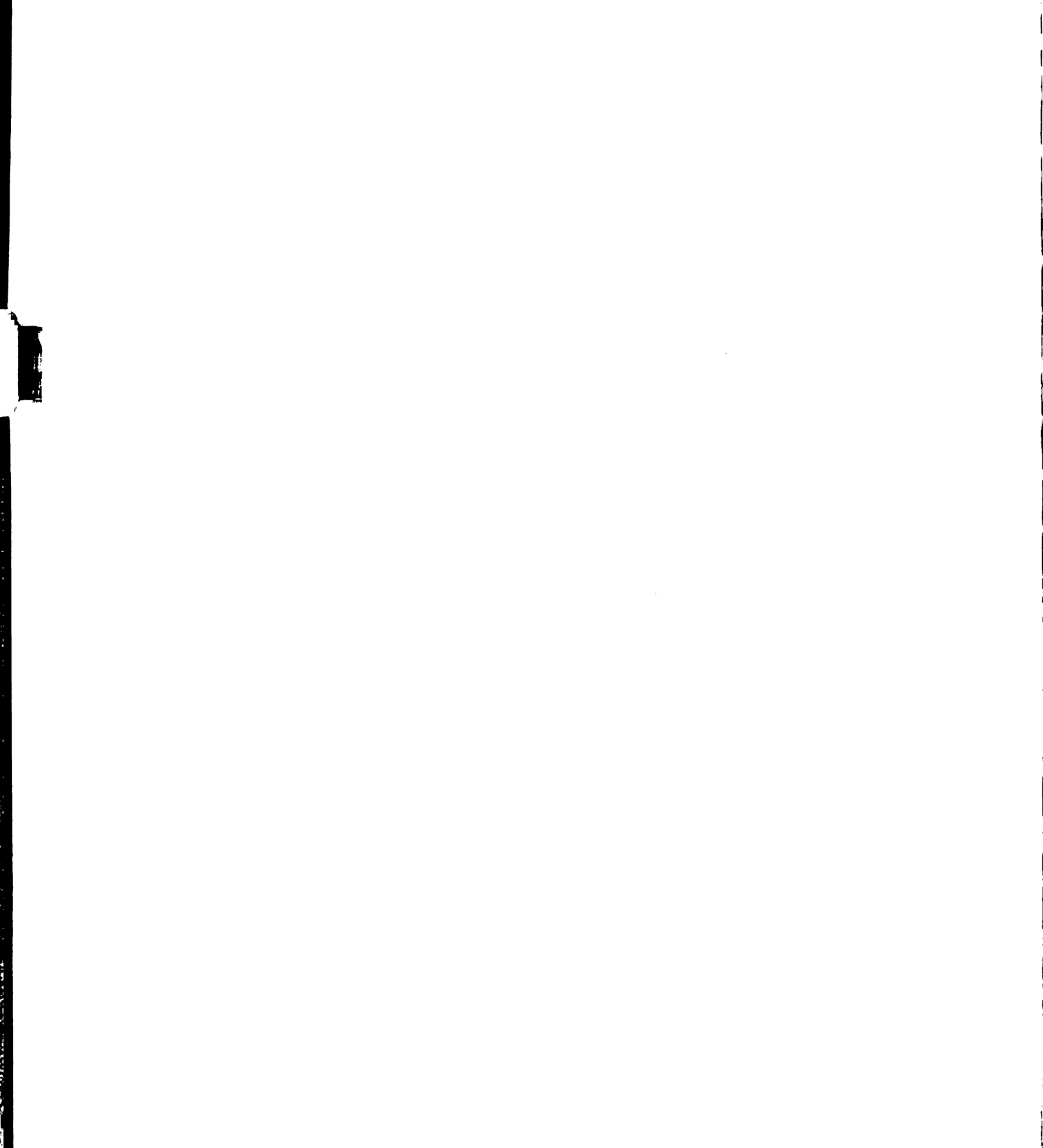
AB

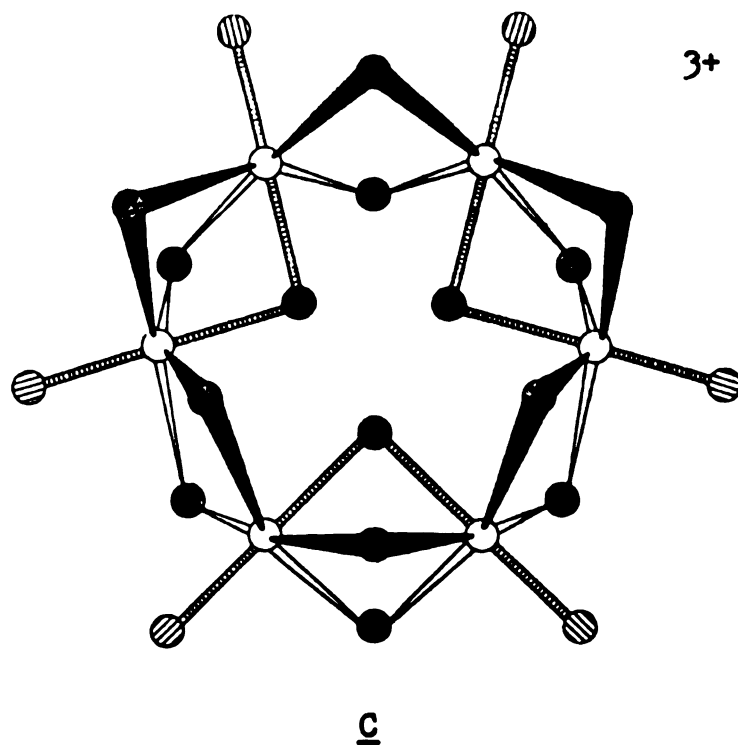
○ = Aluminum

⊖ = Ethanol

● = Ethoxide

Figure 34A. Various Proposed Structures for Aluminum (III) in Absolute Ethanol.





○ = Aluminum

⊖ = Ethanol

● = Ethoxide

Figure 34B. Various Proposed Structures for Aluminum (III) in Absolute Ethanol.

Low temperature aluminum-27 nmr might reveal the inequality among the aluminum ions. Unfortunately, no known studies have revealed a splitting of the single resonance signal which is observed at room temperature. This would indicate that structure A may be incorrect. In addition, another factor makes this structure improbable. All the bridges between the aluminum ions are identical. If this were the actual structure, it would be expected that chelates other than the 2:1 and 6:1 species would be formed, i.e., the 3:1, 4:1 and 5:1 chelates. Since this is not the case, it would appear that all the bridges are not identical and structure A would have to be disregarded. However, structures B and C seem to fit all of the criteria. All of the aluminum ions are environmentally identical, and the bridges alternate between two different types. These structures seem to be intuitively sound, since the attack by flavonol to form the chelates should favor one of the bridge types over the other. Therefore, either structure B or C could represent the structure of aluminum ions in absolute ethanol.

Acidic Solutions

In acidic solutions, aluminum ions are generally believed to have all six coordination sites occupied by solvent molecules because of a shift in the equilibrium given below:

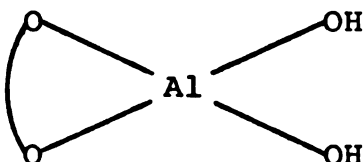


The extent of polymerization is not known although it is believed that at least a dimer exists since a 2:1 metal-to-ligand chelate has been found to exist in acidic absolute ethanol solutions.

CHELATE STRUCTURES

Basic Solutions

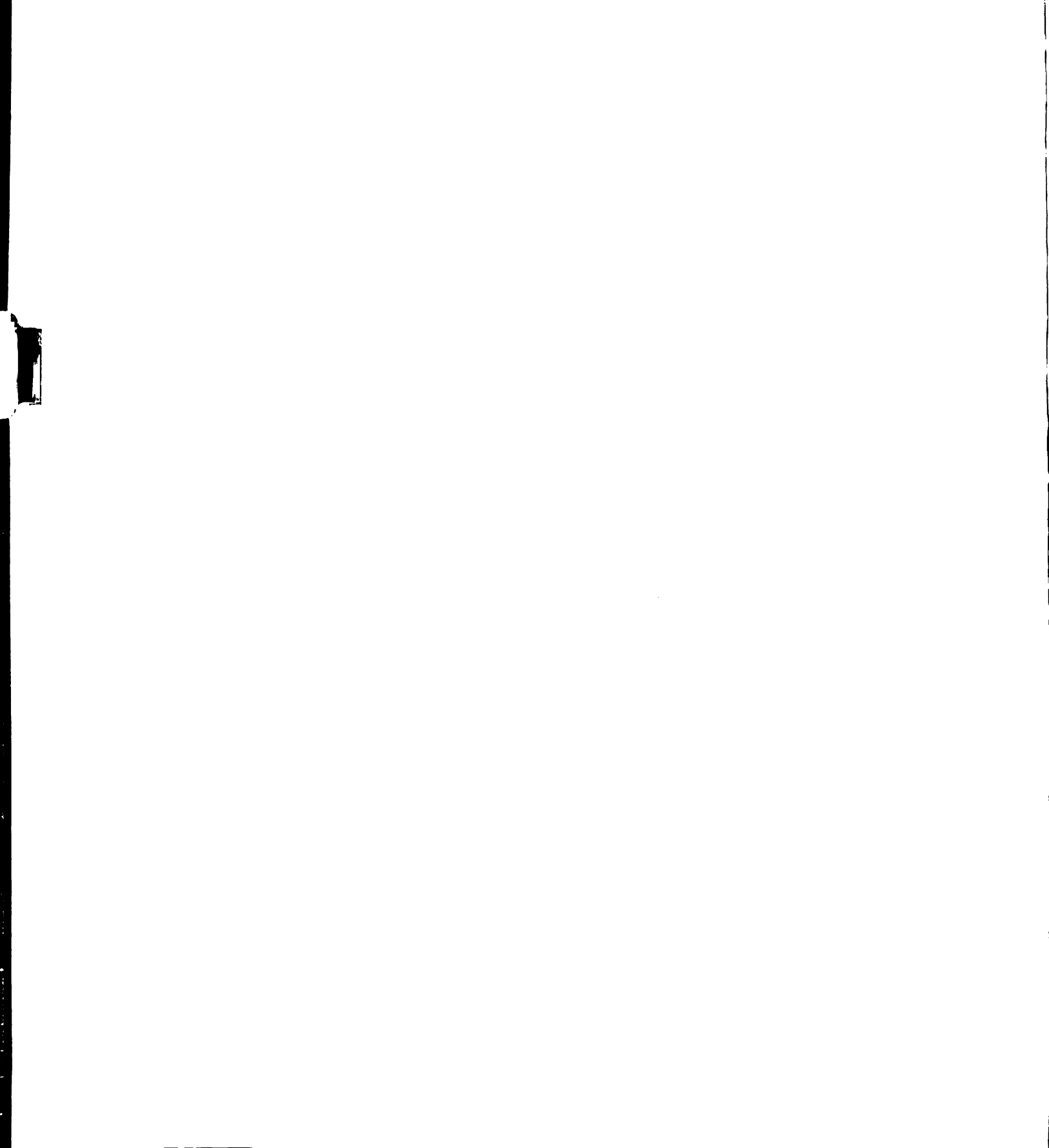
As proposed by Porter and Markham (56) for aluminum-flavonol chelates in methanol, the structure of the 1:1 chelate in basic absolute ethanol is probably a dihydroxy complex.



This structure is reasonable because the chelate should be formed from the reaction of flavonate, $F1O^-$, and aluminate.



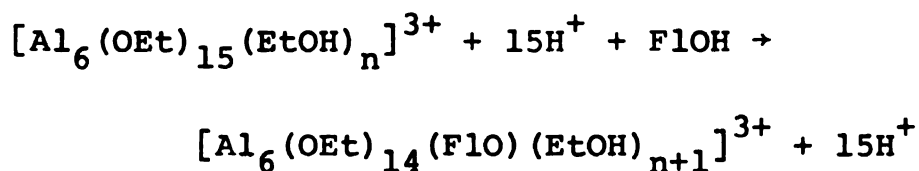
Apparently, flavonol is able to compete effectively with the hydroxide ions for the coordination sites on the aluminum ion if the concentration of hydroxide is relatively low. However, at high concentrations, the equilibrium shown



above is shifted to the left and little or no chelate formation is indicated.

"Neutral" Solutions

Since it is logical to assume that the formation of the 2:1 and 6:1 chelates occurs in a similar manner, the simplest case, which should be the formation of the 6:1 species, will be considered first. As indicated in the previous section of this chapter, the point of attack by flavonol should favor one of the bridge types in the two proposed aluminum ion structures (Figure 34). From the potentiometric titration studies, it has been shown that the formation of the 6:1 chelate occurs with no net change in the number of free protons. This indicates that there must be a loss of one ethoxide ion which is converted into an ethanol molecule. This ethoxide ion is then replaced

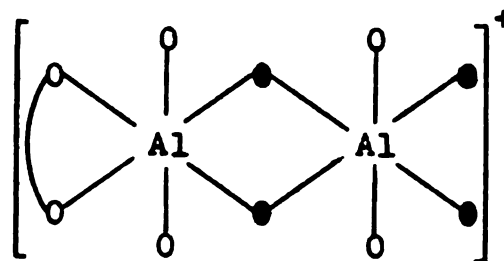
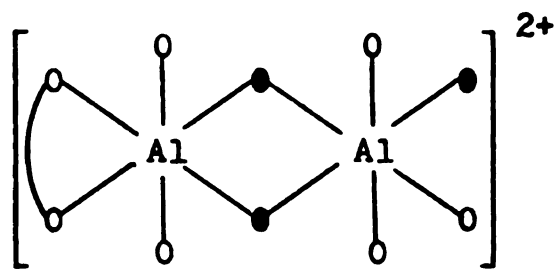
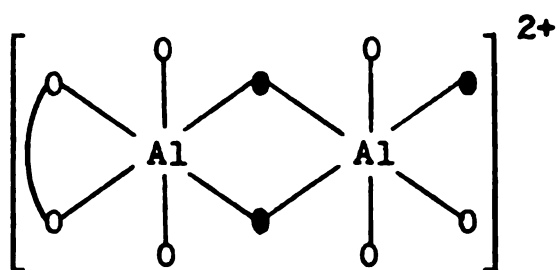
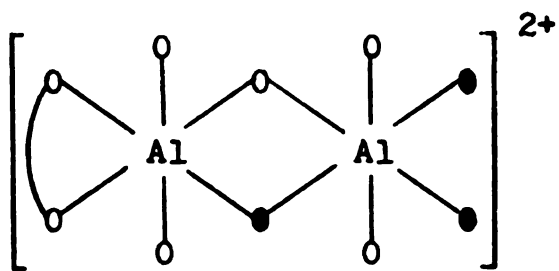
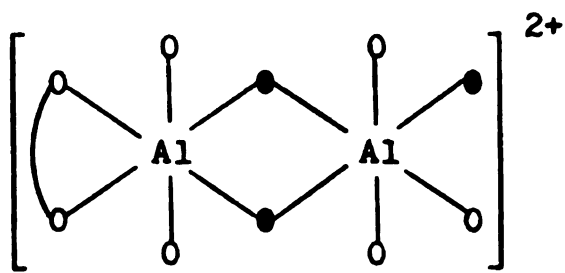


by a flavonate ion. Figure 35 shows the possible structures for the 6:1 chelate based on the proposed aluminum structures in absolute ethanol. The chelate structures have been linearized for clarity but there is a possibility that the 6:1 chelate may still have a cyclic structure. For aluminum structure B (Figure 34), attack at the bridge

type a should lead to the structure which is shown in Figure 35A while attack at bridge type b produces the chelate structure shown in Figure 35B. Obviously, an attack at either bridge type produces a chelate which fits the potentiometric titration data. For aluminum structure C (Figure 34), attack at bridge type c should lead to the chelate structure shown in Figure 35C, while attack at bridge type d produces the structure in Figure 35D. Again, it appears that the attack at either bridge type leads to a chelate which fits the titration data. Consequently, neither of the two proposed aluminum ion structures can be eliminated from consideration on the basis of the 6:1 chelate formation.

For the 2:1 chelate, the potentiometric titration curve had two breaks. The first break occurred at a proton to aluminum ratio of two and indicates that there are four free protons in solution after the formation of one chelate molecule is completed. The second break, which occurs at a proton to aluminum ratio of 2.5, indicates that one additional proton is abstracted from the chelate at higher pH's. Based on these results, the formation of the 2:1 chelate must occur with the production of four free protons, and in addition, it must have one ethanol molecule within its coordination sphere which is easily ionized. Figure 36 shows the 2:1 chelate structures which could possibly be formed from the two proposed aluminum ion structures.

For aluminum structure B (Figure 34), attack by flavonol



O = Ethanol

● = Ethoxide

 = Flavonate

Figure 36. Various Proposed Structures for the 2:1 Aluminum to Flavonol Chelate in Absolute Ethanol.

at bridge types a and b yields the structures which are shown in Figures 36A and 36B, respectively. For aluminum structure C (Figure 34), attack by flavonol at the bridge types c and d produces the structures shown in Figures 36C and 36D, respectively. Note that structures A, C and D are identical, and it is expected that the proton abstraction which occurred during the potentiometric titration involves one of the ethanol molecules on the aluminum ion which is not bound directly to flavonol. The reason behind this expectation is that this aluminum ion is relatively more electropositive than the one bound directly to the flavonate ion with its large resonance system. On the other hand, structure B in Figure 36 is quite different from the others. In this case, proton abstraction would probably occur at the bridging ethanol molecule. Note that this abstraction results in a molecule which is identical to structures A, C and D after proton abstraction. In any case, with the experimental evidence presently available, it is impossible to predict which bridging type undergoes attack by flavonol, and in addition, neither of the proposed aluminum ion structures can be eliminated.

For the 1:1 chelate which is produced from the 2:1 chelate upon aging, the potentiometric titration indicates that four free protons are present in solution for every two aluminum ions, and no proton abstraction was observed. Although no mechanism can be proposed at this time, the length of time needed for the conversion indicates that a

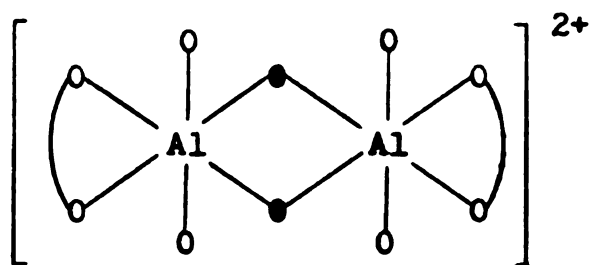
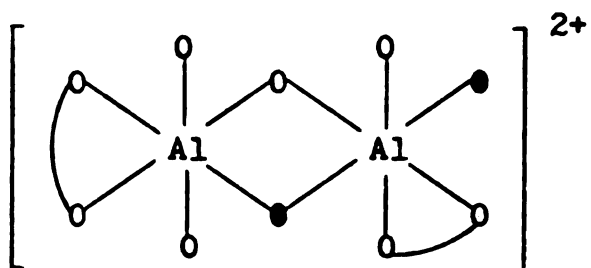
gross structural change takes place. The proposed structures for the 1:1 chelate are presented in Figure 37. Structure A results from the replacement of one ethoxide ion and one ethanol molecule in structures A, C and D in Figure 36. Structure B results from the same process for structure B in the same figure. It is quite reasonable to expect that structure B for the 1:1 chelate would undergo a proton exchange and rearrangement for reasons of symmetry. The resultant structure would then be identical to structure A.

Acidic Solutions

The structures of the chelates in acidic solutions should be identical to those which are found in "neutral" absolute ethanol solutions although the compositions change due to the protonation of the associated ethoxide ions. The proposed structures for the 1:1 and 2:1 chelates are shown in Figure 38.

CHELATE QUANTUM EFFICIENCIES

During the course of this study, an interesting trend was noticed. Apparently, the amount of fluorescence, which is produced from the excitation of a chelate, is dependent upon the chelate stoichiometry and its ionic charge. This correlation has been tabulated in Table V. For the 1:1 chelate, the change in ionic charge seems to have only

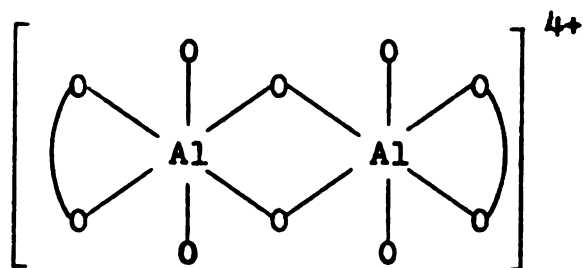
AB

O = Ethanol

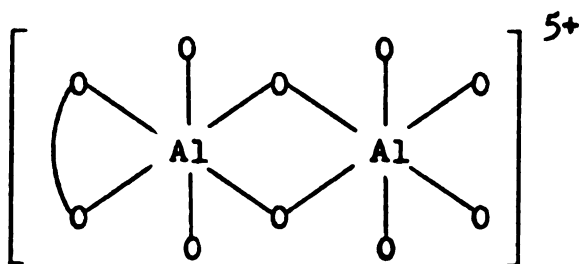
● = Ethoxide

= Flavonate

Figure 37. Various Proposed Structures for the 1:1 Aluminum to Flavonol Chelate in Absolute Ethanol.



1:1 Chelate



2:1 Chelate

Figure 38. Proposed Structures for the 1:1 and 2:1 Aluminum to Flavonol Chelates in Acidic Absolute Ethanol.

Table V
Correlation of Quantum Efficiency with
Chelate Stoichiometry and Ionic Charge

Solution pH	Chelate Stoichiometry	Ionic Charge	Quantum Efficiency
Basic	1:1	0	0.01
Neutral	1:1	+2	0.01
Neutral	2:1	+2	0.03
Neutral	6:1	+3	0.70
Acidic	1:1	+4	0.03
Acidic	2:1	+5	0.45

a slight effect on the chelate quantum efficiency. On the other hand, the quantum efficiency of the 2:1 aluminum-to-flavonol chelate undergoes a large increase as its ionic charge changes from +2 to +5.

At this point, it is important to note that even though there seems to be a correlation between ionic charge and quantum efficiency, it is actually the number of aluminum ions in each of the chelates which causes the change in quantum yield. Consider the chelates which are formed in "neutral" absolute ethanol. As the ratio of aluminum to flavonol increases, the quantum efficiencies also undergo a drastic increase. The same is true for the two chelates

which are formed in acidic solutions. This phenomenon may be explained by considering the structures of the chelates themselves.

For the chelates formed in "neutral" ethanol solutions, the large increase in quantum efficiency between the 2:1 and 6:1 chelates could be caused by an increase in structural rigidity. This may indicate that the 6:1 chelate has a cyclic structure similar to that of aluminum (III) in absolute ethanol. On the other hand, the quantum efficiency difference for the two chelates formed in acidic solutions is not so easily explained. Upon the addition of acid, it is expected that the ethoxide ions involved in the chelate structures should be neutralized. Consequently, the electropositivity of the aluminum ions would increase, and this should result in a depletion of electron density on the attached flavonate ion(s). It would appear that this change in electron density might account for the difference in quantum efficiency for the acidic chelates.

Generally, increases in quantum efficiency are attributed to increases in rigidity, planarity and/or to the raising of a (n, π^*) transition energy relative to a (π, π^*) transition. However, an increase in rigidity or planarity does not seem to explain the large difference in quantum efficiency for the acidic chelates. On the other hand, it is possible that the apparent change in electron density on flavonol does result in raising the (n, π^*) transition energy since some non-bonding electrons are utilized in the formation of the chelates. This should decrease the rate of intersystem crossing and increase the fluorescence efficiency.

PREPARATION OF SOLID CHELATES

Throughout this investigation, repeated attempts were made to obtain the solids of the chelates which presumably existed in solution. Unfortunately, it seems that all attempts have ended in failure. In light of the results which were obtained from the Raman, infrared and aluminum-27 NMR studies, prospects for success in this venture are dim since it appears that only one chelate is formed at high aluminum-flavonol concentrations. However, a brief outline of the recovery attempts is given below.

Evaporation to dryness of solutions which contained the appropriate stoichiometric ratios led to the formation of crystalline powders. The powders obtained from the solutions of the 2:1 and 6:1 chelates gave identical X-ray powder diffraction patterns. The infrared spectra of these same powders in KBr pellets also indicated that they were structurally identical.

Crystallization by the addition of various solvents such as carbon tetrachloride, chloroform, benzene and cyclohexane to ethanolic solutions of the chelates proved unsuccessful. However, crystals were obtained over a period of four days by allowing ethyl ether to diffuse into ethanolic chelate solutions. Unfortunately, the crystals were too small and irregular for a X-ray crystallographic structure analysis. In addition, it is believed that the chelate, which was formed by the above procedure, was identical to that of the powders which were obtained through evaporation.

IV. SUMMARY AND CONCLUSIONS

From photometric and fluorometric spectral studies, a new electronic absorption band in the spectrum of flavonol has been discovered. The band is located in the spectral region near 410 nm, and excitation at this wavelength results in the emission of fluorescence at 484 nm. Tentatively, this electronic absorption band has been assigned to a (n, π^*) transition although the experimental results are somewhat inconclusive. Further, support for this assignment might be obtained by the conversion of flavonol to the corresponding oxime (62). If the absorption band disappears from the absorption spectrum of the oxime, there is a strong indication that the band is caused by a (n, π^*) transition. Unfortunately, this method of assignment has only been shown to be reliable for nitrogen heterocyclic compounds and consequently, further tests with oxygen heterocycles would have to be carried out before a definite assignment could be made. In addition, the conversion of flavonol to its oxime in concentrated alkaline medium would have to be modified since flavonol is unstable in concentrated base.

Based on the work of various investigators (55,59-61), numerous aluminum-27 nmr studies, and the results of this study, various structures for aluminum (III) in absolute ethanol have been proposed. Of the three presented, all

are hexameric cyclic structures, and only one of these could be eliminated on the basis of the available experimental evidence. The two remaining structures (Figure 34, B and C) seem to fit the experimental criteria of identical environments for all of the aluminum ions, an ethoxide to aluminum (III) ratio of 2.5, and an alternating bridge configuration.

The work of Urbach and Timnick (53,54) has been re-examined in detail. The formation of a 1:1 chelate in dilute base and the 1:1, 2:1 and 6:1 aluminum-to-flavonol chelates in "neutral" absolute ethanol solutions has been confirmed. In addition, this study has also shown that 1:1 and 2:1 aluminum-to-flavonol chelates also exist in acidic ethanol solutions. Based upon the proposed aluminum (III) structures in absolute ethanol and a series of potentiometric titrations, various structures for these chelates have been proposed. Although the 6:1 aluminum-to-flavonol chelate in "neutral" absolute ethanol has been pictured in a linear form, there is no experimental evidence to warrant this representation. Indeed, there exists a good possibility that this chelate actually has a cyclic structure which is similar to that of aluminum (III) in absolute ethanol. As far as the structures for the other chelates are concerned, some are similar or identical to the ones proposed by Porter and Markham (56) for the aluminum-flavonol chelates in absolute methanol.

Fluorescence quantum efficiency measurements on the chelates in solution have revealed an interesting trend. It appears that as the number of aluminum ions in the chelate structures increases, the quantum efficiencies of the chelates also increase. For example, in "neutral" ethanolic solutions, the existence of three chelates is indicated. These are the 1:1, 2:1 and 6:1 aluminum-to-flavonol chelates. The quantum efficiency of the 2:1 chelate is about three times larger than that of the 1:1 chelate, and the 6:1 species exhibits an efficiency that is about seventy times as large. If the 6:1 chelate has a cyclic structure, the increase in rigidity over the 1:1 and 2:1 chelates should account for the large increase in quantum yield. An increase in quantum efficiency can also be observed in the 1:1 and 2:1 chelates which are formed in acidic ethanol solutions. There is approximately a fifteen fold increase in quantum efficiency for the 2:1 chelate over the 1:1 species. This effect cannot be explained by an increase in rigidity or planarity. However, it might be explained by a decrease in the rate of intersystem crossing caused by raising the energy of the (n, π^*) transition relative to the (π, π^*) transition of the chelates. This rise in energy could be caused by a depletion of non-bonding electron density on the chelate flavonate ion(s), which is caused by an increase in the electropositivity of the chelated aluminum ions. Since this effect should be much larger in the 2:1 chelate, a large increase in quantum efficiency over the 1:1 chelate is expected.

The prospects for obtaining the solids of the chelates, which presumably exist in dilute absolute ethanol solutions, appear to be quite small. Crystallization by the addition of various solvents to the ethanolic chelate solutions has proved unsuccessful. However, evaporation of the solvent from the same ethanolic solutions did yield crystalline powders. Unfortunately, the crystals were unsuitable for an X-ray crystallographic structure analysis. Studies by using Raman, infrared and aluminum-27 nmr spectroscopy have all indicated that only one chelate is formed in concentrated solutions and in the solid state. Comparison of the solid state infrared spectra, which were obtained during the course of this study, with the infrared spectrum of the solid chelate obtained by Urbach, indicates that the solids in both studies might be the same. Consequently, it is assumed that the solid chelate obtained in this study probably has an aluminum-to-flavonol ratio of 1:3.

APPENDICES

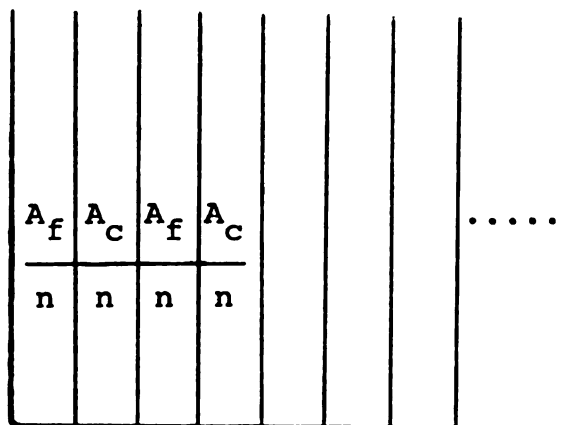
APPENDIX ONE

MATHEMATICAL PROOF OF ASSUMPTION FOUR

Assumption four states that the ratio of the fluorophore absorbance, A_f , to the total absorbance, A_t , in the cell is equal to the ratio of the quanta, Q_f , absorbed by the fluorophore to the total quanta absorbed, Q_t .

$$\frac{A_f}{A_t} = \frac{Q_f}{Q_t}$$

The mathematical proof of this statement is presented by the use of the following approach. The cell is assumed to contain a fluorophore and a constant number of chromophores. The cell is then divided in a fashion such that the fluorophore and the chromophores are segregated into alternating equal volume slices as shown below:



A constant fraction, $1/n$, of the fluorophore is contained in the first slice. The second slice contains the same

fraction of the chromophores while the third slice contains $1/n$ of the fluorophore and so on.

At this point, the following definitions are made:

- (1) A_f is the total absorbance due to the fluorophore.
- (2) A_c is the total absorbance due to the chromophores.
- (3) A_t is the total absorbance, $A_f + A_c$.
- (4) The total number of cell slices is equal to $2n$.

Consequently, the absorbance of the fluorophore in each of the odd numbered slices is A_f/n , while the absorbance for the chromophores in each of the even numbered slices is A_c/n . From the general expression for the exponential attenuation of the excitation beam, the following expression may be written:

$$I = I_0 e^{-abc} = I_0 e^{-A} \quad (1)$$

where a , b , c and A have the usual Beer's Law meanings. From Equation 1, it follows that the intensity of the excitation beam after passing through the first slice is

$$I_1 = I_0 e^{-(A_f/n)} \quad (2)$$

and $I_0 - I_1$, is the number of quanta absorbed by the fluorophore in the first slice. The total number of quanta absorbed by the fluorophore, Q_f , across the whole cell is given by the following expression

$$Q_f = I_o \sum_{q=1}^n [e^{-(q-1)(A_t/n)} - e^{((q-1)(A_t/n) + A_f)/n}] \quad (3)$$

By factoring Equation 3, the following expression is obtained

$$Q_f = I_o (1 - e^{-(A_f/n)}) (e^{(A_t/n)}) \int_1^n e^{(A_t/n)q} dq \quad (4)$$

The total quanta absorbed within the cell is given by an expression which is similar to Equation 3

$$Q_t = I_o \sum_{q=1}^n [e^{-(q-1)(A_t/n)} - e^{-q(A_t/n)}] \quad (5)$$

By factoring, Equation 5 yields

$$Q_t = I_o (e^{(A_t/n)} - 1) \int_1^n e^{-q(A_t/n)} dq \quad (6)$$

Consequently,

$$\frac{Q_f}{Q_t} = \frac{(1 - e^{-(A_f/n)}) (e^{(A_t/n)})}{e^{(A_t/n)} - 1} \quad (7)$$

It should be noted at this point that as n approaches infinity, the cell model used in this proof approaches reality and since

$$\lim_{n \rightarrow \infty} e^{(A_t/n)} = 1$$

then,

$$\frac{Q_f}{Q_t} = \frac{1 - e^{-(A_f/n)}}{e^{(A_t/n)} - 1} \quad (8)$$

Unfortunately, Equation 8 cannot be evaluated in this form because the denominator goes to zero as n approaches infinity. To circumvent this difficulty, Equation 8 can be expressed as the series expansion of e^x . Expansion leads to the following expressions

$$e^{-(A_f/n)} = 1 - (A_f/n) + \frac{(A_f/n)^2}{2!} - \dots$$

and

$$e^{(A_t/n)} = 1 + (A_t/n) + \frac{(A_t/n)^2}{2!} + \dots$$

Consequently, Equation 8 may now be written as

$$\frac{Q_f}{Q_t} = \frac{[(A_f/n) + \frac{(A_f/n)^2}{2!} - \dots]}{[(A_t/n) + \frac{(A_t/n)^2}{2!} + \dots]} \quad (9)$$

As n approaches infinity and for reasonable values of A_t , it is easily recognized that all of the terms in each series go to zero infinitely faster than the first term. Therefore,

$$\frac{Q_f}{Q_t} = \frac{(A_f/n)}{(A_t/n)} = \frac{A_f}{A_t}$$

and assumption four has been shown to be valid.

APPENDIX TWO
BUFFERED DIGITAL I/O PIN CONFIGURATIONS
(DEC DR8-EA)

INPUT

- (1) A 1 → 0 transition at any input bit leaves a 1 in the corresponding accumulator bit.
- (2) After clearing the input register, reading the register into the accumulator leaves the accumulator a logical 0.

OUTPUT

- (1) Logical 1's in the accumulator give logical 0's at the corresponding output bits.

ASSIGNMENTS

<u>BIT</u>	<u>PIN</u>
0	V2
1	S1
2	T2
3	P1
4	S2
5	M1
6	P2
7	L1

<u>BIT</u>	<u>PIN</u>
8	M2
9	J1
10	K2
11	H1

The assignments given above are for both the input and output registers. The electrical ground for both registers has been assigned to pin F2.

APPENDIX THREE

INSTRUCTIONS FOR THE CONSTRUCTION AND IMPLEMENTATION OF AN EMISSION DETECTION SYSTEM CORRECTION TABLE

The emission system correction table is normally used in conjunction with the fluorimeter computer program, FLUORO, to correct the measured fluorescence for changes in sensitivity, as a function of wavelength, of the emission optical system and photomultiplier tube. The correction table resides in field one of core memory, starts at address 4000_8 and can extend up to address 4700_8 . Consequently, there is room for 512 correction factors. The table consists of integer factors which can range from 0 to 2047 and are stored as a function of wavelength. Location 4000_8 contains the correction factor for a wavelength of 200 nm, location 4001_8 contains the factor for 201 nm, etc. Stored in this fashion, there is enough room for all the correction factors from 200 to 700 nm.

The general process for the construction of the correction table is fairly simple. The process entails the comparison of the emission system response with that of a linear detector. In this case, the linear detector is a quantum counter. The comparison is made by placing a reflectance plate in the sample position so that the excitation beam is directed through the emission detection system when the vibrating bridge is in the sample position. The true intensity of the excitation beam is then measured by the quantum counter

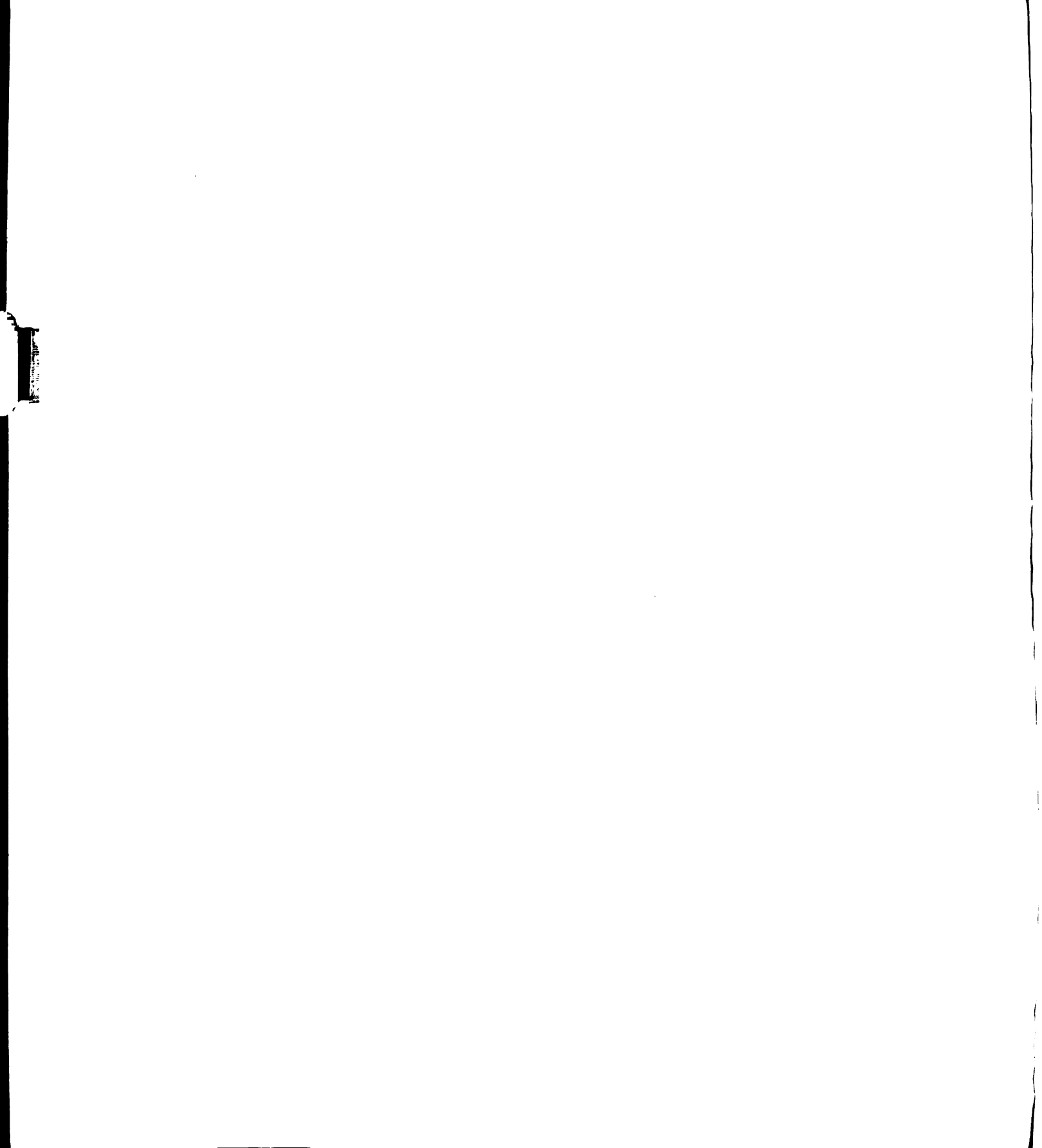
when the vibrating bridge is in the reference position. The ratio of the reference signal to the emission signal, R/F , is then the correction factor for a particular wavelength. The factors for the entire wavelength range are obtained by scanning the emission and excitation monochromators in tandem and by measuring and outputting the ratio, R/F , at one nanometer intervals.

Unfortunately, the use of just one quantum counter over the wavelength range of 200 to 700 nm is not possible. Since the rhodamine B quantum counter is only useful from 250 to about 600 nm, it must be used in conjunction with a methylene blue counter in order to cover the entire wavelength region. Fortunately, there is a considerable overlap in the useful wavelength ranges of these two counters. Since with the proper filter, the methylene blue counter is useful in the range from 550 to 700 nm, the overlap between 550 and 600 nm can be used to normalize the correction factors obtained from the two counters.

BUILDING THE CORRECTION TABLE

Rhodamine B Section

- (1) Load the main fluorometer program into the computer and set up the instrument for a normal excitation scan. A one nanometer data interval should be used.



- (2) Wire the excitation and emission monochromators in parallel so that they scan in tandem.
- (3) Place the reflectance plate, which has been recently coated with Kodak's White Reflectance Standard, in the sample cell position.
- (4) Manually scan both monochromators to assure that the reference and emission signals do not saturate the analog-to-digital converter.
- (5) Reset the monochromators and scan from 200 to 610 nm. Note that the fluorometer program requires that the scan be started at 200 nm even though meaningful correction factors are obtained only from 250 to 610 nm.
- (6) At the end of the scan, make sure that the absorption and photomultiplier corrections are inactive.
- (7) To output the correction factors, the user types PUNCH: R/F and the teletype responds with TURN ON THE PUNCH. Once the paper tape punch is ready, the user types a SPACE and the R/F values as a function of wavelength are punched out.
- (8) Steps 5 through 7 are then repeated four additional times so that five individual paper tapes are generated. These tapes will be processed at a later time.

Methylene Blue Section

- (1) The rhodamine B quantum counter is removed from the instrument, and the rhodamine B solution and the 610 nm sharp cut-off filter are replaced with the methylene blue solution and a 700 nm sharp cut-off filter. The quantum counter is then placed back in the instrument.
- (2) Steps 4 through 8 in the rhodamine B section are then repeated except that the wavelength scans are now from 550 to 700 nm.

PROGRAM PMT

The paper tapes which were obtained from the fluorometer scans are processed by a FORTRAN program named PMT. This program serves several functions. First, it enables the user to average the multiple scans for each quantum counter in order to minimize the random errors in the correction table. Second, the correction factors may be scaled so that the full integer range may be used and so that the tables from the two quantum counters can be normalized and finally merged. Finally, program PMT allows the user to punch out the factors in a form which is compatible with PAL8 assembly. A program listing and flowchart appear on the following pages.

PROGRAM PMT

```

1  DIMENSION ARRAY(500), N(125), L(10)
   R = 1.
   WRITE(1,2)
2  FORMAT(//, 'TYPE IN THE BEGINNING AND ENDING WAVELENGTH IN NM')
   READ(1,3) ISTART
   READ(1,3) IEND
3  FORMAT(1I3)
   LENGTH = IEND - ISTART + 1
   NUMBER = LENGTH/4
   LOGOS = NUMBER * 4
   LOG = LOGOS + 1
   DO 4 I = 1, LENGTH
   ARRAY(I) = 0.
4  CONTINUE
5  J = 1
   WRITE(1,28)
28  FORMAT(//, 'PLACE THE TAPE IN THE READER AND TURN THE READER ON')
   READ(1,30) Z
30  FORMAT(1A6)
   READ(1,6) A, B, C, D, E, F, G
6  FORMAT(7A6)
   READ(1,7) H, O, P, Q
7  FORMAT(4A6)
   DO 9 I = 1, LOGOS, 4
   A1 = ARRAY(I)
   A2 = ARRAY(I+1)
   A3 = ARRAY(I+2)
   A4 = ARRAY(I+3)
   READ(1,8) N(J), ARRAY(I), ARRAY(I+1), ARRAY(I+2) - ARRAY(I+3)
8  FORMAT(1I4, 4E16.7)
   ARRAY(I) = ARRAY(I) + A1
   ARRAY(I+1) = ARRAY(I+1) + A2
   ARRAY(I+2) = ARRAY(I+2) + A3
   ARRAY(I+3) = ARRAY(I+3) + A4
   J = J+1
9  CONTINUE
   IF (LENGTH - LOGOS) 11, 11, 27
27  A1 = ARRAY(LOG)
   A2 = ARRAY(LOG+1)
   A3 = ARRAY(LOG+2)
   READ(1,10) N(J), (ARRAY(I), I = LOG, LENGTH)
17  FORMAT(1I4, 3E16.7)
   ARRAY(LOG) = ARRAY(LOG) + A1
   ARRAY(LOG+1) = ARRAY(LOG+1) + A2
   ARRAY(LOG+2) = ARRAY(LOG+2) + A3
11  WRITE(1,11)
12  FORMAT(//, 'TYPE IN THE RUN MODE: ', /, '1 = DATA INPUT: ', /,
   '1*2 = PRINT OUT AVERAGED SCALED DATA', /, '3 = PUNCH OUT
   2DATA', /, '4 = RESTART THE PROGRAM', /)

```

```

13 READ(1,13) IANS
   FORMAT(111)
   GO TO (14,29,29,38) IANS
14 R = R + 1.
   GO TO 5
29 DO 15 I = 1, LENGTH
   ARRAY(I) = ARRAY(I)/R
15 CONTINUE
   WRITE(1,16)
16 FORMAT(/, 'TYPE IN THE SCALE FACTOR', /)
   READ(1,17) SCALE
17 FORMAT(1F14.5)
   DO 18 I = 1, LENGTH
   ARRAY(I) = ARRAY(I) * SCALE
18 CONTINUE
   RSCALE = SCALE
   GO TO (21,21,19,38) IANS
19 WRITE(1,20)
20 FORMAT(/, 'PRESS CONTINUE ON THE CONSOLE WHEN YOU HAVE THE
   1PUNCH READY', /)
   PAUSE
   CALL OPEN
21 WRITE(1,22)
22 FORMAT(/, '*4000', /, 'DECIMAL')
   NUM = (LENGTH/10) * 10
   NUM1 = LENGTH - NUM
   DO 34 I = 1, NUM, 10
   M = I
   DO 39 J1 = 1, 10
   L(J1) = ARRAY(M)
   M = M + 1
39 CONTINUE
   WRITE(1,23) (L(N1), N1 = 1, 10)
23 FORMAT(9(114,';',1X), 114)
34 CONTINUE
   IF (NUM1) 36,36,35
35 M = NUM + 1
   DO 41 I = 1, NUM1
   L(I) = ARRAY(M)
   M = M + 1
41 CONTINUE
   WRITE(1,23) (L(N1), N1 = 1, NUM1)
36 WRITE(1,24)
24 FORMAT(/, '$')
   DO 37 I = 1, LENGTH
   ARRAY(I) = ARRAY(I) * R/SCALE
37 CONTINUE
   GO TO (26,26,25,38) IANS
25 PAUSE
   CALL OPEN
26 GO TO 11
38 GO TO 1
   CONTINUE
   END

```

PROGRAM PMT FLOWCHART

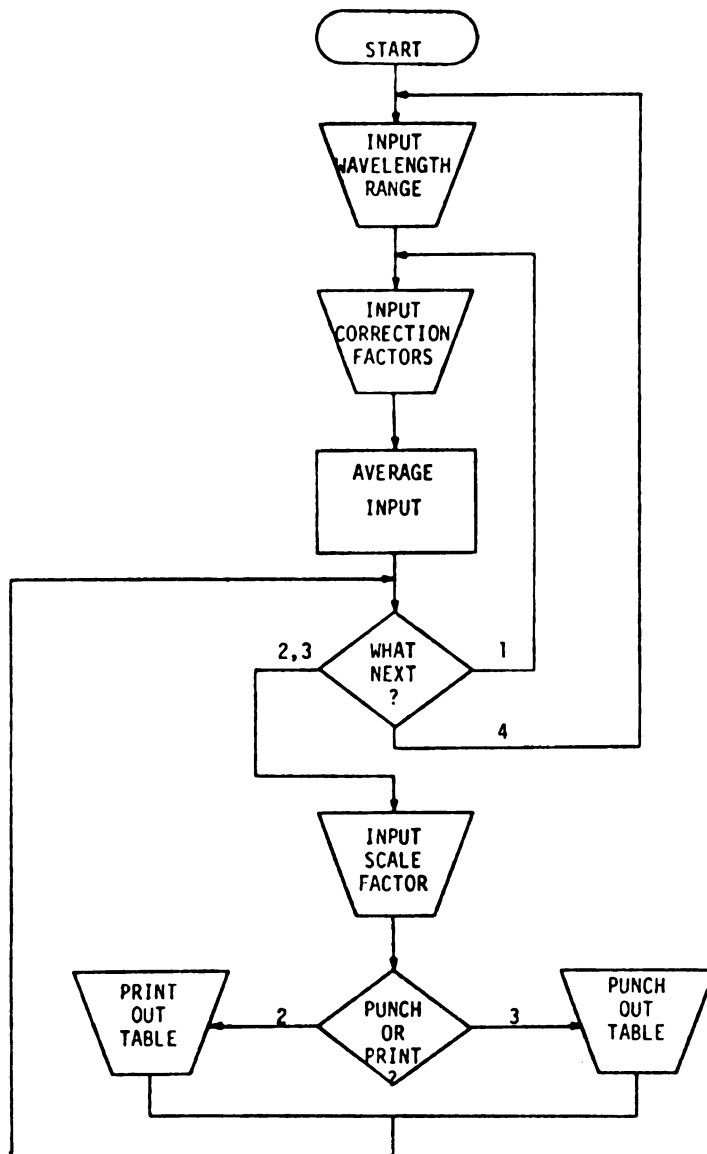


Figure 39. Program PMT Flowchart.

DATA PROCESSING

The paper tapes from the methylene blue quantum counter are processed first. This is because the methylene blue table will contain the largest correction factor.

- (1) Load program PMT into the computer.
- (2) The teletype will respond with TYPE IN THE BEGINNING AND ENDING WAVELENGTH IN NM. The user then types in the appropriate information in integer format.
- (3) The teletype will then respond with PLACE THE TAPE IN THE READER AND TURN THE READER ON.
- (4) Subsequently, one of the five paper tapes for the particular counter which is being processed, is read into the program. Although the program reads the heading at the beginning of each paper tape, this information is not used.
- (5) The teletype then responds with:

TYPE IN THE RUN MODE:

1 = DATA INPUT

2 = PRINT OUT AVERAGED SCALED DATA

3 = PUNCH OUT DATA

4 = RESTART THE PROGRAM

If more tapes are to be read into the program, the user types a 1. Steps 3 through 5 are then repeated until all the tapes for a particular quantum counter have been read.

- (6) At this point, the user should type a 2 in response to the alternatives given above.
- (7) The teletype will then respond with TYPE IN THE SCALE FACTOR. The user should now locate the largest correction factor and calculate the scale factor which, when multiplied by this largest factor, gives a number of about 2000.
- (8) The user then enters this scale factor into the program and the scaled correction table is printed out.
- (9) When the teletype responds with the list of alternatives again, the user types a 3.
- (10) Again, the teletype responds as in step 7 and the user enters the calculated scale factor.
- (11) The teletype will then type out PRESS CONTINUE ON THE CONSOLE WHEN YOU HAVE THE PUNCH READY.
- (12) Once the CONTINUE switch is pressed, the PAL8 compatible correction table will be punched out on paper tape. This tape is saved for final editing and assembly.
- (13) Once the punching process is completed, the CONTINUE switch is pressed again, and the teletype will print out the alternatives. The user then chooses alternative 4, and the program is restarted and ready for more input.
- (14) The rhodamine B correction table is processed in a similar manner except for steps 7 and 8. For

step 7, the user should type in the same scale factor which was used for the final output of the methylene blue correction factors. For the methylene blue counter, all of the correction factors between 570 and 590 nm are averaged. The same is done for the rhodamine B correction factors which were obtained from step 7. The final scaling factor for the rhodamine B table is merely the ratio of the methylene blue average to the rhodamine B average, multiplied by the scale factor used in step 7.

- (15) The two PAL8 compatible paper tapes are then read into the OS/8 EDITOR. The rhodamine B table is read in first, then the other table. The two tables are then merged at a point in the 570 to 590 nm interval where two of the correction factors are close to being identical. The overall correction table should be edited until the following form is obtained:

*4000

DECIMAL

.

.

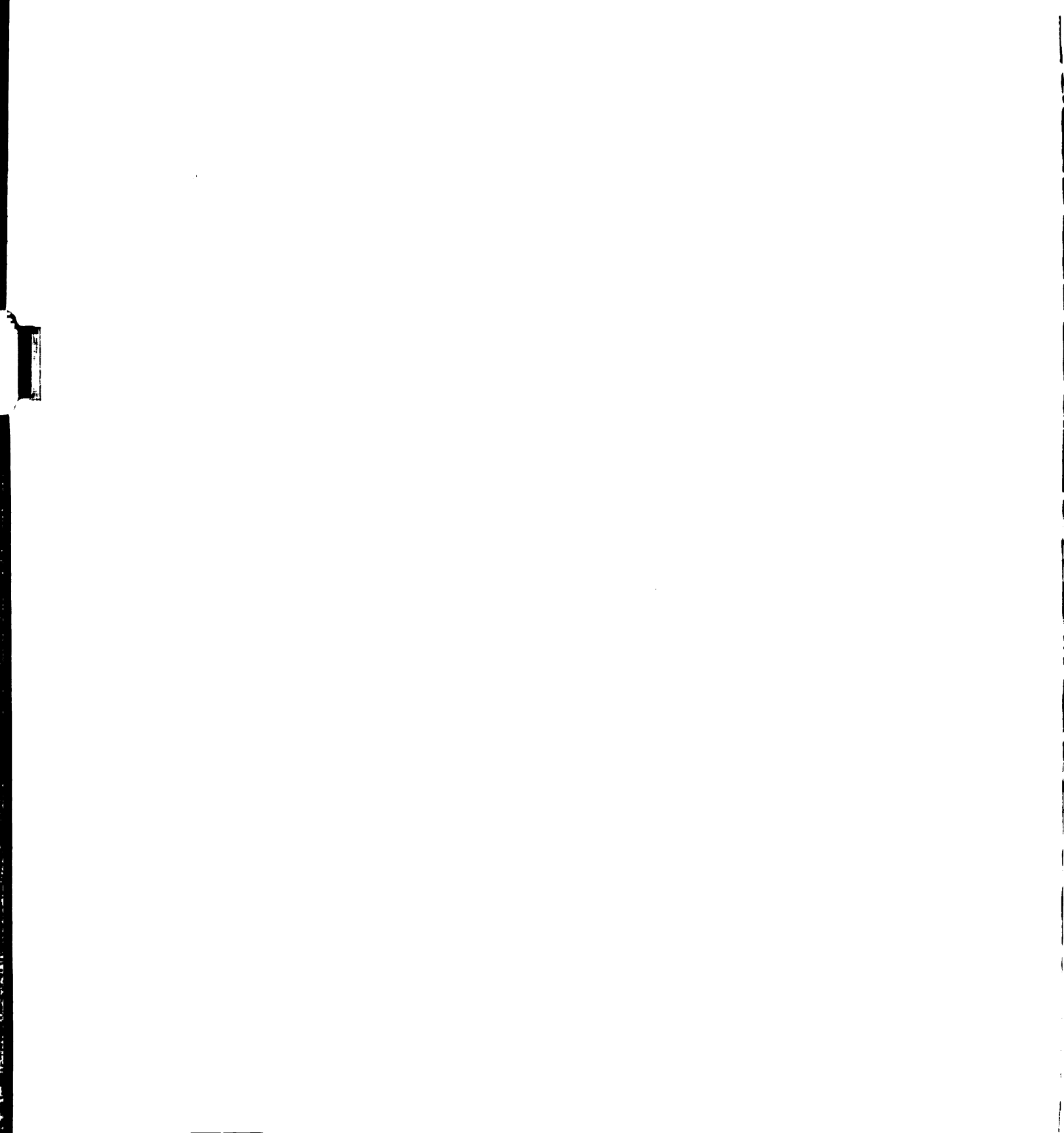
table of correction factors

.

.

\$

- (16) The file produced from EDITOR is then assembled by the PAL8 assembler into a file named PMT.BN. This file is loaded into field one when the main FLUORO program is processed into an OS/8 SAVE file.
- (17) The effectiveness of the completed correction table can be tested by running a tandem scan for each quantum counter. If the table has been constructed properly, the ratio of the reference signal to the emission signal, R/F , when plotted as a function of wavelength, should be a straight horizontal line. Obviously, the photomultiplier correction routine should be operative for these tests.
- (18) Once the tests are completed, the rhodamine B quantum counter should be installed for routine use.



APPENDIX FOUR
INSTRUCTIONS FOR THE IMPLEMENTATION OF
ABSORPTION-CORRECTED FLUORESCENCE MEASUREMENTS

As indicated in the Theoretical chapter of this thesis, the absorption corrections on source-corrected fluorescence measurements are dependent upon the size of the fluorescence observation window and the geometry of the emission optical system. Consequently, absorption-corrected fluorescence measurements are only possible if the geometry of the optical system is not altered and the size of the observation window can be determined. Since the geometry of the optical system will not be changed once it is installed in the instrument, the only impediment to the implementation of routine absorption-corrected fluorescence measurements is the determination of the window size. Unfortunately, this process is somewhat tedious, but happily it is also a one time venture.

Since absorption-corrected fluorescence deals with pure fluorophore solutions as well as mixtures of fluorophores and chromophores, these types of chemical systems are used in the determination of the observation window dimensions. The system of choice for the pure fluorophore solutions is quinine sulfate in either 1.0 or 0.1 N sulfuric acid. This system was chosen because quinine sulfate is stable in solution over long periods of time; it can be

obtained in high purity; it has a constant quantum efficiency and there is little overlap between the emission and absorption spectra.

For the mixtures of fluorophores and chromophores, several systems have been found to be satisfactory. Of these, the best are quinine sulfate and either 2-thiouracil or 2,5-dihydroxybenzoic acid in 0.1 N sulfuric acid. The 2-thiouracil is the best chromophore from the standpoint of stability in solution but decomposition in the solid state is a problem. On the other hand, 2,5-dihydroxybenzoic acid is somewhat unstable in solution, and lifetimes of about one week can be expected. The acid also has one more minor drawback in that it tends to dimerize in concentrated solutions, but the problem is not severe enough to warrant its dismissal as a test chromophore.

In any case, at least two series of solutions should be prepared for test purposes. The pure fluorophore series should range in concentration so that the solution absorbances go from about 0.005 up to about 2.0. In the case of quinine sulfate where the fluorescence at 450 nm is excited at 312 nm, the solutions should range from about 1×10^{-6} to about 3.1×10^{-4} M. In the case of the fluorophore-chromophore series, the first solution, which is pure fluorophore, should have an absorbance of at least 0.1 so that a reasonable amount of fluorescence is generated. Obviously, this fluorescence is going to be severely

attenuated by the presence of large amounts of chromophore. Consequently, there must be enough fluorophore present in order to generate a quantity of fluorescence which can be accurately measured even under conditions of severe attenuation. The concentration for quinine sulfate chosen for this study was 1×10^{-5} M but more concentrated solutions could be used. Whatever the concentration chosen, it should be the same for the whole series. The chromophore concentrations should range so that the solution absorbances, which do not include the fluorophore absorbance, run from about about one-fourth that of the fluorophore all the way to about 2.0. The chromophore absorbances in this study ranged from 0.013 to about 1.85.

Once all of the solutions have been prepared, the source-corrected fluorescence and transmittance of each solution are measured. These data are then processed through a series of FORTRAN programs.

PROGRAM LSSQ

Program LSSQ is a utility program which is divided into two sections. The first section, which is connected with run mode alternatives 1 and 2, is used to prepare the source-corrected fluorescence and transmittance data for input to the fitting program, RTFACT. The second section, which is associated with alternatives 3 and 4, accepts the window dimensions obtained from RTFACT as input. These

dimensions are then used in conjunction with the experimental data in order to calculate the absorption-corrected fluorescence for each solution in the series. All the information is then output in tabular form. This table may then be used to determine whether the absorption-corrected fluorescence is linear with the absorbance.

Program LSSQ is used in the following manner:

Section One

- (1) The program is loaded into the computer and the teletype immediately responds with
TYPE IN THE RUN MODE:
1 = LEAST SQUARES FIT FOR A PURE FLUOROPHORE
2 = FIT FOR A FLUOROPHORE AND CHROMOPHORE MIXTURE
3 = CALCULATION ROUTINE FOR A PURE FLUOROPHORE
4 = CALCULATION ROUTINE FOR A MIXTURE
- (2) The user then enters a 1 if the data are for a pure fluorophore or a 2 if they are for a mixture.
- (3) In both cases, the teletype prints TYPE IN THE NUMBER OF DATA POINTS AND YOUR DATA. The user then enters the appropriate information. An integer format is used for the number of data points whereas the transmittance and fluorescence data are entered as real numbers. The data are arranged in the following order:

```

transmittance           /first solution
source-corrected fluorescence
transmittance           /second solution
source-corrected fluorescence
.
.
.
etc.

```

The data for the least absorbant solution should always appear first and the rest of the data are ordered sequentially in increasing absorbance.

- (4) If the user chose the first option, the teletype responds with TYPE IN THE NUMBER OF DATA POINTS TO BE USED IN THE LEAST SQUARES FIT. The user then enters in the number of pure fluorophore solutions which have an absorbance under 0.05.
- (5) The teletype then prints out TYPE IN THE ESTIMATED W1 AND W2, RESPECTIVELY. The required information is entered and the program then calculates the absorption-corrected fluorescence for the solutions to be used in the fit. The equation of the best straight line is then calculated, and the program prints out the values for the slope and intercept. This equation is then used to calculate the absorption-corrected fluorescence for the remaining solutions in the series.
- (6) If option 2 was chosen, the teletype prints out TYPE IN THE ABSORPTION-CORRECTED FLUORESCENCE FOR THE PURE FLUOROPHORE. This value can be calculated from the window dimensions which were obtained

from RTFACT for the series of pure fluorophore solutions. The user then types in this fluorescence value.

- (7) At this point, the teletype responds to options 1 and 2 with PRESS CONTINUE ON THE CONSOLE WHEN YOU HAVE THE PUNCH READY. The user takes the appropriate action and presses the switch. The program then punches out the data in a form which is compatible with the input format of RTFACT. When the punching process is completed, the program pauses and the tape can be removed from the punch. The user then presses the CONTINUE switch to restart the program.

Section Two

- (8) Upon loading or restarting the program, the alternatives are typed out as in step one.
- (9) The user then enters a 3 if the calculations are to be performed for a pure fluorophore series or a 4 if they are for a mixture series.
- (10) The teletype then responds as in step three and again, the user supplies the needed input.
- (11) If alternative 3 was chosen, the program follows the same dialogue as outlined in steps three through five. If alternative 4 was chosen, the dialogue is the same as in step six.

- (12) At this point, the teletype responds to options 3 and 4 with TYPE IN W1 and W2, RESPECTIVELY. The user then enters the observation window dimensions which were obtained from RTFACT.
- (13) The program will next type out a table which consists of four pieces of information for each solution in a particular series: the absorbance, the source-corrected fluorescence, the theoretical absorption-corrected fluorescence used in the RTFACT fit, and the calculated absorption-corrected fluorescence which was obtained by using the window dimensions output by RTFACT.
- (14) The user may now plot the calculated absorption-corrected fluorescences against the solution absorbances to determine whether the window dimensions are satisfactory.

A program listing as well as a flowchart for LSSQ appear on the following pages.

PROGRAM RTFACT

Program RTFACT is a program based on a modified Simplex optimization technique. This program fits the experimental source-corrected fluorescence measurements to the LSSQ calculated absorption-corrected fluorescences by varying the window parameters, w_1 and w . When a fit has been

PROGRAM LSSQ

```

DIMENSION XARRAY(100), YARRAY(100), ZARRAY(100), WARRAY(100)
DIMENSION GARRAY(30)
32 SUMXY = 0.
SUMX = 0.
SUMY = 0.
SUMY2 = 0.
WRITE(1,1)
1  FORMAT(//, 'TYPE IN THE RUN MODE:',/, '1 = LEAST SQUARES FIT
FOR A PURE FLUOROPHOPE',/, '2 = FIT FOR A FLUOROPHOPE AND
2CHROMOPHOPE MIXTURE',/, '3 = CALCULATION ROUTINE FOR A PURE
3FLUOROPHOPE',/, '4 = CALCULATION ROUTINE FOR A MIXTURE',/)
READ(1,2) INPUT
2  FORMAT(111)
WRITE(1,3)
3  FORMAT(//, 'TYPE IN THE NUMBER OF DATA POINTS AND YOUR DATA', /)
READ(1,4) INTER
4  FORMAT(113)
DO 6 I = 1, INTER
READ(1,5) XARRAY(I)
READ(1,5) ZARRAY(I)
5  FORMAT(1F10.4)
6  CONTINUE
GO TO (11,7,11,7) INPUT
7  WRITE(1,8)
8  FORMAT(//, 'TYPE IN THE ABSORBANCE CORRECTED FLUORESCENCE FOR
THE PURE FLUOROPHOPE',/)
READ(1,9) PUPE
9  FORMAT(1F10.4)
DO 10 I = 1, INTER
YARRAY(I) = PUPE
GO TO (10,10,10,31) INPUT
31 WARRAY(I) = -(ALOG(XARRAY(I)))/2.30258
10 CONTINUE
GO TO 16
11 WRITE(1,12)
12 FORMAT(//, 'TYPE IN THE NUMBER OF DATA POINTS TO BE USED IN
THE LEAST SQUARES FIT',/)
READ(1,13) NHIEST
13 FORMAT(113)
WRITE(1,35)
35 FORMAT((', 'TYPE IN THE ESTIMATED W1 AND W2, RESPECTIVELY',/)
READ(1,27) W3
READ(1,27) W4
DO 14 I = 1, NHIEST
GARRAY(I) = ZARRAY(I)*(ALOG(XARRAY(I)))*(W4-W3)/((XARRAY(I)**
14) - (XARRAY(I)**W3))

```

```

X = -(ALOG(YAPPAY(I))/2.30258)
SUMXY = SUMXY + (OAPPAY(I) * X)
SUMX = SUMX + X
SUMY = SUMY + OAPPAY(I)
SUMX2 = SUMX2 + X**2.
14 CONTINUE
NHIEST = NHIEST
SLOPE = ((NHIEST*SUMXY) - (SUMX*SUMY))/((NHIEST*SUMX2) -
1(SUMX**2.))
RINTER = ((SUMY*SUMX2)-(SUMX*SUMY))/((NHIEST*SUMX2)-(SUMX**2.))
DO 16 I = 1, INTER
YAPPAY(I) = SLOPE * (-(ALOG(XAPPAY(I))/2.30258) + RINTER
GO TO (16,16,15,15) INPUT
15 WAPPAY(I) = -(ALOG(XAPPAY(I)))/2.30258
16 CONTINUE
GO TO (17,19,17,25) INPUT
17 WRITE(1,18) SLOPE, RINTER
18 FORMAT(/, 'SLOPE = ', 1E13.6, /, 'INTERCEPT = ', 1E13.6)
GO TO (19,19,25,25) INPUT
19 WRITE(1,20)
20 FORMAT(/, 'PRESS CONTINUE ON THE CONSOLE WHEN YOU HAVE THE
1PUNCH READY',/)
PAUSE
CALL OPEN
DO 24 I = 1, INTER
WRITE(1,23) XAPPAY(I), YAPPAY(I), ZARRAY(I)
23 FORMAT(2(1F10.4, /), 1F10.4)
24 CONTINUE
GO TO 30
25 WRITE(1,26)
26 FORMAT(/, 'TYPE IN V1 AND V2, RESPECTIVELY', /)
READ(1,27) V1
READ(1,27) V2
27 FORMAT(1F10.4)
WRITE(1,28)
28 FORMAT(/, 'ABSORBANCE', 6X, 'FLUORESCENCE', 6X, 'THEOR-AB-FLUOR',
16X, 'CALC-AB-FLUOR')
DO 30 I = 1, INTER
A = ZARRAY(I)*(ALOG(XAPPAY(I)))*(V2-V1)/((XAPPAY(I)**V2)
1-(XAPPAY(I)**V1))
WRITE(1,29) WAPPAY(I), ZARRAY(I), YAPPAY(I), A
29 FORMAT(/, 1F10.4, 7X, 1F10.4, 9X, 1F10.4, 9X, 1F10.4)
30 CONTINUE
PAUSE
CALL OPEN
GO TO 32
END

```

PROGRAM LSSQ FLOWCHART

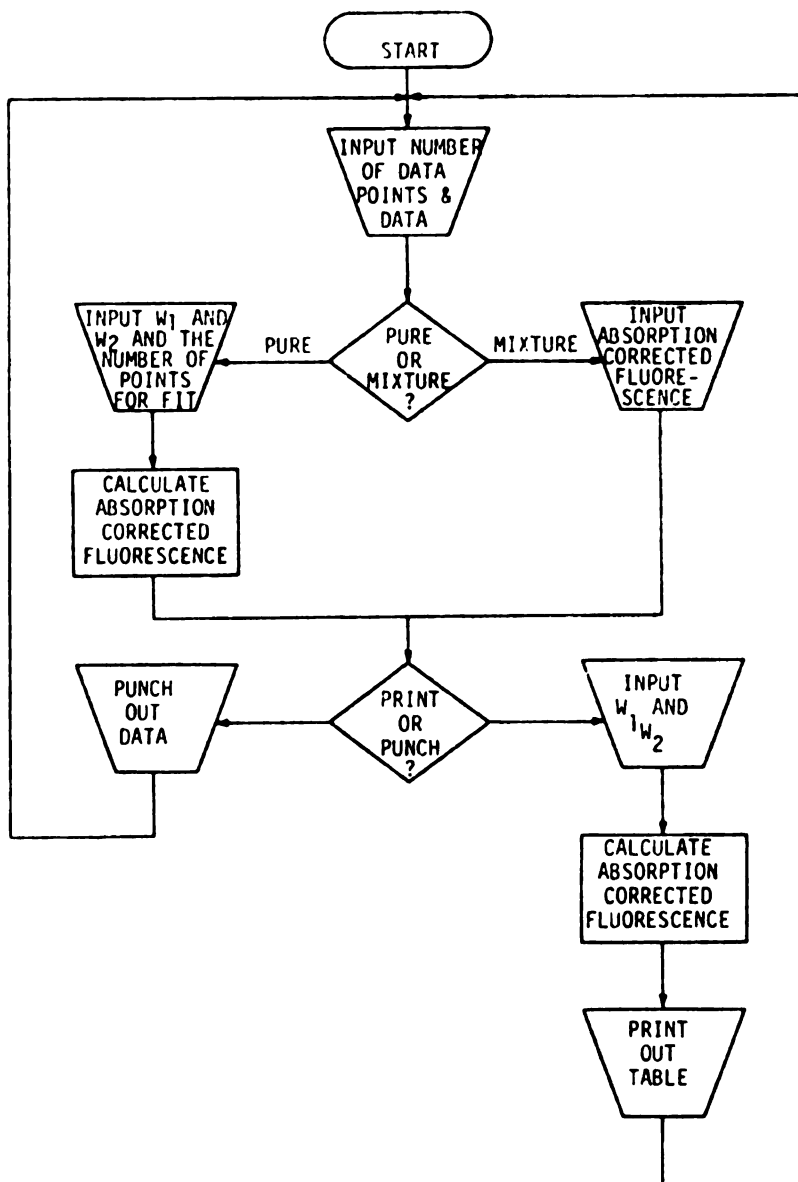


Figure 40. Program LSSQ Flowchart.

obtained within the specified convergence limit, the program outputs the window parameters as well as a value for the residual which is a measure of the exactness of the fit. Consequently, a low residual indicates that a good fit has been obtained. The input format for program RTFACT is given below:

```

1           /uneven data intervals
20          /number of data points
transmittance /output from LSSQ
absorption-corrected fluorescence
source-corrected fluorescence
.
.
.
2           /number of variables
.100        /estimate of  $w_1$ 
.800        /estimate of  $w$ 
.01         /convergence limit of 1%
```

Once convergence has been attained, the window parameters, w_1 and w , are converted to w_1 and w_2 which are quantities utilized by programs LSSQ and ARTCAL. The program listing for RTFACT appears on the following pages. No flowchart is supplied because the program is well commented.

PROGRAM ARTCAL

Once the user is satisfied with the values for the observation window parameters, they must be placed in the FLUORO program subroutine which calculates the absorption-correction factor, f_a . Since this subroutine calculates f_a by using the first seven terms of a Taylor expansion,

PROGRAM RTFACT

```

DIMENSION XARRAY(100), YARRAY(100), GUESS(10,9), RSDL(10)
DIMENSION K(10), BAD(10), OLD(9), PRES(9), RNEW(5,9), RENEV(5)
DIMENSION FIND(10), ZARRAY(100)
KL = 1
ITT = 0
NE = 0
WATCH = 0.
C TYPE IN THE KIND OF INPUT DATA: A 0 FOR DATA TAKEN AT
C EQUAL INTERVALS; A 1 FOR DATA TAKEN AT UNEQUAL INTERVALS
READ(1,1) INPUT
1 FORMAT(111)
IF (INPUT - 0) 2,2,6
C TYPE IN THE EQUAL INTERVAL DATA INPUT PARAMETERS: FIRST AND
C LAST INDEPENDENT VARIABLES, AND DATA INTERVAL
2 READ(1,3) START, FINISH, XINTER
3 FORMAT(3(1F10.3))
INTER = (FINISH - START + XINTER)/XINTER
FILL = START
C LOAD THE INDEPENDENT AND DEPENDENT VARIABLES IN XARRAY AND
C YARRAY, RESPECTIVELY
DO 4 I = 1, INTER
XARRAY(I) = FILL
FILL = FILL + XINTER
4 CONTINUE
READ(1,5) (YARRAY(I), I = 1, INTER)
5 FORMAT(1F10.3)
GO TO 10
C TYPE IN THE NUMBER OF VARIABLES AND LOAD THE INDEPENDENT
C AND DEPENDENT VARIABLES IN XARRAY AND YARRAY, RESPECTIVELY
6 READ(1,7) INTER
7 FORMAT(1110)
DO 9 I = 1, INTER
READ(1,8) XARRAY(I)
READ(1,8) YARRAY(I)
READ(1,8) ZARRAY(I)
8 FORMAT(1F10.4)
9 CONTINUE
C TYPE IN THE NUMBER OF UNKNOWNNS
10 READ(1,11) IUNKN
11 FORMAT(111)
RIUNKN = IUNKN
IUNK1 = IUNKN + 1
C TYPE IN THE INITIAL ESTIMATES FOR THE UNKNOWNNS
READ(1,12) (GUESS(1,I), I = 1, IUNKN)
12 FORMAT(1F10.3)

```

```

C      TYPE IN THE CONVERGENCE LIMIT
      READ(1,93) QED
93     FORMAT(1F10.4)
C      CONSTRUCT THE INITIAL SIMPLEX
13     DO 16 I = 1, IUNKN
      DO 15 J = 2, IUNK1
      GUESS(J,I) = GUESS(1,1)
      IF (J - I - 1) 15,14,15
14     GUESS(J,I) = .1 * GUESS(J,I) + GUESS(J,I)
15     CONTINUE
16     CONTINUE
C      CALCULATE THE THEORETICAL DEPENDENT VARIABLES
      DO 20 J = 1, IUNK1
17     RESID = 0.
      DO 18 L = 1, INTER
C      THIS IS THE THEORETICAL EQUATION
      A = ZARRAY(L) * (ALOG(XARRAY(L))) * (GUESS(J,2))/((XARRAY(L)
      1**GUESS(J,2) + GUESS(J,1))) - (XARRAY(L)**GUESS(J,1))
      RESID = RESID + (ABS(A - YARRAY(L)))**2.
18     CONTINUE
      IF (KL - 1) 19,19,31
C      SAVE THE RESIDUAL FOR EACH VERTEX
19     RSDL(J) = RESID
20     CONTINUE
C      START SORTING THE RESIDUALS;  WORST RESID IN BAD(1)
21     DO 22 I = 1, IUNK1
      FIND(I) = RSDL(I)
22     CONTINUE
      DO 25 J = 1, IUNK1
      B1 = 0.
      DO 24 I = 1, IUNK1
      IF (B1 - FIND(I)) 23,24,24
23     B1 = RSDL(I)
      K1 = I
24     CONTINUE
      FIND(K1) = 0.
      BAD(J) = B1
      K(J) = K1
25     CONTINUE
C      SORTING COMPLETED;  START GENERATION OF THE NEW SIMPLEX
C      THE NEXT DO LOOP IS USED TO AVOID HAVING THE SIMPLEX STRANDED
C      IT IMPLEMENTS THE USE OF OTHER VERTICES (RATHER THAN THE
C      WORST VERTEX) FOR THE CONSTRUCTION OF A NEW SIMPLEX
      DO 56 INDEX = 1, IUNKN
      I = K(INDEX)
C      GENERATION OF THE HYPERFACE
      DO 28 N = 1, IUNKN
      PRES(N) = 0.
      DO 27 J = 1, IUNK1
      IF (J - I) 26,27,26
26     PRES(N) = PRES(N) + GUESS(J,N)/RIUNKN
27     CONTINUE
28     CONTINUE
C

```

```

C      GENERATE NEW SIMPLEX USING THE FOLLOWING ALGORITHM
C      REFLECT THE WORST VERTEX (W) ACROSS THE HPERFACE TO FORM
C      A NEW VERTEX (R).  IF (R) IS NOW THE BEST VERTEX, EXPAND
C      THE SIMPLEX TO (S).  IF (S) IS NOW THE BEST, KEEP (S);  IF
C      NOT, KEEP (R).  IF (R) IS NEITHER THE BEST NOR THE
C      WORST VERTEX, KEEP (R).  IF (R) IS THE WORST VERTEX AND
C      WORSE THAN (W), THEN CONTRACT INTERNALLY.  IF (R) IS BETTER
C      THAN (W), THEN CONTRACT EXTERNALLY.  IF INTERNAL OR EXTERNAL
C      CONTRACTION RESULTS IN THE NEW VERTEX BEING THE WORST,
C      THE SIMPLEX IS FURTHER DIMINISHED
      NV = 1
      FACK = 1.
C      DIRECT REFLECTION
29     DO 30 N = 1, IUNKN
      RNEW(NV,N) = PRES(N) + FACK * (PRES(N) - GUESS(I,N))
      GUESS(I,N) = RNEW(NV,N)
30     CONTINUE
      KL = 2
      J = 1
      GO TO 17
31     RENEW(NV) = RESID
      GO TO (32,37,42,42) NV
32     IF (BAD(IUNK1) - RESID) 33,36,36
33     IF (BAD(2) - RESID) 39,39,34
34     WATCH = 0.
      DO 35 N = 1, IUNK1
      GUESS(I,N) = RNEW(NV,N)
35     CONTINUE
C      KEEP DIRECTLY REFLECTED VERTEX
      RSDL(I) = RENEW(NV)
      GO TO 47
C      EXTERNALLY EXPAND SIMPLEX
36     NV = 2
      FACK = 2.
      GO TO 29
C      KEEP EXPANSION; GO TO STATEMENT 34
37     IF (BAD(IUNK1) - RESID) 38,34,34
C      KEEP THE DIRECT REFLECTION
38     NV = 1
      GO TO 34
39     IF (BAD(1) - RESID) 40,40,41
C      INTERNALLY CONTRACT THE SIMPLEX
40     NV = 3
      FACK = -.5
      GO TO 29
C      EXTERNALLY CONTRACT THE SIMPLEX
41     NV = 4
      FACK = .5
      GO TO 29
42     IF (BAD(2) - RESID) 58,58,34
C      RECONSTRUCT THE SIMPLEX USING THE BEST VERTEX
43     WRITE(1,44)
44     FORMAT(//, 'THE PROGRAM WILL RECONSTRUCT THE SIMPLEX
      1 AND CONTINUE')

```

```

NE = NE + 1
C THE PROGRAM IS ONLY ALLOWED TO RECONSTRUCT 25 TIMES
IF (NE - 25) 45,45,54
45 DO 46 N = 1, IUNKN
IBEST = K(IUNK1)
GUESS(1,N) = GUESS(IBEST,N)
46 CONTINUE
KL = 1
GO TO 13
C COUNT ITERATIONS AND SEE IF CONVERGENCE WAS ATTAINED
47 ITT = ITT + 1
DO 49 N = 2, IUNK1
IF (ABS(PSDL(1) - PSDL(N)) - QED) 49,49,48
C CONTINUE CONVERGING IF THE MAXIMUM NUMBER OF ITERATIONS
C HAS NOT BEEN EXCEEDED
48 IF (ITT - 600) 21,54,54
49 CONTINUE
WRITE(1,50)
50 FORMAT(//, 'CONVERGENCE ATTAINED!')
C PRINT OUT THE UNKNOWNNS
51 N = K(IUNK1)
DO 53 I = 1, IUNKN
WRITE(1,52) I, GUESS(N,I)
52 FORMAT(//, 'W', III, ' = ', 1E12.6)
53 CONTINUE
WRITE(1,63) PSDL(1)
63 FORMAT(//, 'RESIDUAL = ', 1E12.6)
GO TO 62
C FAILURE TO CONVERGE CAN BE DUE TO TOO MANY RECONSTRUCTIONS
C OR EXCEEDING THE MAXIMUM NUMBER OF ITERATIONS
54 WRITE(1,55)
55 FORMAT(//, 'CONVERGENCE WAS NOT ATTAINED!')
C LIST THE UNKNOWNNS
GO TO 51
C A JUMP TO STATEMENT 56 MEANS THAT THE PROGRAMS IS USING
C THE SECOND WORST VERTEX TO AVOID BEING STRANDED
56 CONTINUE
C A JUMP TO STATEMENT 43 MEANS THAT THE SIMPLEX IS STANDED
C AND CONSEQUENTLY, THE SIMPLEX WILL HAVE TO BE RECONSTRUCTED
GO TO 43
C A JUMP TO STATEMENT 58 MEANS THAT THE PROGRAM IS DIMINISHING
C THE SIMPLEX EITHER INTERNALLY OR EXTERNALLY TO AVOID BEING
C STRANDED.
58 IF (WATCH - 9.) 59,59,56
59 GO TO (56,56,60,61) NV
60 FACK = FACK + .06
GO TO 29
61 FACK = FACK - .06
GO TO 29
62 CONTINUE
END

```

the constant part of each term must be calculated and the resultant numbers converted into binary floating point notation. Program ARTCAL is used for this task. Upon prompting from the program, the user types in the values of w_1 and w_2 which were obtained from RTFACT. The program responds by outputting the decimal value for each term constant as well as the binary floating point equivalent. ARTCAL calculates the term constants for the second through eleventh terms of the Taylor series. This is done so that the user can be assured that the eighth through eleventh terms are negligible compared to the first seven terms. The term constants ART1 through ART6 are then substituted into FLUORO and the user is now ready to make automated absorption-corrected fluorescence measurements. A program listing and flowchart for ARTCAL appear on the following pages.

PROGRAM ARTCAL

```

DIMENSION IHOLD(20), IBASE(60), IEX(4), NOUT(20), ART(10)
DIMENSION APTN(10)
KJ = 0
WRITE(1,28)
28  FORMAT(/,'TYPE IN W1 AND W2, RESPECTIVELY')
READ(1,29) W1
29  FORMAT(1E12.6)
READ(1,30) W2
30  FOPMAT(1E12.6)
DO 32 NN=1,10
FACT=1.
L=NN+1
DO 31 JJ=1,L
R = JJ
FACT=FACT*R
31  CONTINUE
EX=NN+1
APT(NN)=((W2**EX)-(W1**EX))/(FACT*(W2-W1))
I2=1
J=1
ISCORE=1
INDEX=2
NEX=0
APT(NN)=APT(NN)
DO 2 I=1,20
APT(NN)=APT(NN)*8.
NUMBER=APT(NN)
IHOLD(I)=NUMBER
REALM=NUMBER
2  APT(NN)=APT(NN)-REALM
CONTINUE
DO 3 I=1,60
IBASE(I)=0
3  CONTINUE
DO 4 I=1,60,3
M=I+1
N=I+2
IHOG=IHOLD(J)+1
GO TO (12,5,6,7,8,9,10,11), IHOG
5  IBASE(N)=1
GO TO 12
6  IBASE(M)=1
GO TO 12
7  IBASE(M)=1
IBASE(N)=1

```

```

      GO TO 12
8     IBASE(I)=1
      GO TO 12
9     IBASE(I)=1
      IBASE(N)=1
      GO TO 12
10    IBASE(I)=1
      IBASE(M)=1
      GO TO 12
11    IBASE(I)=1
      IBASE(M)=1
      IBASE(N)=1
12    IF (J-20) 13,4,4
13    J=J+1
4     CONTINUE
      DO 24 I=1,60
      GO TO (14,17,18), ISCORE
14    IF (IBASE(I)) 16,15,16
15    NEX=NEX+1
      GO TO 24
16    ISCORE=ISCORE+1
      NOUT(I)=IBASE(I)*2
      GO TO 24
17    NOUT(I)=NOUT(I)+IBASE(I)
      ISCORE=ISCORE+1
      GO TO 24
18    GO TO (19,20,21), IZ
19    NOUT(INDEX)=IBASE(I)*4
      IZ=IZ+1
      GO TO 22
20    NOUT(INDEX)=IBASE(I)*2+NOUT(INDEX)
      IZ=IZ+1
      GO TO 22
21    NOUT(INDEX)=IBASE(I)+NOUT(INDEX)
      IZ=IZ+1
22    IF (IZ-4) 24,23,24
23    IZ=1
      INDEX=INDEX+1
24    CONTINUE
      IF (NEX) 42,40,42
40    DO 41 JP = 1,4
      IEX(JP) = 0
41    CONTINUE
      GO TO 43
42    PNEX = NEX
      DECIMAL=4095.-PNEX
      DIV=DECIMAL/8.
      IDIV=DIV
      SAVOP=IDIV
      PDIV=SAVOP*8.
      IEX(1)=DECIMAL-RDIV+1.
      GO TO 34
37    RDEC = IDIV

```

```
DIV=RDEC/8.
IDIV=DIV
PDIV=IDIV*8
IEX(2)=PDEC-RDIV
GO TO 34
38 RDEC = IDIV
DIV=RDEC/8.
IDIV=DIV
RDIV=IDIV*8
IEX(3)=RDEC-RDIV
GO TO 34
39 IEX(4) = IDIV
43 KJ = 0
WRITE(1,33) NN, ARTN(NN)
33 FORMAT(///, 'ART', I12, ' = ', 1E12.6)
WRITE(1,25) IEX(4), IEX(3), IEX(2), IEX(1)
25 FORMAT(/, 'THE EXPONENT = ', 4I1)
WRITE(1,26) NOUT(1), NOUT(2), NOUT(3), NOUT(4)
26 FORMAT(/, 'THE UPPER MANTISSA = ', 4I1)
WRITE(1,27) NOUT(5), NOUT(6), NOUT(7), NOUT(8)
27 FORMAT(/, 'THE LOWER MANTISSA = ', 4I1)
GO TO 32
34 KJ = KJ + 1
IF (IEX(KJ)-8) 36,35,35
35 IEX(KJ) = 0
IDIV = IDIV + 1
36 GO TO (37,38,39) KJ
32 CONTINUE
END
```

PROGRAM ARTCAL FLOWCHART

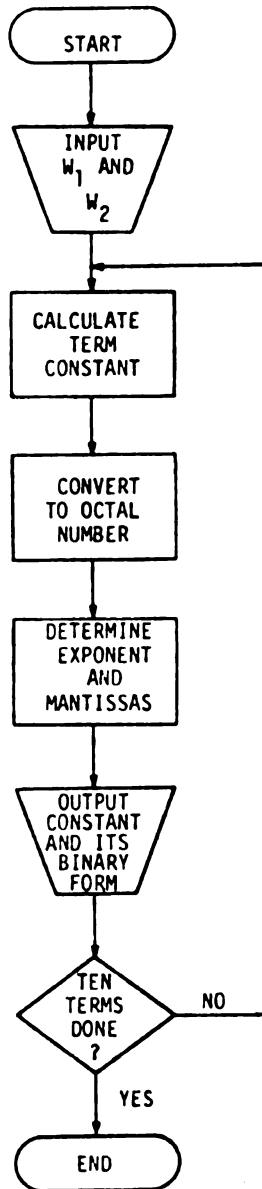


Figure 41. Program ARTCAL Flowchart.

BIBLIOGRAPHY

BIBLIOGRAPHY

1. Hitachi, Ltd., New Marunouchi Bldg., Tokyo, Japan, Model MPF-2A.
2. Photovolt Corp., 1115 Broadway, New York, Lumetron 402 EP.
3. Klett Mfg. Corp., 179 E. 87th Street, New York, Model 2070.
4. Parker, C. A., *Nature*, 82, 1000 (1958).
5. Slavin, W., Mooney, R. W. and Palumbo, D. T., *J. Opt. Soc. Am.*, 51, 93 (1961).
6. Lipsett, R. P., *J. Opt. Soc. Am.*, 49, 673 (1959).
7. American Inst. Co., Bull. 2392 D (1967).
8. Perkin Elmer Corp., *Instrument News*, 21 (2) 12 (1970).
9. Turner, G. K., *Science*, 146, 364, 183 (1964).
10. Cravitt, S. and Van Duuren, B., *Chem. Inst.*, 1, 71 (1968).
11. Howerton, H. K., "Fluorescence", Dekker, New York, Chapter 5 (1967).
12. Parker, C. A. and Rees, W. T., *Analyst*, 85, 587 (1960).
13. Witholt, B. and Brand, L., *Rev. of Sc. Inst.*, 39, (9), 1271 (1968).
14. Melhuish, W. H., *J. Opt. Soc. Am.*, 52, 1256 (1962).
15. Lee, J. and Saliger, H. H., *Photochem. Photobiol.*, 4, 1015 (1965).
16. Argaver, R. and White, C. E., *Anal. Chem.*, 36, 2141 (1964).
17. Parker, C. A., *Anal. Chem.*, 34, 502 (1962).
18. Holland, J. F., Teets, R. E. and Timnick, A., *Anal. Chem.*, 45, 145 (1973).
19. Price, J. M., Kaibara, M. and Howerton, H. K., *App. Opt.*, 1, 521 (1962).

20. Hermans, J. J. and Levinson, S., J. Opt. Soc. Am., 41, 460 (1951).
21. Van Slageren, R., Den Boef, G. and Van der Linden, W. E., Talanta, 20, 501 (1973).
22. Hercules, D. M., "Fluorescence and Phosphorescence Analysis", John Wiley and Sons, New York (1966).
23. Passwater, R. A. and Hewitt, J. W., Fluorescence News, 4, 9 (1969).
24. Longsworth, J. W., Photochem. Photobiol., 8, 589 (1968).
25. Parker, C. A. and Barnes, W. J., Analyst, 82, 606 (1957).
26. Parker, C. A. and Rees, W. T., Analyst, 87, 83 (1962).
27. Ohnesorge, W. E., Anal. Chim. Acta., 31, 484 (1964).
28. Gill, J. E., Appl. Spectrosc., 24, 588 (1970).
29. Holland, J. F., Teets, R. E., Kelly, P. M. and Timnick, A., submitted to Anal. Chem. for publication.
30. Michaelson, R. C. and Loucks, L. F., J. Chem. Ed., 52, 652 (1975).
31. Seely, G. R., J. Phys. Chem., 73, 125 (1969).
32. Eastman Kodak Co., publications JJ-31 and JJ-32.
33. Deming, S. N. and Morgan, S. L., Anal. Chem., 45, 278A (1973).
34. Katyal, M., Talanta, 15, 95 (1968).
35. Nevskaya, E. M. and Nazarenk, V. A., Zh. Analit. Khim., 27, 1699 (1972).
36. Korac, A., Wiadom. Chem., 23, 345 (1969).
37. Wilson, C. A., J. Am. Chem. Soc., 61, 2303 (1939).
38. Taubak, K., Naturwiss., 30, 439 (1942).
39. Hörhammer, L. and Hansel, R., Arch. Pharm., 285, 286 (1952).
40. Hörhammer, L. and Hansel, R., Arch. Pharm., 286, 447 (1953).

41. Hörhammer, L. and Hansel, R., Arch. Pharm., 288, 315 (1955).
42. Hagadorn, P. and Neis, R., Arch. Pharm., 286, 486 (1953).
43. Kohara, H. and Ishibashi, N., Japan Analyst, 16, 470 (1967).
44. Battei, R. and Trusk, B., Anal. Chem., 35, 1910 (1963).
45. Battei, R. and Trusk, B., Anal. Chim. Acta., 37, 409 (1967).
46. Bozhevol'nov, E. A., "Luminescent Analysis of Inorganic Materials", Khimiya, Moscow (1966), p. 86.
47. Kanno, T., Sci. Repts. Res. Inst. Tohoku Univ., A12, 532 (1960).
48. Kanno, T., Sci. Repts. Res. Inst. Tohoku Univ., A13, 91 (1961).
49. Kohara, H., et al., Japan Analyst, 16, 315 (1967).
50. Kohara, H., et al., Japan Analyst, 15, 938 (1966).
51. Elinson, S. V. and Petrov, K. I., "The Analytical Chemistry of Zirconium and Hafnium", Nauka, Moscow (1965), p. 150.
52. Jurd, L. and Geissman, T. A., J. Org. Chem., 21, 1395 (1956).
53. Urbach, F. L., Ph.D. Thesis, Michigan State University, East Lansing, Michigan (1964).
54. Urbach, F. L. and Timnick, A., Anal. Chem., 40, 1269 (1968).
55. Ohnesorge, W. E. and Capotosto, Jr., A., J. Inorg. Nucl. Chem., 24, 829 (1962).
56. Porter, L. J. and Markham, K. R., J. Chem. Soc. (C), 1970, 344.
57. Wheland, G. W., "Advanced Organic Chemistry", 3rd ed., John Wiley and Sons, New York (1960), pp. 683-693.
58. Aveston, J., J. Chem. Soc., 1965, 4438.
59. Brosset, C., Biedermann, G. and Sillen, L. G., Acta Chem. Scand., 8, 1917 (1954).

60. Kohlschütter, H. W. and Hantelmann, P., Z. Anorg. Allegem. Chem., 248, 319 (1941).
61. Ohnesorge, W. E., J. Inorg. Nucl. Chem., 29, 285 (1967).
62. Yoshihara, K. and Kearns, D. R., J. Chem. Phys., 45, 1991 (1966).

MICHIGAN STATE UNIV. LIBRARIES



31293000733075